University of Cincinnati

Date: 6/11/2014

I, Jacob Haseman , hereby submit this original work as part of the requirements for the degree of Master of Science in Aerospace Engineering.

It is entitled:

Experimental Investigation of Stability and Low-NOx Potential of a Lean-Direct-Injection Combustor Concept

Student's name: **Jacob Haseman**

This work and its defense approved by:

Committee chair: San-Mou Jeng, Ph.D.

Committee member: Shaaban Abdallah, Ph.D.

Committee member: Jongguen Lee, Ph.D.

17298

Experimental Investigation of Stability and Low- NO_x Potential of a Lean-Direct-Injection Combustor Concept

A thesis submitted to the Graduate School of the University of Cincinnati
In partial fulfillment of the requirements for the degree of

MASTER OF SCIENCE (M.S.)

In the Department of Aerospace Engineering and Engineering Mechanics
of the College of Engineering and Applied Science

June 2015

By

JACOB HASEMAN

B.S. Aerospace Engineering and Engineering Mechanics
University of Cincinnati, 2013

Committee Chair: Dr. San-Mou Jeng

Abstract

Current trends with swirler/combustor designs tend towards lower emissions in accordance with ICAO standards, with the main problems inherent in common lean-direct-injection (LDI) designs being poor stability and autoignition or flashback issues. The LDI design is meant to combine the good stability and performance of a traditional rich-burn quick-quench lean-burn (RQL) combustor with the ultra-low NO_x emissions of a lean-premixed-prevaporized (LPP) combustor. The goal of this research is to investigate the feasibility of using swirlers with varying swirl strengths in an LDI combustor array by performing a series of combustion tests at atmospheric pressure. Three configurations were designed and tested which contained different arrangements of two counter-rotating radial-radial swirler designs with varying swirl strengths in a 3x3 array format.

All nine swirlers contained a fuel nozzle with very similar flow numbers and were all set to the same insertion depth with respect to the swirlers' flare exits. Two nozzle insertion depths were investigated to see how the performance changes with changing insertion depth. Three fuel circuits supplied fuel to the nine fuel nozzles to the center, sides, and diagonal swirlers respectively. Testing was conducted by placing the hardware on a horizontally-oriented test rig connected to an air intake manifold, with the inlet air preheated to approximately 400°F and the pressure drop across the swirler set to 4% of atmospheric pressure. These tests investigated fuel staging configurations at various simulated engine throttle settings and flight conditions to gauge the steady-state combustion and LBO characteristics and low- NO_x potential of this design.

The results of this testing show that all three configurations tested were able to achieve stable-burning with low equivalence ratios for the three simulated flight conditions tested, as

well as across a number of other investigated parameters. The two high-strength swirler configurations performed better than the baseline configuration in terms of LBO, stability, and flame uniformity, but all three configurations achieved stable combustion at comparable equivalence ratios to traditional combustor designs currently in use in industry. The low fuel flow rates required for ignition with the larger flow number fuel nozzles also demonstrates the practicality of this design in a real-world scenario. These tests also demonstrate that the deeper nozzle insertion depth performed better than the shallow insertion depth, and that future testing should focus on the high-strength swirler configurations.

Acknowledgements

First and foremost I would like to thank my advisor, Dr. Jeng. Without his constant advice, support, and encouragement, I would not have had the distinct pleasure of cooping at the combustion lab, let alone earning my master's degree under his careful guidance.

I would also like to thank my defense committee members, Dr. Jongguen Lee and Dr. Shaaban Abdallah, for taking time out of their schedules to critique my defense and give me valuable feedback.

My sincerest thanks to everyone at the combustion lab who has helped me the past five years: Samir, Curt, Ryan, Wessam, Geoff, Brendan, Derick, Xionghui, and many others. Your support, help, and friendship have made my time at UC not simply bearable, but enjoyable.

To the UC Track & Field team, I owe a deep debt of gratitude. For teaching me valuable time management skills, pushing me to my very limits both mentally and physically, helping me understand that "tiredness is just a state of mind", and teaching me truly unyielding motivation. Those lessons learned and friendships forged I will hold dear for the rest of my life.

And of course, to my mother and father. For making me into the man I am today.
And for fueling the fire.

Table of Contents

Abstract i

Acknowledgements iii

List of Figures vii

List of Tables x

List of Symbols and Abbreviations xi

Chapter 1 : Introduction 1

1.1 Gas Turbine Engines 3

1.2 NO_x Emissions 6

1.3 LPP Combustors 10

1.4 LDI Combustors 13

1.5 Isothermal Aerodynamics 23

1.6 Goals and Expectations 29

Chapter 2 : Hardware Design 30

Chapter 3 : Test Matrix 47

Chapter 4 : Experimental Setup 48

Chapter 5 : Results 51

5.1 Equivalence Ratios for Steady-State Combustion 52

5.2 Steady-State Combustion Pictures 52

5.3 Acoustic Instability 59

5.4 Ignition and Lean-Blowout 61

Chapter 6 : Discussion 62

6.1 Steady-State Burning Equivalence Ratios 62

6.2 Comparison of Combustion Pictures with PIV Data 65

6.3 Standard Video 75

6.4 High-Speed Video 79

6.5 Acoustic Instabilities 85

6.6 Large Fuel Nozzle Ignition/LBO Testing 89

Chapter 7 : Conclusion 91

Chapter 8 : References 93

List of Figures

Figure 1-1: NO Formation Rate vs. Equivalence Ratio (Correa, 1993) 8

Figure 1-2: Relationship Between NOx and CO for a 36-point MPIM 10

Figure 1-3: Sketch of TAPS Configuration 13

Figure 1-4: Comparison of Swirler Orientations for 25-point MPIM 18

Figure 1-5: Comparison of 9, 25, 36, and 49-point LDI Arrays 22

Figure 1-6: Velocity Profiles for Axial Swirler, a) Isothermal, b) Reacting 28

Figure 1-7: Comparison of Reacting/Non-reacting Axial Velocity Profiles for Axial Swirler 29

Figure 2-1: Cross-Sectional View of CAD Model of UCRI-1 (a) and UCRI-2 (b) 31

Figure 2-2: UCRI-1 Axial Velocity Contours 32

Figure 2-3: UCRI-2 Axial Velocity Contours 32

Figure 2-4: Configuration 1 Swirler Orientation: 35

Figure 2-5: Configuration 2 Swirler Orientation 35

Figure 2-6: Configuration 3 Swirler Orientation 35

Figure 2-7: Upstream Side of Faceplate showing Swirler Proximity 37

Figure 2-8: Schematic of Fuel Circuits/Nozzles 38

Figure 2-9: Simulated Fuel Spray Cone for UCRI-1, Deep Insertion Depth 41

Figure 2-10: Simulated Fuel Spray Cone for UCRI-2, Deep Insertion Depth 41

Figure 2-11: Simulated Fuel Spray Cone for UCRI-1, Shallow Insertion Depth 41

Figure 2-12: Simulated Fuel Spray Cone for UCRI-2, Shallow Insertion Depth 42

Figure 2-13: Steady-State Burning Fuel Nozzle Orientation 43

Figure 2-14: Configuration 1 Swirler Orientation 43

Figure 2-15: Configuration 2 Swirler Orientation (UCRI-2 in red, UCRI-1 in black) 43

Figure 2-16: Configuration 3 Swirler Orientation (UCRI-2 in red, UCRI-1 in black) 44
Figure 2-17: 3D CAD Model of LDI Combustion Chamber, Airbox, and Fuel Circuits 45
Figure 2-18: Test Setup with Horizontal Rig, Heater, and LDI Rig 46
Figure 2-19: CAD Model of LDI Rig in High Pressure Combustion Chamber 46
Figure 4-1: Schematic of Horizontal Rig Test Facility 49
Figure 5-1: Configuration 1, Deep Insertion, Idle, 6-0-0, φ=0.21 52
Figure 5-2: Configuration 1, Deep Insertion, Cruise, 4-12-0, φ=0.55 53
Figure 5-3: Configuration 1, Deep Insertion, SLTO, 3-8-10, φ=0.74 53
Figure 5-4: Configuration 1, Deep Insertion, SLTO, 3-9-9, φ=0.74 53
Figure 5-5: Configuration 2, Deep Insertion, Idle, 5-0-0, φ=0.18 54
Figure 5-6: Configuration 2, Deep Insertion, Cruise, 2.5-12-0, φ=0.48 54
Figure 5-7: Configuration 2, Deep Insertion, SLTO, 2.5-9-11, φ=0.77 54
Figure 5-8: Configuration 3, Deep Insertion, Idle, 5-0-0, φ=0.18 55
Figure 5-9: Configuration 3, Deep Insertion, Cruise, 3-12-0, φ=0.48 55
Figure 5-10: Configuration 3, Deep Insertion, SLTO, 3-9-11, φ=0.76 55
Figure 5-11: Configuration 1, Shallow Insertion, Idle, 12-0-0, φ=0.42 56
Figure 5-12: Configuration 1, Shallow Insertion, Cruise, 8-12-0, φ=0.70 56
Figure 5-13: Configuration 1, Shallow Insertion, SLTO, 6-12-12, φ=1.06 56
Figure 5-14: Configuration 2, Shallow Insertion, Idle, 10-0-0, φ=0.35 57
Figure 5-15: Configuration 2, Shallow Insertion, Cruise, 6-10-0, φ=0.55 57
Figure 5-16: Configuration 2, Shallow Insertion, SLTO, 6-12-12, φ=1.04 57
Figure 5-17: Configuration 3, Shallow Insertion, Idle, 9-0-0, φ=0.31 58
Figure 5-18: Configuration 3, Shallow Insertion, Cruise, 6-12-0, φ=0.62 58

Figure 5-19: Configuration 3, Shallow Insertion, SLTO, 5-10-12, φ=0.94 58
Figure 5-20: Output from Audacity showing Dominant Frequency of 567Hz 60
Figure 5-21: Sample Acoustic Spectrum for Acoustic Instability 60
Figure 6-1: Configuration 1 Axial Velocity Contours at y/D=0.3 65
Figure 6-2: Configuration 1 Axial Velocity Contours at y/D=0.74 65
Figure 6-3: Configuration 1 Axial Velocity Contours at y/D=1.0 65
Figure 6-4: Magnification of CTRZ Interaction Zone 67
Figure 6-5: Magnification of Flame-Front Interaction 67
Figure 6-6: Vertical Cross-Sections of Axial Velocity for Configuration 1 68
Figure 6-7: Configuration 2 Axial Velocity Contours at y/D=0.3 69
Figure 6-8: Configuration 2 Axial Velocity Contours at y/D=0.74 69
Figure 6-9: Configuration 2 Axial Velocity Contours at y/D=1.0 69
Figure 6-10: Vertical Cross-Sections of Axial Velocity for Configuration 2 71
Figure 6-11: Configuration 3 Axial Velocity Contours at y/D=0.3 72
Figure 6-12: Configuration 3 Axial Velocity Contours at y/D=0.74 72
Figure 6-13: Configuration 3 Axial Velocity Contours at y/D=1.0 72
Figure 6-14: Vertical Cross-Sections of Axial Velocity for Configuration 3 75
Figure 6-15: Image of Configuration 1 from Standard Video 77
Figure 6-16: Image of Configuration 2 from Standard Video 77
Figure 6-17: Still of Configuration 2 with Circuits 1&2 Active, Shallow Insertion 79
Figure 6-18: High-Speed Video Sequence of Configuration 2 at φ=0.94 (a) 83
Figure 6-19: High-Speed Video Sequence of Configuration 2 at φ=0.94 (b) 84

List of Tables

Table 2-2: Measured and Projected Mass Flow Rates for UCRI-1 Swirlers 33

Table 2-3: Measured and Projected Mass Flow Rates for UCRI-2 Swirlers 33

Table 2-4: Measured vs. Expected Effective Areas and Mass Flow Rates 36

Table 3-1: Steady-State Combustion Pictures and φ Test Plan 47

Table 3-2: Complete Testing Matrix 48

Table 5-1: Steady-State Combustion Equivalence Ratios for Various Fuel Circuits Active 52

Table 5-2: Flow Rates for Acoustic Instability, Configuration 1 59

Table 5-3: Flow Rates for Acoustic Instability, Configuration 2 59

Table 5-4: Flow Rates for Acoustic Instability, Configuration 3 59

Table 5-5: Fuel Flow Rates for Ignition and LBO with FN 3.0 Fuel Nozzle 61

Table 5-6: Equivalence Ratios for Ignition and LBO with FN 3.0 Fuel Nozzle 61

Table 5-7: Equivalence Ratios for Ignition and LBO with FN 0.9 Fuel Nozzles 61

Table 6-1: Visual Frequency Analysis of High-Speed Videos 80

List of Symbols and Abbreviations

Φ	Equivalence Ratio
ρ	Density
$\dot{m}$	Mass Flow Rate (lb/s or kg/s)
θ	Swirler Vane Angle (degrees)
G_x	Axial Flux of Axial Momentum
G_θ	Axial Flux of Tangential Momentum
P_3	Inlet Pressure
T_3	Inlet Temperature
ΔP	Pressure drop across swirler
CTRZ	Central Toroidal Recirculation Zone
EI	Emissions Index (g/kg_{fuel})
EI NO_x	Emissions Index for NO_x (g NO_x per kg fuel)
FAR	Fuel-Air Ratio
FFT	Fast-Fourier Transform
GTC	Gas Turbine Combustor
ICAO	International Civil Aviation Organization
LDI	Lean Direct-Injection
LDV	Laser Doppler Velocimetry
LPP	Lean-Premixed-Prevaporized
MPIM	Multi-Point Injector Module
NO_x	Oxides of Nitrogen
PIV	Particle Image Velocimetry
RQL	Rich-Burn Quick-Quench Lean-Burn
SN	Swirl Number
TAPS	Twin Annular Premixing Swirler
TKE	Turbulent Kinetic Energy

Chapter 1 : Introduction

With the current exponentially-increasing trend of technology and the application of that technology to aircraft engines, engine pressures and inlet temperatures are increasing every year, and will continue to do so as long as materials can be found to withstand those extreme conditions. The drawback to this ever-increasing trend is the concurrent increase in environmentally-damaging emissions that accompany a these high temperatures and pressures. A significant component of these emissions is known as NO_x, or oxides of nitrogen, and contributes both directly and indirectly to the production of smog, acid raid, climate change, and harmful respiratory ailments.

Internal combustion engines are a major contributor to the above-mentioned issues via the production of NO_x that accompanies combustion at typical operating conditions. While aircraft are not currently the major contributor to NO_x and other harmful emissions, the largest contributors (energy, industry, and forestry) utilize technology which is markedly easier to improve and implement emissions-reducing solutions. Cutting-edge technology applied to these sources may cause major inconveniences in the case of malfunction; potential loss-of-life would be the outcome if applied to commercial aircraft. For this reason, proposed advancements to gas turbine engines may take up to 20 years to come to fruition on an actual aircraft, and so those crucial technologies must start being developed now to keep pace with the other contributors of emissions. Additionally, land-based power-generators use nearly identical technology to aircraft engines, so advancements to actual engine technology has a direct and immediate carryover to the energy industry.

The arguments and desires to reduce harmful gas emissions are fairly obvious, and need not be discussed further. The question then becomes how to go about implementing these

improvements to reduce emissions from gas turbine combustion engines. Recently, design advancements have tended towards an array of smaller swirler cups arranged in multiple concentric rings in the combustor. A considerable amount of work has been done on this subject, with the majority being performed by Tacina et. al. In 1990, the similarities and differences between LPP and LDI combustors were investigated by measuring the NO_x at various pressures and physical measurement locations, finding a good correlation with empirical equations used to predict NO_x (Tacina 1990). A series of flame-tube tests were conducted in 2002 with both a 36-point 6x6 array and a 25-point 5x5 array by testing a matrix of inlet pressures and temperatures and measuring the emissions index for NO_x ($EINO_x$). In 2002 the multi-point injection module (MPIM) concept was tested, which used 36 small nozzle/swirler assemblies in an LDI configuration meant to replace the popular twin-annular combustor configuration, in a 4x9 arrangement, and was able to sustain combustion with 75% of the nozzles turned off. The trend continued to 2003 with a 49-point 7x7 array under similar conditions to the previous tests. In 2008, testing was again performed with a 9-point 3x3 array of axial swirlers and compared with the 25, 36, and 49 point arrays (Tacina et al 2002, 2003, 2008).

All of the examples listed here are either LPP or LDI combustors; however the only metric tested were emissions. No testing was done to evaluate stability or lean-blowout limits, which is the inherent downfall in the LPP design. The primary reason for the shift in research focus from LPP to LDI is because of the poor stability of the LPP design combined with its increased risk for flashback and autoignition due to the fuel being partially vaporized and nearing autoignition temperatures in the swirl cup. In principle the LDI design has a greatly reduced risk of flashback or autoignition because the fuel is injected directly into the air stream of the swirler. This is as opposed to traditional RQL designs in which fuel impinges onto the venturi and transitions from

sheet-breakup to droplet-breakup before encountering the shear layer of the two interacting air streams of the swirler. Previous testing on LDI designs has shown that they can achieve comparable emissions to LPP with lower risk of flashback and/or autoignition, however little testing has been done on their stability and lean blow-out limits. The goal of this research is to lay the groundwork for high-pressure combustion testing by investigating the stability behavior of an LDI design at atmospheric conditions.

1.1 Gas Turbine Engines

Gas turbine engine technology has made leaps and bounds since the first GTC-powered aircraft flew in 1939. Compressor pressure ratios have been increasing at a logarithmic rate, and now many commercial engines operate at 50 or 60 atmospheres, with inlet temperatures exceeding 1100°F. However the basic principles of operation for these engines have remained unchanged in their 75+ years of operation. A compressor or fan draws in and increases the pressure of the incoming air. The air is combined with fuel and combusted, converting the chemical energy into thermal energy and increasing the temperature and pressure of the resulting gases. This high-pressure gas expands through the turbine, where some of the energy is harnessed to drive the compressor or fan blades and the rest is ejected through the nozzle and converted to thrust.

There are three main types of combustor burner configurations. The most common design is called a rich-burn quick-quench lean-burn combustor, or RQL. This design burns fuel-rich locally near the dome and then introduces dilution air further downstream to reduce the turbine inlet temperatures. Many aircraft engines and land-based power generators use this design

because it is very stable and reliable; however the drawback with this design is that it produces harmful ozone-depleting emissions of NO, CO, and OH radicals. Because of this, recent research has been focusing on trying to design a combustor with a fuel-lean primary zone and good emissions, which has led to the development of the LPP and LDI combustors. The lean-premixed-prevaporized design relies on a gaseous fuel to achieve extremely quick combustion and uniform fuel-air mixing, which reduces harmful NO_x emissions and allows the engine to run cooler overall. While emissions are better with this design, there is a tradeoff in that the stability is inherently reduced due to the lean primary zone, and an even more significant drawback with the increased risk of flashback and autoignition. (Beer (1972), Lefebvre (2010))

A new design has been in development since the early 1990's dubbed lean-direct injection (LDI), which injects fuel directly into the combustion zone and commonly relies on a series of very small air swirlers to atomize and combine the fuel/air mixture. By injecting directly into the combustion zone the risk of autoignition is greatly reduced due to the time necessary for droplet evaporation and the reduced proximity to the burner dome. The reduced swirl cup assembly size shortens the residence time of the combustion process and subsequently NO_x emissions, ensures a more uniform burning process via increased overall turbulent kinetic energy (TKE) which reduces local hotspots which contribute to NO_x emissions, and reduces the overall length and weight of the engine which reduces cost and size requirements. (Lefebvre, 2010)

All combustor designs have a fuel injector to supply fuel for combustion and an air swirler to thoroughly break up the fuel and combine with the air in the combustor. The performance of the swirler is crucial to the efficiency and operation of the combustor, and subsequently the engine as a whole. If the fuel/air mixture is not thoroughly mixed or the fuel droplets are too big then local temperatures may grow too high for the combustor liner materials for higher power

conditions. For low-power conditions, poor mixing or atomization may lead to an engine blowout or blow-off, an extremely dangerous situation especially at higher altitudes where the incoming air pressure and temperatures are not conducive to combustion without pre-pressurization. The air swirlers and fuel nozzles must be designed to provide sufficient atomization and droplet breakup at lower power conditions and supply enough fuel for high-power conditions. Additionally, the swirler must be able to anchor the flame to ensure stable combustion across all power conditions while maintaining good combustion efficiency and performance. (Turns, 2012)

The swirler serves to create a central toroidal recirculation zone (CTRZ) by imparting tangential velocity to the flow. This creates a low-pressure zone near the centerline of the swirler, causing the flow to recirculate in a "bubble" near the swirler exit with a local negative axial velocity. Hot combustion products further downstream are brought back upstream by this CTRZ to aid in the combustion of fresh fuel droplets from the fuel nozzle. The amount of swirl is characterized and standardized by the swirl number (SN). The swirl number is the ratio of the axial flux of tangential momentum to the axial flux of axial momentum, normalized by the swirler exit radius, and represented by equation 1-1 below.

$$SN = \int_0^\infty \frac{G_\phi}{G_x R} \qquad (1\text{-}1)$$

Traditionally, any swirling flow with a swirl number greater than roughly 0.6 is considered to be "strong", and a closed CTRZ will develop. (Gupta et al (1984), Lilley (1977))

The size, shape, and strength of the CTRZ are all very important to the stability and performance of a gas turbine combustor. Very generally, a smaller CTRZ will be stronger and

slightly less stable, with "strength" either being defined as the average magnitude of the reverse flow velocity inside the CTRZ or the largest value of the reverse flow velocity. In accordance with the conservation of mass, for a given mass flow a larger average positive axial velocity will yield an equally-large average negative axial velocity. Accordingly, a larger CTRZ has lower average negative axial velocity, which is beneficial to stability as this allows the flame speed of the hot combustion products to more closely match the incoming unburned air/fuel mixture and propagate the flame more successfully. The characteristics of the swirler and CTRZ dictate the aerodynamics in the burner, which subsequently dictates the formation of various combustion products and the uniformity of the flow prior to entering the turbine inlet. (Gupta et al (1984), Lilley (1977))

1.2 NO_x Emissions

The term "oxides of nitrogen" or "NO_x" comprises two chemicals: NO and NO_2, both of which are produced during combustion. NO is a radical which depletes the ozone layer and naturally degrades to NO_2 over time in the atmosphere. NO_2 is a toxic gas which forms both smog and acid rain, as well as produces O_3 near the ground. NO_2 can then convert again to NO via reaction with ultraviolet light, continuing the cycle. In light of this, the international civil aviation organization (ICAO) has set standards in place which govern the maximum allowable amount of NO_x for aircraft engine emissions. These regulations were first enacted in 1981 when an original limit on NO_x emissions was set, and these limits have been becoming increasingly stringent since then, with new limits set in 1996, 2004, and 2008. (ICAO Annex, 2008)

Past efforts to design low-NO_x combustor concepts include the High Speed Research Program (HSR), the Advanced Subsonic Technology Program (AST) (Friedl, 1997), the Experimental Clean Combustor Program (Niedzwiecki, 1974), and the Ultra-Efficient Engine Technology Program (UEET) (Daggett, 2002). These programs were created to voluntarily begin developing technology and designing combustors with lower NO_x emissions before the ICAO guidelines took effect. All of these efforts have produced technology which has reduced NO_x emissions to between 40% and 80% below the limit proposed in 1996 by the ICAO, with the HSR, AST, and UEET demonstrating emissions reductions of 90%, 50%, and 70% respectively compared to the 1996 ICAO standard (Tacina 2008). Recent testing by Tacina (2002) with 25-point and 36-point arrays demonstrated NO_x emissions that were 80% below the 1996 limit. More testing performed with a 49-point array yielded a NO_x emissions index of 9, performing similarly to the 25-point array previously tested (Tacina 2003).

The mechanisms by which NO_x is generated are well-known and are used to aid in the design of low- NO_x swirlers and combustors. There are three primary mechanisms by which NO_x is produced in gas turbine engines; the thermal mechanism, the prompt mechanism, and the nitrous oxide mechanism. The two main chemical reaction equations for the formation of NO in fuel-lean conditions are as follows.

$$O + N_2 \Leftrightarrow NO + N$$

$$N + O_2 \Leftrightarrow NO + O \quad (1\text{-}2)$$

The thermal mechanism is only significant at temperatures above ~1800K, and is given by the following equation.

$$w = A[N_2][O_2]^{1/2} e^{-\frac{E_a}{RT}} \qquad (1\text{-}3)$$

There is a very strong and direct relationship between temperature and oxygen concentrations and NO_x formation, and thus an indirect but equally as strong relationship between NO_x and oxygen concentrations and equivalence ratio, as illustrated in figure 1-1. (Semerjian et al (1997), Correa et al (1993))

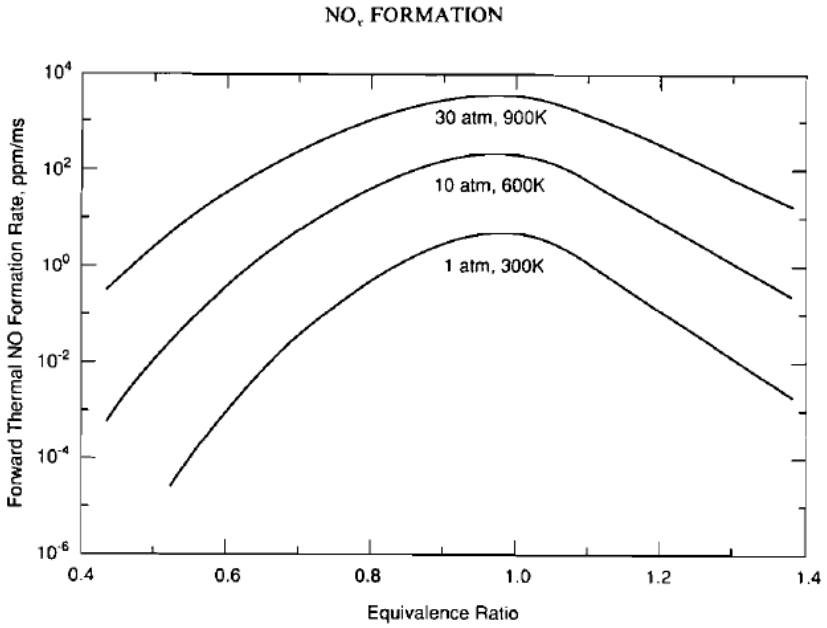

Figure 1-1: NO Formation Rate vs. Equivalence Ratio (Correa, 1993)

The prompt mechanism plays a more dominant role in NO_x production at lower temperatures and accordingly lower equivalence ratios. As the name implies, prompt NO_x is produced almost instantaneously in the flame, partly due to the thermal mechanism and super-equilibrium radicals, and partly due to hydrocarbon and nitrogen synthesis. NO_x produced by this mechanism accounts for roughly 30% of the total production of oxides of nitrogen. The nitrous oxide mechanism is similar to the thermal mechanism and contributes more to the overall production of NO_x at low temperatures and in the post-flame region. Here, nitrous oxide is

produced as an intermediary step before being converted to NO, or being reduced to N_2. (Bowman (1973), Turns (2012))

$$N_2 + O + M \Leftrightarrow N_2O + M$$

$$H + N_2O \Leftrightarrow NO + NH$$

$$O + N_2O \Leftrightarrow NO + NO \quad (1\text{-}4)$$

NO_x production is a kinematically-limited process, with equilibrium levels hovering around 1000ppm for combustion. This means that NO_x may be reduced by having very short residence times in the combustion zone. A number of researchers have investigated this avenue by trying to make the combustion process as quick as possible, which is usually accomplished by having a very short flame with a very small, compact recirculation zone. Tacina et al (2002), Correa (1993), Fletcher et al (1971), and others have also demonstrated that NO_x production is a logarithmic/power function of flame temperature, so another method of reducing NO_x is by reducing the equivalence ratio to reduce the temperature. This can be accomplished by reducing either the local equivalence ratio for a multi-swirler array or the global equivalence ratio for a single or multi-swirler array, and is the reason for the recent shift towards LPP and other lean-burn combustor designs.

There exists a delicate balance between flame stability, NO_x production, and combustion efficiency. A shorter residence time and quicker combustion process means less time for combustion to complete, which decreases combustion efficiency and increases CO production. Tacina illustrates the inverse relationship between NO_x and CO, and concurrently the combustion efficiency, in figure 1-2 below. As it will be discussed further in the next section, a number of solutions already exist to the issue of NO_x production, with some designs already

producing ultra-low emissions of less than $5g_{NOx}/kg_{fuel}$. The issue inherent in these designs however is stability and the lean blow-out limit. (Lefebvre, 2010)

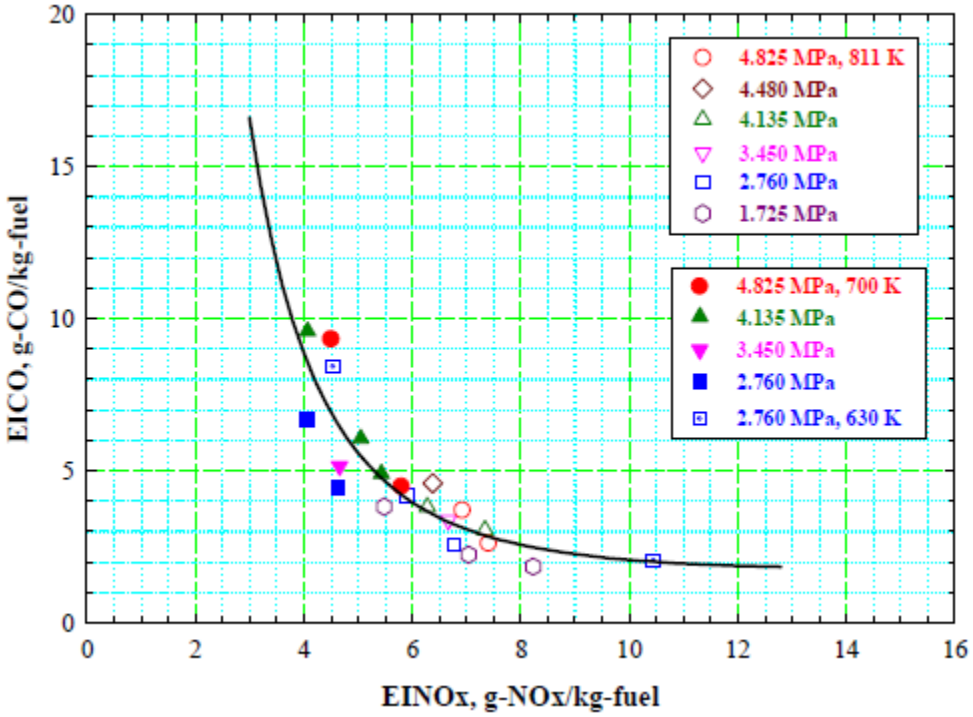

Figure 1-2: Relationship Between NO_x and CO for a 36-point MPIM

1.3 LPP Combustors

While the RQL combustor design relies on a fuel-rich zone for flame-holding and dilution air holes downstream to lean burn prior to the turbine inlet, the LPP combustor is designed to have an overall fuel-lean flame at the burner exit with little to no dilution air compared to the RQL design. It is able to achieve this by vaporizing and mixing the fuel with air prior to the swirler exit, generally by injecting fuel perpendicularly to the air stream through a series of very small holes spaced equally around the swirler cup. This gaseous fuel-air mixture is able to combust at a

lower equivalence ratio than liquid fuel, leading to a shorter flame and a more uniform temperature profile across the combustor exit. (Lefebvre)

The concept of vaporizing fuel prior to combustion in gas turbine engines is not a new one: the first GTC engine designs used to power manned aircraft in 1939 relied on pre-vaporized fuel. However the first experiments to investigate the NO_x emissions from a pre-vaporized combustor were not performed until 1974 by Anderson, where it was found that the LPP design had superior emissions performance compared to RQL combustors. His work continued to 1975 where he was able to obtain an emissions index of NO_x ($EINO_x$) of 0.3 at inlet conditions of 620°F and an equivalence ratio of 0.4, as well as draw a correlation between equivalence ratio and $EINO_x$ which is in accordance with the above-mentioned dependence of NO_x production with temperature. Tacina's work in 1990 detailed the necessary balance between allowing enough time and high enough temperatures for complete combustion while keeping them low enough to limit NO_x production. In 1995, Hayashi investigated the relationship between NO_x production and combustion efficiency and compared the performance and stability of a LDI and LPP configuration. At inlet temperatures of 350°F the LDI nozzle had roughly 5 to 6 times lower NO_x emissions than the LPP for equivalence ratios between 0.6 and 0.8, and at 710°F the NO_x emissions were roughly 4 to 5 times lower for the LDI nozzle. Smith (1992) performed a full-scale engine test on a 5500 horsepower Centaur Type H gas turbine in 1992. With an inlet pressure and temperature of 9.4 atmospheres and 605°F respectively and a combustor outlet temperature of 1850°F, Smith measured NO_x, CO, and UHC emissions of <25ppm, <50ppm, and <50ppm respectively at 15% O_2.

In 1981, Anderson proposed a theoretical upper limit to inlet temperatures of 1900K to keep the flame temperature low enough to keep thermal NO_x production under control; however they

noted that combustion occurred before the fuel and air had a chance to fully mix, and that the fuel spontaneously self-ignited upon introduction to the heated air stream. This highlights one of the inherent dangers with the LPP design; autoignition. Because the fuel is allowed to interact with the preheated air prior to the combustion zone, there exists a risk that the fuel/air mixture will become hot enough to ignite before reaching the combustion zone, possibly damaging parts of the combustor that were not designed to withstand combustion temperatures. Marek et al investigated this issue in 1977 by studying the ignition delay times and flashback velocities for various air pressures and temperatures and fuel/air ratios. The ignition delay was found to decrease with increasing pressure and temperature, and the flashback velocity to increase with equivalence ratio in the range of 0.7 to 1.0. For a simulated engine pressure ratio of 30:1 (438psia) and inlet temperature of 1040°F, the ignition delay was around 5 milliseconds; for typical engine pressure ratios of 40:1 to 50:1 that time would be markedly shorter.

A recent LPP combustor design developed by GE is known as TAPS, or twin-annular premixing swirler, which is currently used in the GEnx engines to power the 787 and a 747 variant aircraft. A report in 2012 details the reduction in NO_x possible with this design, showing a 52% reduction in NO_x levels below the CAEP/6 standards while keeping good combustion efficiency with an overall pressure ratio of around 43:1. A basic sketch of the operating principle for this combustor's swirl cup is shown below in figure 1-3. Twin axial swirlers begin the mixing and atomization process via the shear layer interaction between the two rotating air streams. A pilot flame zone is formed shortly downstream of the swirler exit, which acts to anchor the flame and provide stability during low power conditions. At higher engine power fuel was supplied to cyclone mixer which premixes the air and fuel and generates uniform air/fuel mixer at the

cyclone exit. This air/fuel mixer creates a secondary lean burning zone, which pushes the combustion further away from stoichiometric conditions. (Foust, 2012)

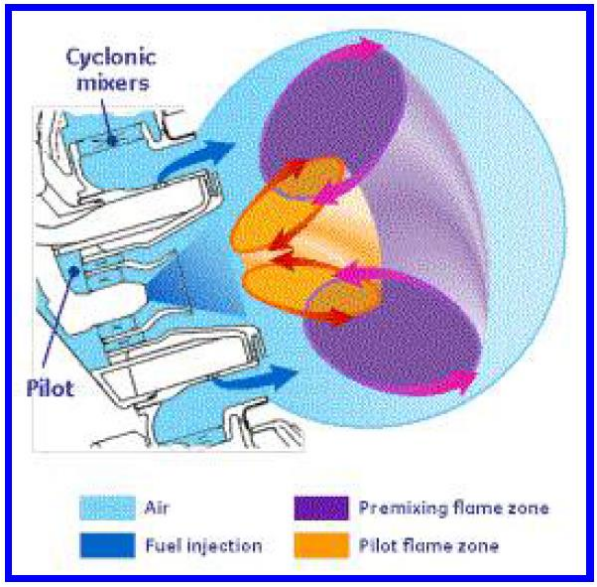

Figure 1-3: Sketch of TAPS Configuration

1.4 LDI Combustors

The concept for the LDI combustor was designed with the intention of combining the good stability and LBO performance of the traditional RQL combustor with the ultra-low NO_x emissions of the LPP design. For the RQL design, fuel is sprayed onto a venturi encompassing a primary air stream, where fuel is allowed to form onto a sheet and then break up into strands and droplets shortly before the combustion zone. In an LDI combustor, however, fuel is injected directly into the shear layer between either two counter-rotating or co-rotating air streams or the flame front. This greatly limits the amount of time the fuel droplets spend in the heated air stream before ignition, serving to reduce the risk of flashback/autoignition while also keeping the primary zone fuel-lean and producing relatively low levels of NO_x. Hayashi performed some of the earliest experiments on direct injection combustors in 1995, conveniently comparing them to

a nearly identical LPP configuration with the same dual-swirler setup. While his design was not robust enough to allow combustion in the "ultra-lean" range with an equivalence ratio of less than 0.6, the NO_x levels for LDI were consistently lower than LPP for the same conditions, with the difference slightly more pronounced for lower inlet temperatures. Additionally, the fact that both test setups were identical with the exception of the addition of the premixing tube for the LPP configuration means that more direct comparisons can be drawn between the two concepts and $EINO_x$ values can be compared more accurately. (Tacina, 1990)

Terasaki et al (1995) demonstrated the ultra-low NO_x potential of a dual-swirler combustor using gaseous fuel, measuring $EINO_x$ values of 0.5 for a dual-swirler arrangement and 1.1 for a single-swirler arrangement. His results show that the dual-swirler arrangement may have lower NO_x emissions than that of a single swirler due to the aerodynamic interactions present in the dual swirler configuration. However since Terasaki's testing used gaseous fuel injected directly into the flame, it can be thought of as a hybrid between LPP and LDI and be treated as a "stepping-stone" to LDI work performed in the early 21^{st} century.

Tacina (1990) gives a thorough overview and comparison of these three designs, covering experiments performed by Anderson, Semerjian, Alkabie, Hussain, and others. Over the next 18 years, Tacina developed a wide range of multi-swirler arrays with lean-direct-injection fuel nozzles, testing 25, 36, 49, and 9-injector concepts. The purpose of having an array constructed in this fashion was to replace the commonly used twin-annular combustor concept with a series of much smaller swirl cups which would each have a much smaller CTRZ and concurrently shorter residence times and reduced NO_x emissions. Additionally, the reduction in the required length as a result of the size reduction of the swirl cups would reduce the overall length of the combustor and subsequently the engine, reducing both weight and cost.

The first experiments were a series of flame-tube tests designed to gauge the feasibility of using a multi-point injection array, testing both a 25-point array and a 36-point array with a variety of inlet pressures and temperatures and two swirler configurations. The swirlers tested had swirl numbers of either 0.5 or 0.8, and were arranged in either a co-rotating or counter-rotating configuration. The pressure drop across the swirler was varied slightly from 3% ($\Delta P/P_3$) to 5% and inlet pressures ranged from 930kPa to 2760kPa, with inlet temperatures ranging from 590K to 810K. The 25-point array had the most diverse testing matrix, with 4 series of experiments conducted for an array consisting of swirlers all having a SN of 0.5 co-rotating, all 0.8 co-rotating, 0.5 and 0.8 combined co-rotating, and 0.5 and 0.8 combined counter-rotating. The 36-point array was tested with SN 0.5 and 0.8 swirlers in combination and a co-rotating swirler configuration.

NO_x emissions were measured for all tests and plotted against the flame temperature on a log plot. All data sets have a linear or nearly-linear trend, indicating that the dependence of NO_x on temperature is exponential, as predicted. At the highest inlet pressure and temperature conditions and a 4% pressure drop, all four configurations of the 25-point array show a very similar behavior, with the configuration with all 0.8 SN swirlers showing slightly lower NO_x for a given flame temperature. The 36-point array is markedly lower however, with $EINO_x$ values down to 2 g/kg for the lowest flame temperatures. The trend continues with testing performed at 1380kPa and 810K for a 4% pressure drop, as well as a 5% pressure drop for 2760kPa and 810K; the 25-point array performs fairly uniformly across configurations while the 36-point is markedly lower.

As expected, when the inlet temperature was reduced from 810K to 700K the NO_x emissions dropped off accordingly across all configurations tested, and continued to drop when the inlet temperature was reduced further to 590K. Overall, the lowest NO_x emissions were generally

achieved with the 36-point array operating at the lowest inlet temperatures, with the inlet pressure and pressure drop playing a smaller role in NO_x formation. To simulate low-power conditions, testing was also performed at relatively mild inlet conditions of 930kPa and 464K to 590K with 12 of the 25 fuel circuits shut off for the 25-point array with the 0.5 and 0.8 swirl number swirler combination in a co-rotating configuration. $EINO_x$ of 0.6 g/kg were achieved with inlet temperatures of 533K, which was neither the highest nor the lowest temperature tested. It is speculated that this is due to the tradeoff between the heat required to improve fuel atomization and subsequently the combustion efficiency, and the low inlet temperatures necessary for ultra-low NO_x emissions. However, a FAR of >0.0397 was required to maintain good combustion efficiency for all fuel-staged testing, which is too fuel-rich for typical gas turbine applications unless a large amount of dilution air were to be introduced further downstream. The results of the testing indicate that a minimum flame temperature of approximately 1500K is necessary to achieve >99.5% combustion efficiency for all test conditions. (Tacina et al, NASA, 2002)

The previous flame-tube testing evolved to a more representative engine test, comprising a 15° sector arc of a mock combustor with the 36-point array shifting to a 4x9 configuration rather than the 6x6 configuration. These 36 swirler/fuel nozzle assemblies were chemically-etched laminate radial-inlet swirler assemblies and dubbed the multi-point integrated module combustor concept (MPIM). Inlet conditions were around 4.8MPa and 866K, meant to mimic a theoretical 55:1 engine pressure ratio, with a 4% pressure drop across the swirler. Two sets of air swirlers were tested again, one having a swirl number of 0.5 and another with a swirl number of 0.8, and tested in various configurations and orientations. A number of parameters were varied to see their effect on NO_x emissions, including the fuel/air ratio, inlet pressure, inlet temperature,

swirler configuration, and swirler orientation. The combustion efficiency was also measured for high-power conditions only and found to hold constant around 99.8-99.9%. The combustion efficiency was then plotted against NO_x and found to vary inversely with NO_x (e.g. lower NO_x yielded higher CO emissions and subsequently efficiency).

When investigating the effect of fuel-air ratio, combustor exit temperature, and reaction zone temperature on NO_x, most test conditions only had 2 data points with two data sets having three tightly-spaced data points. So while no significant conclusions can be drawn from the 2-point data sets, the data sets with three points show a linear trend on their logarithmic scale, keeping consistent with the previously-mentioned exponential dependency of NO_x on temperature. For all testing done at the same pressure, all NO_x emissions were lower for testing done with the lower temperature. The NO_x emissions were found to have a weak but consistent dependence on pressure across a number of inlet temperatures and fuel-air ratios. The lowest $EINO_x$ values reported were 4 g/kg for a number of configurations corresponding to low flame temperatures (i.e. low FAR, and/or low inlet temperature). When compared with the previous flame-tube testing at the same inlet conditions, the MPIM had slightly higher NO_x emissions than all previous flame-tube test configurations, although only two data points could be compared. A summary of the results is shown below in figure 1-4.

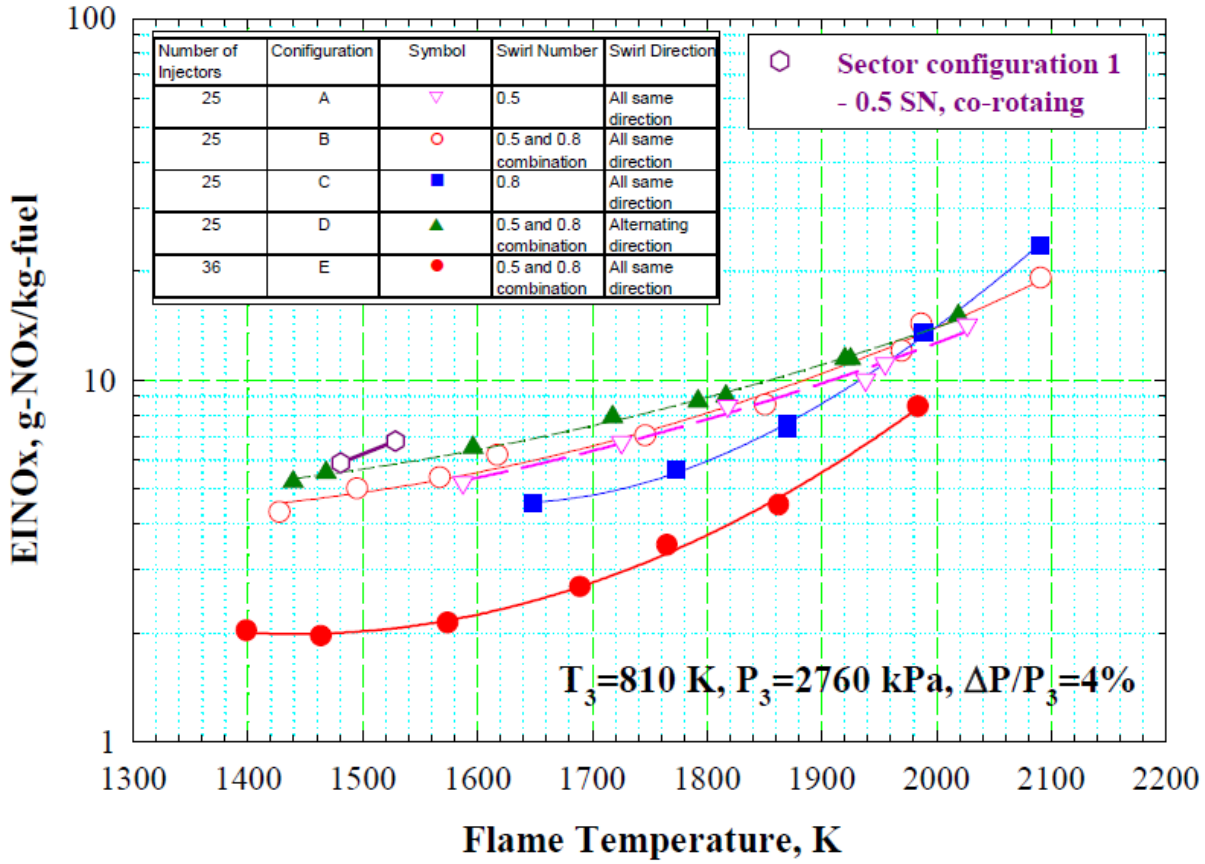

Figure 1-4: Comparison of Swirler Orientations for 25-point MPIM

The effect of fuel-staging was also investigated in the same fashion as the 36-point flame tube testing. The fuel manifold consisted of four fuel lines supplying fuel to the 36 nozzles separated in such a manner that two fuel lines supplied fuel to each of the top and bottom halves, and further divided in a checkerboard fashion. Testing was performed with two fuel circuit configurations; two of the four fuel circuits on, and one of the four fuel circuits on. For the two-circuit configuration, testing was performed at 1.035MPa and 616K, 1.035MPa and 533K, and 0.69MPa and 533K. For the single-circuit, testing was only performed at 0.69MPa and 533K. The results show the same exponential trend for NO_x emissions, however the lowest $EINO_x$ values are around 1.5g/kg, compared with the 0.6g/kg achieved by the flame-tube testing. The author notes that this may be due to the increase in fuel necessary to keep the test parameters

consistent with respect to the global fuel-air ratio; increased local FAR equates to higher local flame temperatures and NO_x generation. A full engine cycle was also simulated based on the various inlet conditions and power settings tested, and a 40% reduction in NO_x was calculated based on the 1996 ICAO standard. (Tacina et al, ASME, 2002)

In 2003 testing evolved yet again from the 36-point array to a 49-point 7x7 array with the expectation that more, smaller swirlers may lead to further NO_x reductions based on the trend from the 25-point array to the 36-point array. The fuel nozzles used for this array are roughly 1/3 the effective area as the previous MPIM testing, and the swirlers' effective area is also reduced by roughly 30% (1361mm^2 to 1030mm^2). Inlet conditions were nearly identical to previous testing and the pressure drops tested remained the same as well. $EINO_x$ values were again higher for higher inlet temperatures and pressures, correlating more heavily on temperature than pressure, and lower for higher pressure drops. The lowest $EINO_x$ values measured were around 1.5g/kg for the lowest inlet temperature and pressure of 615K and 1380kPa respectively at a 4% pressure drop, corresponding to an equivalence ratio of 0.35 and flame temperature of 1500K.

The effect of fuel-staging was much more muted for these experiments, with only two fuel lines supplying fuel in a checkerboard pattern again. At high-power conditions (2760kPa and 810K) the change in $EINO_x$ was around 5% at the most, however the difference was somewhat more pronounced at 1380kPa. Test conditions included two inlet temperatures of 730K and 615K, a 4% pressure drop across both fuel lines, 4% drop across one line, and 3% across one line. The lowest emissions were obtained at the lower inlet temperatures, as expected, and those levels decreased going from 3% drop across fuel line to 4% across one line to the lowest levels at 4% drop across both lines. The reasons for this are the same as the previous experiment; locally fuel-rich combustion zones increased local NO_x production, and reducing the fuel pressure drop

reduces atomization quality, creating larger droplets, longer burning and residence times, and increasing NO_x production.

For equivalence ratios between 0.3 and 0.6, the combustion efficiency remained relatively constant between 99.90% and 99.99%, regardless of inlet pressure, temperature, or pressure drop. However when comparing the effect of fuel staging, the efficiency drops to ~94% for the low-power conditions (1380kPa and 615K) with both fuel lines at 4% and an equivalence ratio of 0.35. With the exception of this point, all other data indicates combustion efficiencies between 99.90% and 99.99% again. The results of this series of testing were compared with the 25-point MPIM flame tube tests and the 36-point MPIM sector tests. Overall, the 49-point array showed average $EINO_x$ results across the range of equivalence ratios tests, performing better than the 25-point co-swirling combination and worse than the 25-point co-swirling 0.8SN configuration.

The last configuration tested by Tacina et al was a series of flametube tests on a 3x3 swirler array in 2008. These swirler assemblies were much larger than the previous 36-point and 49-point array assemblies, using axial swirlers again but with the addition of a converging-diverging venturi. The swirl number for these assemblies was calculated as 1.02 based on the equation proposed by Beer and Chigier in their book, “Combustion Aerodynamics”. Inlet conditions were somewhat similar to previous testing, with inlet pressures ranging from 2800kPa to 5500kPa and temperatures ranging from 755K to 865K. The pressure drop was increased from 4% to 7% however and held constant for the duration of testing, with the exception for one series of tests used for comparison with the previous multi-point array tests. The lowest $EINO_x$ measured were around 5g/kg at an inlet pressure/temperature of 3100kPa and 755K respectively, an equivalence ratio of 0.35, and a 7% pressure drop. The worst $EINO_x$ were around 20g/kg at the highest pressure, temperature, and equivalence ratio tested (5500kPa, 865K, and 0.5 respectively).

The data was then compared with the previous 25-point, 36-point, and 49-point test configurations at the same inlet conditions of 4% pressure drop, 2750kPa inlet pressure, 810K inlet temperature, and FAR spanning 0.017 to 0.04. The 9-point array had the narrowest operability limit, with a FAR from 0.024 to 0.038 while the 36-point was able to achieve good combustion and low NO_x down to a FAR of 0.017. Additionally, the $EINO_x$ was higher for all test conditions for the 9-point array than any other configuration tested. The general trend produced by this comparison is that smaller swirler assemblies may be better for NO_x emissions to an extent, and the likely reason for this is that the flame size/shape is scaled accordingly with the size of the swirler. A shorter recirculation zone means a shorter residence time which correlates to lower NO_x emissions, since NO_x is directly related to both temperature and residence time. A comparison of Tacina's LDI combustor concepts up to this point is shown below in figure 1-5, showing how the measured NO_x emissions change with the fuel-air ratio for the 9, 25, 36, and 49-point combustor concepts.

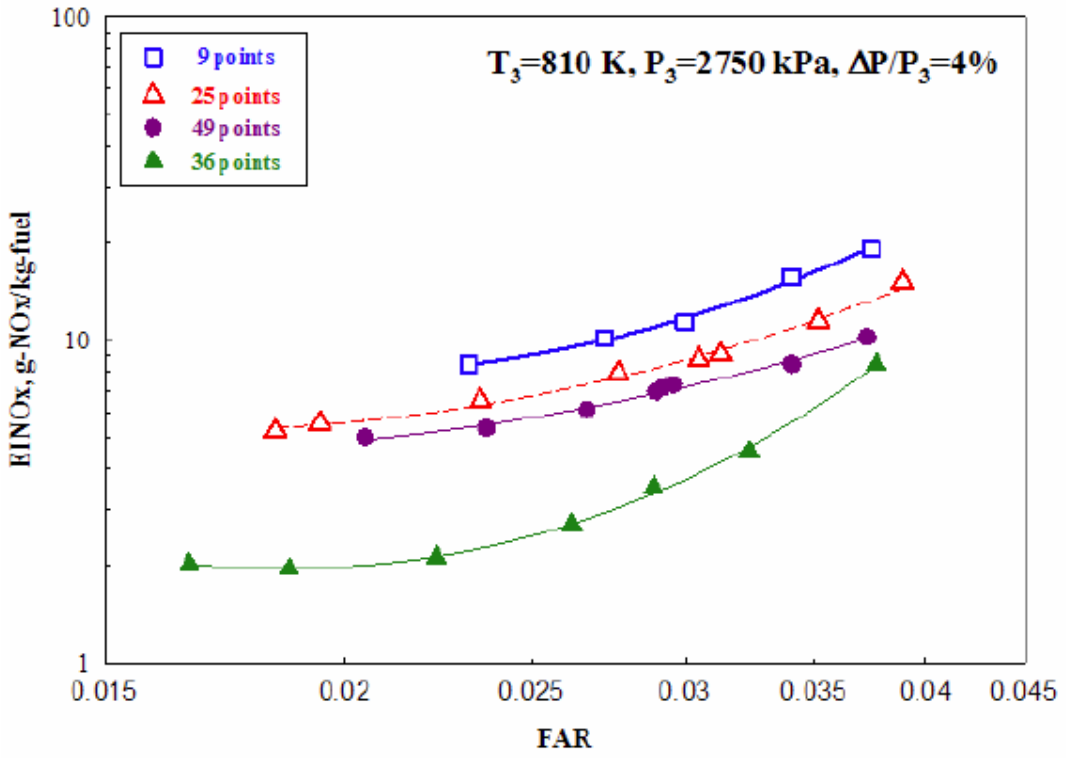

Figure 1-5: Comparison of 9, 25, 36, and 49-point LDI Arrays

The myriad testing done by Tacina et al investigated a variety of inlet parameters, pressure drops, and the effects of fuel-staging. However only very limited testing has been done on how the configuration and orientation of swirlers and their respective swirl strengths can alter the aerodynamics and combustion dynamics. Additionally, these tests were conducted with very small, basic swirlers with a single inlet and relatively "simple" aerodynamics. Most typical gas turbine combustor swirlers are at least dual-inlet, with some combining axial and radial swirl inlets, mixing and matching counter and co-rotating air streams with axial/axial or radial/radial or axial/radial configurations. The aerodynamics of a multiple-swirler array are extremely complicated, especially when different types of swirlers are used and possibly offset/recessed to enhance potential combustion characteristics. For this reason it is extremely prudent to investigate the isothermal aerodynamics of a swirler array to gain crucial insight to the

interactions of various air streams and swirling flows, and extrapolate how they will affect combustion dynamics and what roles those interactions will play on emissions and NO_x production. (Marek et al (1997, 2005), Smith (1992), Tacina (2008))

1.5 Isothermal Aerodynamics

The aerodynamics of a single swirler orientation have been studied very thoroughly for a number of years now, however the velocity profile and aerodynamic characteristics of a single swirler cannot be directly applied to multiple swirlers in an array. Kao (2014), Fu (2007), Cai (2001, 2006), and Endicott (2014) have all explored the effect of swirler-swirler interaction dynamics and shown considerable evidence that the aerodynamics of a single swirler differs considerable when placed in an array of swirlers, even those with identical arrangements. Most aerodynamics performed on swirlers or hardware used in gas turbine engines are done on a single swirler in simulated confinement. While this greatly reduces the complexity of the experiments by reducing the cost of producing hardware, the size of the experimental setup and flow rates required, and the time needed for testing by reducing the measurement domain while keeping the resolution necessary for detailed analysis of the flow-field, it does not adequately capture the whole picture of what is happing in a combustor sector.

Much of this work is predicated on Cai's investigation into the swirler aerodynamics of an axial swirler array. This early investigation into the design of an LDI assembly looks at the interaction and velocity profile of a 3x3 array of axial swirlers with eight discrete jets per swirler. Two configurations are tested; the first arrangement is all nine swirlers in a co-rotating sense, and the second configuration alternates the orientation of neighboring swirlers such that swirlers

immediately on each side are counter-rotating and swirlers on a diagonal are co-rotating. Each swirler is 0.7" in diameter and the swirler separation is 1". Testing was performed at a 4% pressure drop. His results showed that the velocity profile of the co-rotating array exhibited an overall counter-clockwise swirl sense as the flow progressed downstream, with generally smoother velocity contours and the axial jets maintaining their relative strength. For the counter-rotating array, each swirler seemed unaffected by the neighboring swirlers and did not exhibit the overall swirling motion that the co-rotating array did. Additionally the turbulent kinetic energy (TKE) profiles showed higher overall turbulence for the counter-rotating array, which may indicate more thorough fuel-air mixing when applied to a combustion environment.

Fu expanded upon Cai's work, designing a helical-vaned axial swirler with a converging-diverging venture that more closely resembles swirler designs employed in current gas turbine combustors. Like Cai, he looked at the aerodynamics of a swirler array in both counter-rotating and co-rotating configurations for swirlers with a calculated swirl number of 1.0, and also compared the aerodynamics of a single swirler with simulated confinement mimicking the swirler spacing in the swirler array to that of the array itself. Additionally he investigated the effect of recessing the center swirler below the surrounding eight swirlers, comparing the velocity contours and stress contours for both counter-rotating and co-rotating configurations again.

His results indicate that there is a significant different between a single swirler's aerodynamics under simulated confinement and that of a multi-swirler array. While the single swirler produces a strong, compact CTRZ, none of the swirlers in the array have any sort of central recirculation zone, only corner recirculation zones in various locations. The co-swirling configuration seems to have a more uniform axial velocity profile at z/D=0.36 downstream of the

swirler exits, as well as a weak bulk swirling motion that is lacking in the counter-swirling configuration. The very uniform profile at less than one third of an inch downstream is a good indicator that the fuel and air will mix very thoroughly and very quickly, which is an indirect goal of the LDI concept. Quicker mixing means a reduced chance for local hot-spots to develop which would increase NO_x production, as well as a more uniform temperature profile to the turbine inlet.

Most interesting were the results obtained when the center swirler was recessed 1/4D below the other eight swirlers. A global CTRZ developed in the center of the array for both counter-rotating and co-rotating configurations which extended downstream approximately 2/3". At 1.3" downstream a global swirl orientation was observed for the co-swirling configuration whose strength was greater than that of the co-swirling configuration with no swirlers recessed. These results indicate that recessing the center swirler may allow a CTRZ to develop in a 3x3 array where none would form with all swirlers at the same axial level. This may serve to improve the stability and operability of an LDI array as the addition of a CTRZ would allow hot combustion products to recirculate and enhance flame-anchoring capabilities at fuel-lean conditions or in a case where one or several swirl cups extinguish due to aerothermal or aeroacoustic instabilities.

Kao (2013, 2014) also performed a significant amount of research on the effects of various parameters on the aerodynamics of a multi-swirler array, including confinement, swirler-swirler spacing, wall spacing, recession/protrusion of various swirlers, and the number of swirlers in an array. While his experiments were conducted on a one-dimensional array rather than a two-dimensional array, they were conducted with a counter-rotating radial-radial swirler assembly and thus may be more applicable to the results presented in this thesis which use very

similar hardware. The majority of Kao's results indicated an alternating pattern of small/strong with large/weak central recirculation zones for the five-swirler array, and the size/strength of the center swirler was dictated primarily by the inter-swirler spacing.

When the distance between swirler centers was equal to or less than twice the swirler exit diameter (2D), the central swirler was larger. However when the spacing was increased slightly to 2.5D, the flow structure completely reversed, with the center swirler now exhibiting a small, strong CTRZ. Since one of the goals of the LDI concept is to have a number of swirlers as close together as possible, the swirler spacing becomes a very important factor that may be used to predict how the swirlers will interact when placed in an array. A similar trend was observed when investigating the effects of axial offset of the center swirler. With a baseline case of a large, weak CTRZ for the center swirler, by offsetting the center swirler just 0.125D axially downstream the flow structure reversed once again, with the center swirler becoming small and strong. While these results may not directly apply to a 3x3 swirler array, these results along with those of Fu clearly show that very small changes in some key parameters can have a significant impact on the overall aerodynamic structure of a two-dimensional swirler array.

The results of the testing performed in this thesis are predicated most heavily on the work done by Endicott in 2014. His experiments share some similarities to those performed by Tacina in 2002, which investigated the use of swirlers placed in an array with varying swirl strengths and swirl orientations. While those tests were performed with a single swirl orientation per swirler assembly with swirl numbers ranging from 0.5 to 0.8, Endicott used a counter-rotating radial-radial swirler assembly which mimics those currently being used in industry-level gas turbine engines, albeit reduced in size in accordance with the LDI design which uses very small or scaled-down swirler designs. He used a particle-image-velocimetry (PIV) system to measure

the velocity profile with 37 cross-sections for each of three swirler configurations comprised of a mixture of high-swirl and low-swirl swirlers. His results reiterated the fact that a single swirler's aerodynamics cannot be compared to or extrapolated towards a multi-swirler array as the swirlers' interactions alter the flow field considerably.

A baseline case was first examined which was comprised of all low-strength swirlers, with a measured swirl number of roughly 0.6, and used to compare against two other configurations. The second configuration consisted of a single high-swirl swirler in the center of the 3x3 array surrounded by low-swirl swirlers, and the third configuration consisted of a row of three high-swirl swirlers with two rows of low-swirl swirlers on either side. The swirlers in the baseline case all showed similar velocity profiles while the second and third cases with the high-swirl swirlers demonstrated a significant increase in the size of the central recirculation zone. As previously stated this is potentially very beneficial to the stability and operability limits of the array as a larger CTRZ means lower negative axial velocity and better opportunity for flame propagation and flame-anchoring. Additionally the large CTRZ pushes the axial jets radially outwards, allowing them to interact with the other swirlers closer to the swirler exit which would ideally further enhance stability, lean-blowout limits, and flame-anchoring properties.

It should be noted that while isothermal aerodynamic measurements are beneficial to gain insight into the flow properties and how they change with the addition of multiple swirlers in an array configuration, the aerodynamics do change from isothermal measurements to combustion measurements. This has been demonstrated both by Archer et al (2003) and Fu, who measured and compared the non-reacting and reacting flow fields for a single swirler to illustrate the similarities and differences between both profiles. Archer's measurements are shown below in figure 1-6, and Fu's are shown more clearly in figure 1-7. The most notable change is the

significant disparity between the positive and negative axial velocity. The overall axial velocity increases for combustion testing due to the increase in temperature, decrease in density, and subsequent increase in average velocity necessary in keeping with the conservation of mass. However both the positive axial velocities and negative axial velocities have increased in magnitude, indicating a more intense shear layer between the two air streams and a smaller, stronger recirculation zone that starts further downstream from the swirler exit.

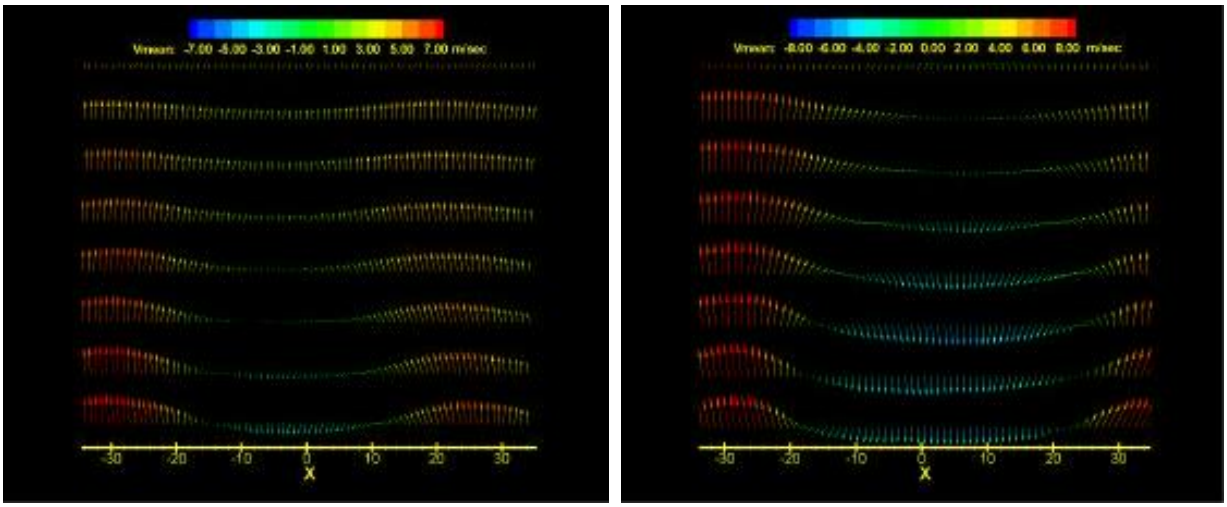

Figure 1-6: Velocity Profiles for Axial Swirler, a) Isothermal, b) Reacting

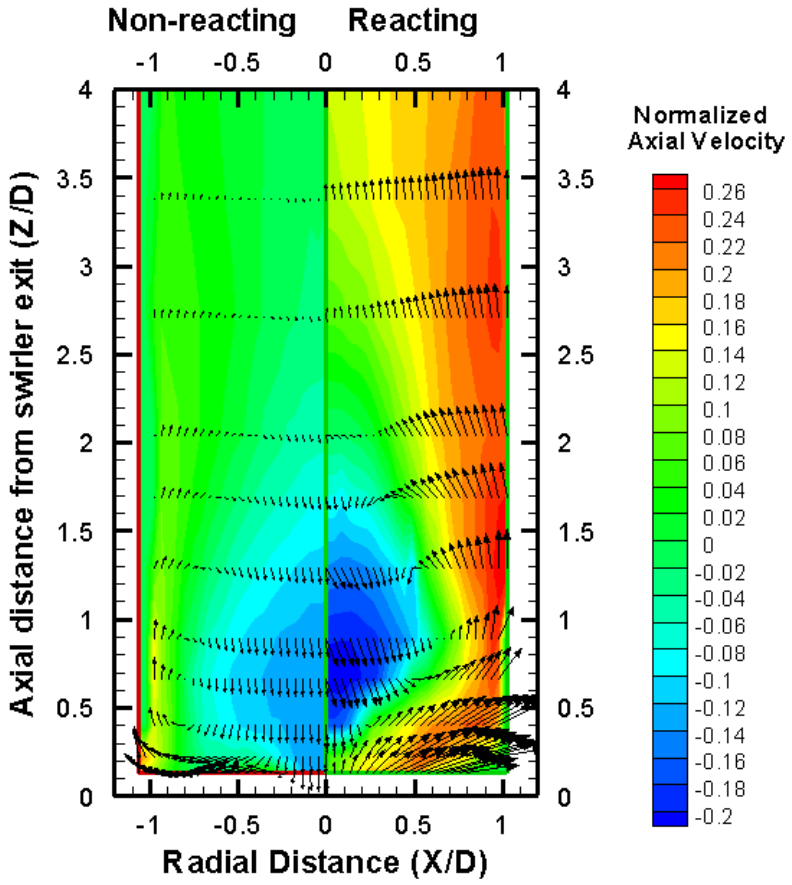

Figure 1-7: Comparison of Reacting/Non-reacting Axial Velocity Profiles for Axial Swirler

1.6 Goals and Expectations

The goal of this research is two-fold: first, to demonstrate the feasibility of using an array of varying swirl-strength swirlers in an LDI configuration by validating the ignition and LBO potential; and secondly to draw comparisons and conclusions with the PIV measurements performed on the isothermal aerodynamics for the same configurations previously tested in Endicott's research. While the velocity profiles may not be compared quantitatively, the effects of using varying swirl-strength swirlers in an array can be observed and evaluated based on images of the combustion at various conditions, and the stability and utility gauged based on ignition and lean-blowout data. The LDI design presented is meant to replace a single combustor

cup or a twin-annular design, and so the direct goal of this research is to achieve stable, lean combustion with all fuel nozzles, investigate the operability limits with various fuel circuits at various equivalence ratios, and observe how the previously-studied isothermal aerodynamics correlate to combustion dynamics for the three swirler configurations.

Chapter 2 : Hardware Design

As previously stated, the purpose of this testing is to gauge the feasibility of using an array of counter-rotating radial-radial swirlers with varying swirl strengths in a lean-direct-injection combustor configuration. The hardware and test apparatuses were designed with the goal of high-pressure combustion testing, but also needed to have the flexibility to change a number of testing parameters without significant modifications to the hardware, while also having the capability for atmospheric testing on a different test rig than the high-pressure chamber. The two swirler designs are dubbed UCRI-1 and UCRI-2 and illustrated below in figure 2-1. UCRI-1 is considered a "high-swirl" swirler, having a calculated swirl number of approximately 1.0, and UCRI-2 is a "low-swirl" swirler, with a swirl number of approximately 0.6. The aerodynamic axial velocity profiles for UCRI-1 and UCRI-2 are shown below in figures 2-2 and 2-3 respectively. Both swirlers have identical vane angles and orientations but different vane inlet and exit areas. The primary vane passage is shown in green and the secondary is shown in purple. The exit diameters of both swirlers are again the same at one inch, however the flare angles vary between designs. UCRI-2 has a flare angle of 36° with respect to the vertical, and UCRI-2 has a flare angle of 54°. Both swirlers have radial inlets for the primary and secondary air passages and a counter-rotating orientation between those passages, with the

primary passage rotating counter-clockwise when viewed looking upstream and the secondary rotating clockwise.

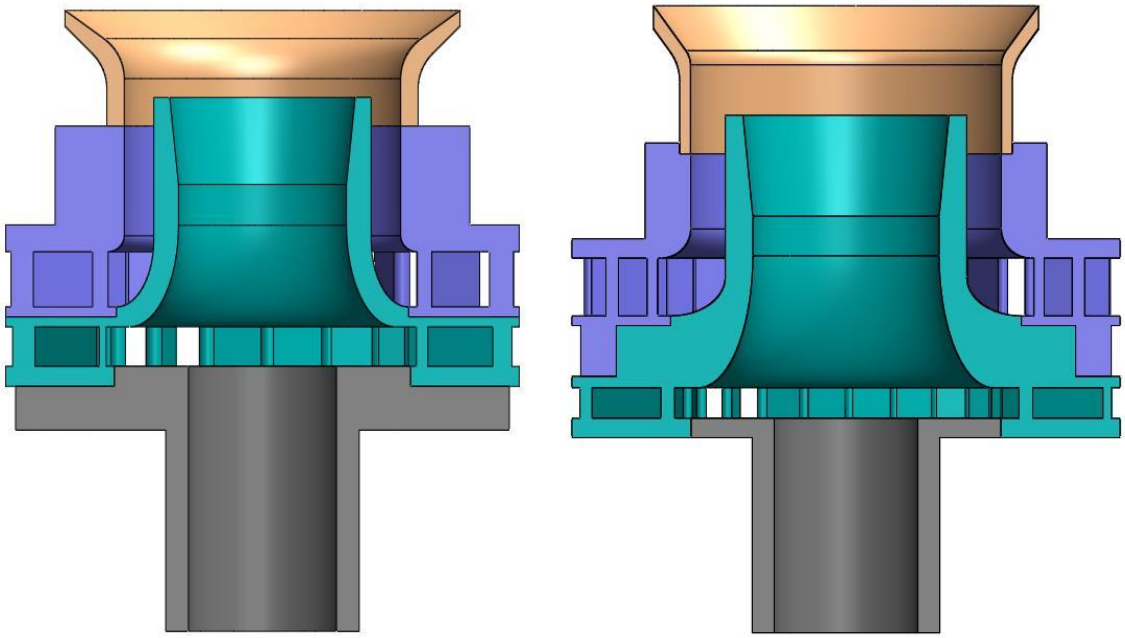

Figure 2-1: Cross-Sectional View of CAD Model of UCRI-1 (a) and UCRI-2 (b)

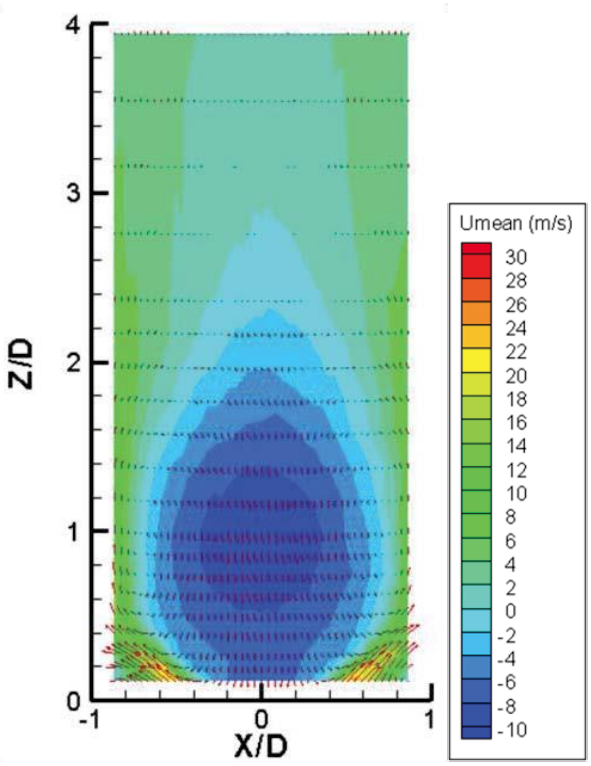

Figure 2-2: UCRI-1 Axial Velocity Contours

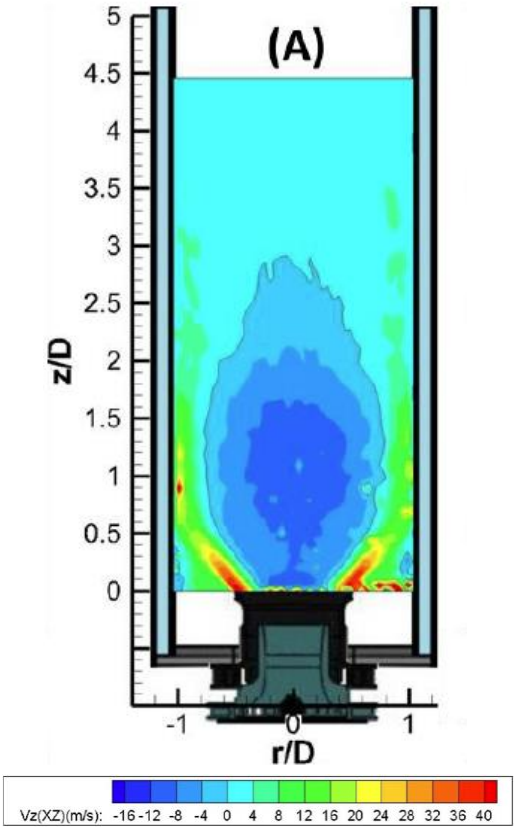

Figure 2-3: UCRI-2 Axial Velocity Contours

Kao, Brennan, and Endicott have all performed aerodynamics analyses on UCRI-1 and/or UCRI-2. Some of their results are shown above in figures 2-2 and 2-3. UCRI-1 clearly has a much wider CTRZ and lower average axial velocity, while UCRI-2 has a narrower CTRZ with stronger axial velocity jets issuing from the flare exit. For this reason, swirler designs typically used in land-based power-generating gas turbine engines employ a lower swirl number swirler. Exhibiting a higher average axial velocity and a smaller recirculation zone, this design tends to have lower NOx emissions at higher engine power conditions. However, there is a higher risk of flame extinction. The higher-strength swirler exhibits better flame anchoring properties due to its wider CTRZ: it draws in hotter combustion gases for recirculation due to its reduced length and has better performance across all power conditions which is more suitable for propulsion-based

gas turbine engines. Both swirlers were designed to have similar inlet areas and were calculated to be around 0.13 in^2 each. Equation 2-1 below was used to calculate the effective area, where the mass flow rate and density were measured with a flow meter and the pressure drop was measured with a differential pressure transducer. A total of ten UCRI-2 swirlers and four UCRI-1 swirlers were manufactured via DMLS 3D printing, however due to manufacturing tolerances there were slight discrepancies between the effective areas for all swirlers. The results are summarized below in tables 2-2 and 2-3.

$$\dot{m} = A_{eff}\sqrt{2\rho\Delta P} \qquad (2\text{-}1)$$

UCRI-1	A_{eff} (in^2)	% Var.	Measured $\dot{m}$ at 4% dp, 60°F (lb_m/hr)	Projected $\dot{m}$ at 4% dp, 400°F (lb_m/hr)
1	0.1286	0.6	65.91	51.25
2	0.1272	-0.5	65.20	50.70
3	0.1292	1.0	66.22	51.49
4	0.1265	-1.1	64.81	50.39

Table 2-1: Measured and Projected Mass Flow Rates for UCRI-1 Swirlers

UCRI-2	A_{eff} (in^2)	% Var.	Measured $\dot{m}$ at 4% dp, 60°F (lb_m/hr)	Projected $\dot{m}$ at 4% dp, 400°F (lb_m/hr)
1	0.1517	6.0	77.74	60.45
2	0.1492	4.4	76.43	59.43
3	0.1371	-4.0	70.27	54.64
4	0.1325	-7.7	67.88	52.78
5	0.1349	-5.7	69.12	53.75
6	0.1385	-3.0	70.99	55.20
7	0.1466	2.7	75.10	58.39
8	0.1393	-2.4	71.39	55.51
9	0.1476	3.4	75.64	58.81
10	0.1490	4.2	76.33	59.35

Table 2-2: Measured and Projected Mass Flow Rates for UCRI-2 Swirlers

The UCRI-1 swirlers have an average measured effective area of 1.3 square inches and vary by roughly 1% from the average at most. This puts their expected flow rate at 4% pressure drop and 400°F at roughly 51 lb/hr. The average effective area of the UCRI-2 swirlers is 0.143 square inches and varies considerably more, roughly ±6%. Each fuel nozzle was also flow checked to determine its flow number, which ranged between 0.84 and 0.91 with jet-A fuel for all nozzles. Thus for each configuration the swirlers with larger effective areas were generally placed around fuel nozzles with larger flow numbers, or swirlers with similar effective areas were paired with fuel nozzles on the same fuel circuit to encourage flame uniformity via similar equivalence ratios for each swirler.

The three configurations tested are illustrated in figures 2-4, 2-5, and 2-6, with the number 1 representing UCRI-1 and the number 2 representing UCRI-2, and are identical to those tested by Endicott (2014). The baseline case consists of all low-swirl swirlers, the second case contains a single high-swirl swirler in the center, and the third case is a row of high-swirl swirlers surrounded by two rows of low-swirl swirlers. The rationale behind the choice of these configurations is that a single high-swirl swirler in the center of the array, or a row of high-swirlers, may prove to have favorable effects on the stability and operability limits by altering the combustion dynamics in a similar manner to that demonstrated by the aerodynamics study performed by Endicott. The average effective area for UCRI-1 is 0.128 in^2 and for UCRI-2 it is 0.143 in^2.

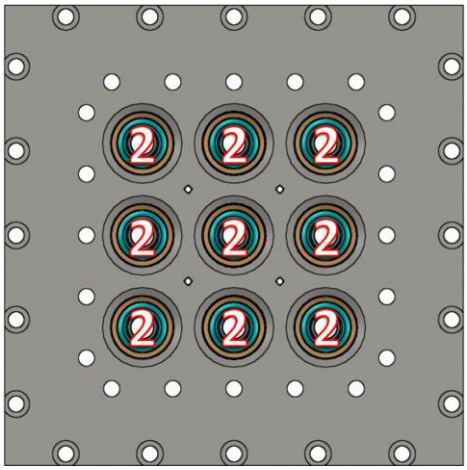

Figure 2-4: Configuration 1 Swirler Arrangement:

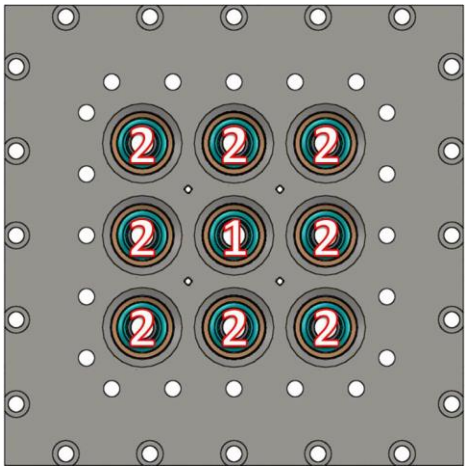

Figure 2-5: Configuration 2 Swirler Arrangement

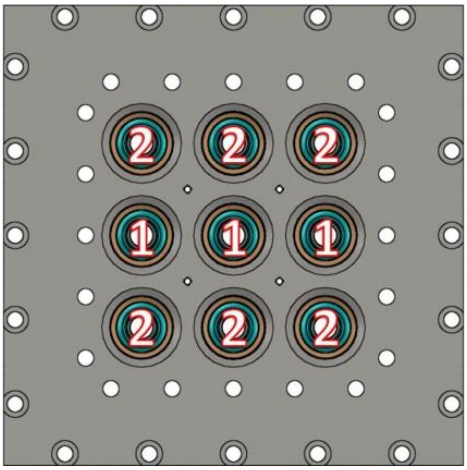

Figure 2-6: Configuration 3 Swirler Arrangement

A summary of the expected and measured effective areas for all three configurations is shown below in table 2-4. The expected mass flow rates were calculated by adding the effective areas of nine swirlers which were expected to be used for testing. Predictably, the expected mass flow rate decreases as the number of UCRI-1 swirlers for each configuration increases, which have a smaller average effective area. However the opposite trend is observed for the measured mass flow rates: the flow rates decrease as number of UCRI-1 swirlers increases. Note that the measured values were averaged from readings taken over 10-15 seconds while the pressure drop and temperature were held constant. Due to the extreme proximity of the swirlers to one another illustrated in figure 2-7 (minimum distance 0.0625") there appear to be some boundary layer effects and aerodynamic interactions which serve to decrease the discharge coefficient and reduce the effective area. This effect is more pronounced for configurations 1 and 2, which have more UCRI-2 swirlers with a larger diameter than UCRI-1 on the upstream side of the faceplate, than configuration 3.

	Expected $\dot{m}$ (lb/hr)	Actual $\dot{m}$ (lb/hr)	Discrepancy	Expected A_{Eff} (in^2)	Actual A_{Eff} (in^2)	Discrepancy
Config. 1	510	418	22.0%	1.280	1.133	20.3%
Config. 2	508	424	19.6%	1.274	1.172	17.9%
Config. 3	492	448	10.0%	1.235	1.159	8.4%

Table 2-3: Measured vs. Expected Effective Areas and Mass Flow Rates

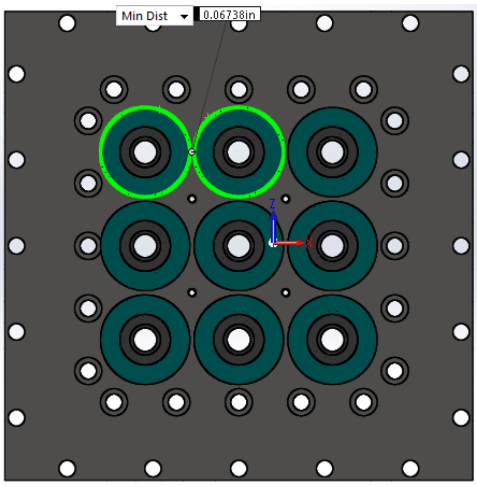

Figure 2-7: Upstream Side of Faceplate showing Swirler Proximity

Fuel was supplied to the nine swirlers via nine fuel nozzles which were connected to three fuel circuits, illustrated below in figure 2-8, with the numbers 1, 2, and 3 representing fuel circuit 1, fuel circuit 2, and fuel circuit 3 respectively. The circuits were designed to allow for fuel staging and separate fuel flow rate manipulation. Circuits 2 and 3 would be selectively turned on or off depending on the simulated power/throttle conditions, as would be the case in a full-scale LDI combustor. The flow rates may also be manipulated selectively to determine what effect, if any, varying fuel flow rates to the different fuel circuits has on stability and operability limits. For example, circuit 1 would likely always be activated and circuits 2 and 3 would be varied to observe the flame shape, color, length, and LBO fuel flow rate to determine and gauge stability; or the fuel to circuit 1 may be increased by 10% and the flow rate to circuits 2 and 3 reduced by 10% each to lower global equivalence ratio while retaining stability with a fuel-rich center swirler. The use of fuel-staging also eliminates the need for two fuel circuits per nozzle for a standard dual-orifice nozzle, as different circuits may simply be activated and adjusted accordingly rather than a new circuit for each nozzle.

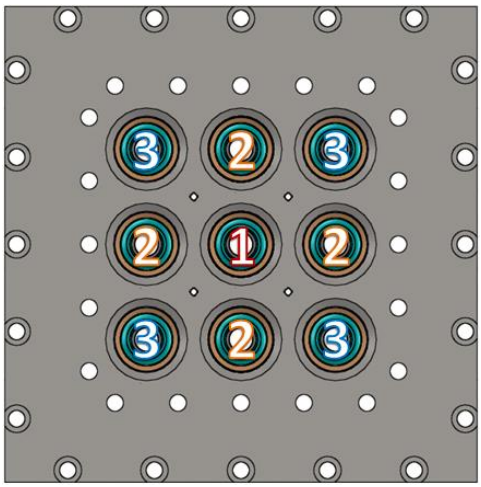

Figure 2-8: Schematic of Fuel Circuits/Nozzles

There were three simulated flight conditions tested: idle, cruise, and sea-level take-off (SLTO), which correspond to circuit 1, circuits 1 and 2, and circuits 1, 2, and 3 being activated. The air pressure and temperature selected for these tests are significantly lower than the steady-state engine operating conditions for all power conditions, and flame anchoring properties in the engine should have a lower minimum air-to-fuel ratio compared to the atmospheric testing performed for this research. The idle conditions (circuit 1 only) in the current test was designed to gauge the operability limits (idle and ignition) of this LDI combustor design, which should be very fuel-lean (i.e. low fuel-to-air ratio) and have stable combustion. The simulated cruise (circuits 1 and 2) and take-off conditions (circuits 1, 2, and 3) were selected primarily to observe the uniformity of energy release which is related of NO_x generation. Actual engine cruise and high power conditions have significantly higher air pressure and temperatures and there will be no issues with flame-anchoring.

All atmospheric testing was performed using fuel nozzles with a flow number of approximately 0.9 to give a representative idea of combustion dynamics, flame characteristics, and operability range. The spray angle for each nozzle was observed to be around 72°. This

information was used to determine the approximate insertion depths used for testing, where insertion depth is the axial location of the fuel nozzle tip with respect to the swirler flare exit. The two insertion depths are shown in figures 2-9, 2-10, 2-11, and 2-12, which include a representative illustration of the approximate spray angle with respect to the swirler venturi and the primary/secondary air streams for both UCRI-1 and UCRI-2. For UCRI-1 the spray impinges on the venturi very briefly, only encountering $1/8^{th}$ of an inch of the venturi when no axial momentum is considered, and likely not even contacting the venturi when the axial momentum of the primary air flow is accounted for. For UCRI-2 only the outermost regions of the spray contact the venturi when axial momentum is not considered, and only for ~$1/16^{th}$ of an inch. When axial momentum is accounted for the spray is certainly past the venturi and meets the classical definition of "direct injection". Note that while the deeper insertion depth may not be classically categorized as "direct" injection, because the spray spends so little time on the venturi and the nozzle is inserted much further downstream than an RQL combustor, it still has the reduced risk of flashback that the LDI concept benefits from while exhibiting characteristics of a low-NO_x swirler configuration. The shallow insertion depth injects fuel directly into the shear layer between the two air streams and the primary combustion zone. This is where the fuel is injected for a typical direct-injection design: here the droplet breakup is done entirely by the shear-layer interaction of the two swirling air streams with no pre-filming via the venturi.

Ignition testing was also performed with a higher flow number fuel nozzle to mimic real-world ignition conditions. This fuel nozzle will be the same one used for future high-pressure combustion test and has been sized appropriately to accommodate both minimum and maximum expected flow rates. The flow number was measured to be approximately 3.0. This nozzle was also characterized to measure the spray angle at various fuel flow rates and determine the

appropriate pressure drop required for sufficient fuel cone shape. At 8 lb/hr, the pressure was enough to open the fuel spray past the classical “tulip-bulb” shape, but not enough to produce a fully-opened spray cone and allow complete fuel droplet atomization. At 12 lb/hr, the spray produced the classic cone shape with a spray angle of approximately 75°. The spray was found to be fully open above 15 lb/hr, which corresponds to a pressure drop of around 25psig, and the spray angle did not change significantly. The significance of these fuel flow rates will be expanded upon later, but a brief explanation is that these flow rates are around those expected for ignition with this larger fuel nozzle. The insertion depth was kept constant for both sets of fuel nozzles as both the spray angle and expected impingement point of the fuel spray on the venturi remained relatively constant for both fuel nozzles near operating conditions. At the lower fuel flow rates expected for ignition, the fuel spray is not fully developed and thus will have poorer performance compared to an appropriately-sized nozzle placed at a deeper insertion depth: the angle will be shallower and the droplets larger, with ignition occurring at higher flow rates.

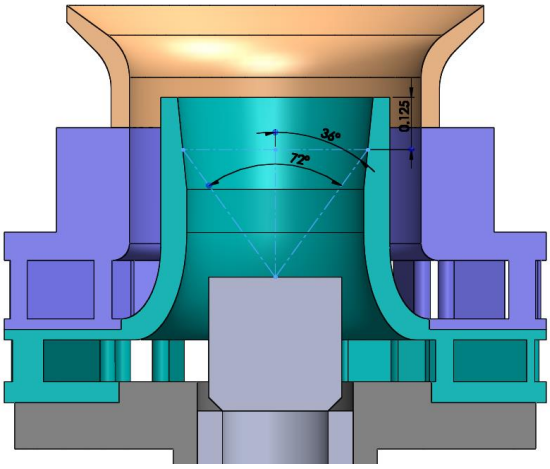

Figure 2-9: Simulated Fuel Spray Cone for UCRI-1, Deep Insertion Depth

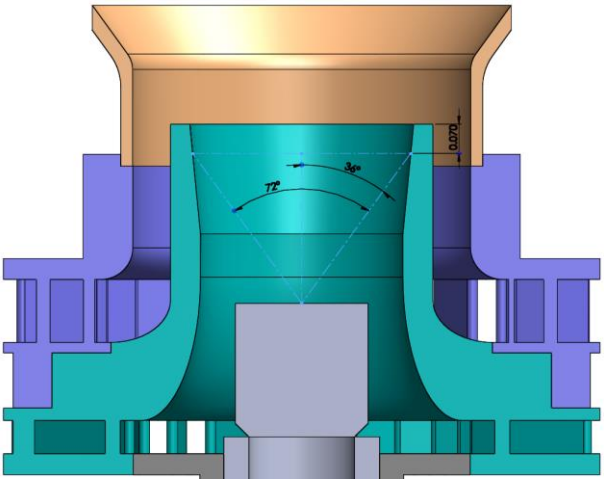

Figure 2-10: Simulated Fuel Spray Cone for UCRI-2, Deep Insertion Depth

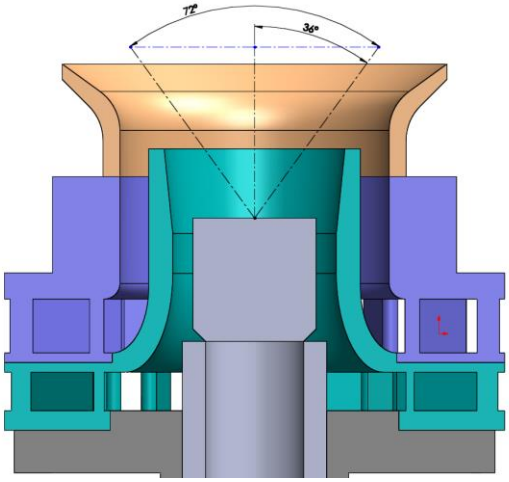

Figure 2-11: Simulated Fuel Spray Cone for UCRI-1, Shallow Insertion Depth

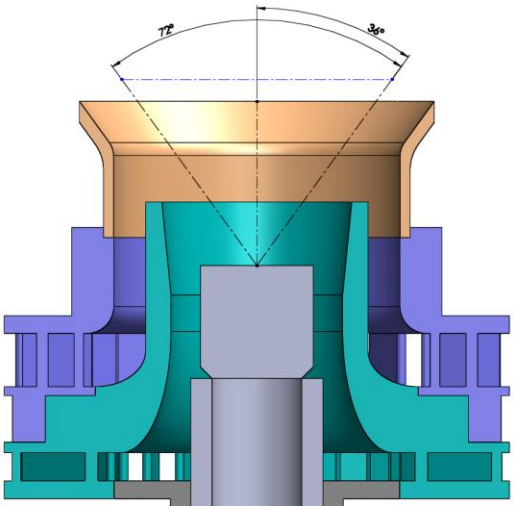

Figure 2-12: Simulated Fuel Spray Cone for UCRI-2, Shallow Insertion Depth

Due to the very small flow number claimed by the manufacturer of the fuel nozzles, the flow number for each nozzle was measured individually to ensure that nozzles connected to the same circuit would receive approximately the same amount of fuel for a given circuit's flow rate. Here the flow number is represented by the following equation, where $\dot{m}$ is represented in lb/hr and ΔP is represented in psig. The calculated result may be roughly considered as a representation of the effective area of the nozzle, where density is not considered. The results are meant to be qualitative rather than quantitative, illustrating the respective differences between similar fuel nozzles, and are shown below in figure 2-13.

Referencing the results of tables 2-2 and 2-3, swirlers were selected for each particular fuel nozzles based on their effective areas and the requirements of each configuration (i.e. swirlers with larger effective areas paired with fuel nozzles with larger flow numbers). The arrangements are shown below in figures 2-14, 2-15, and 2-16.

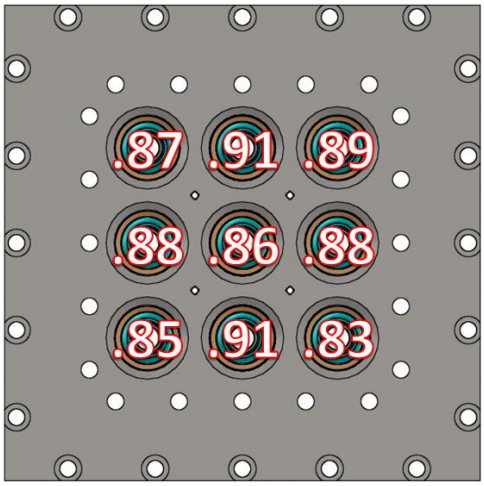

Figure 2-13: Steady-State Burning Fuel Nozzle Orientation

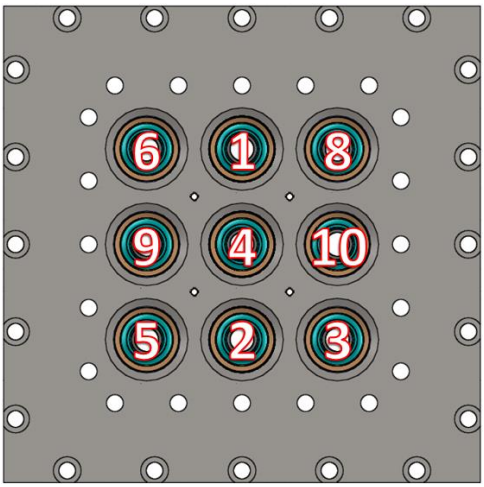

Figure 2-14: Configuration 1 Swirler Orientation

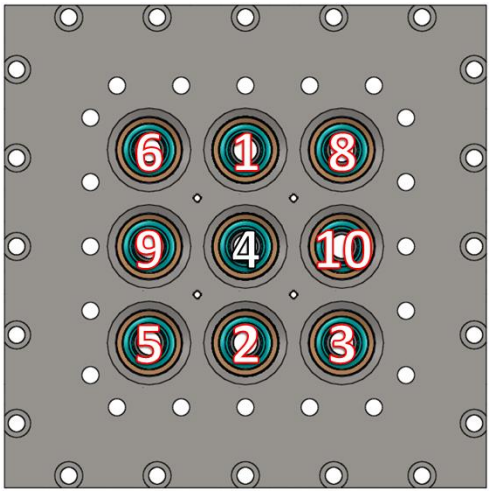

Figure 2-15: Configuration 2 Swirler Orientation (UCRI-2 in red, UCRI-1 in black)

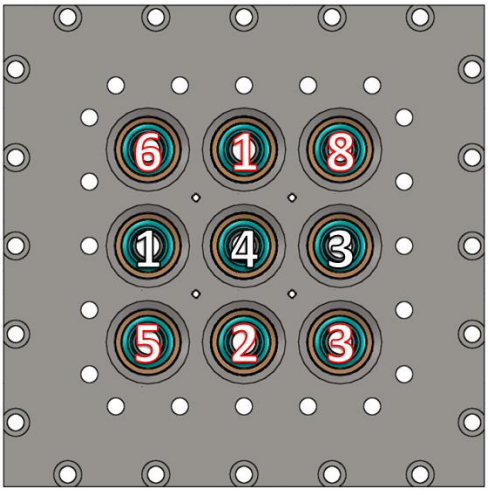

Figure 2-16: Configuration 3 Swirler Orientation (UCRI-2 in red, UCRI-1 in black)

As previously stated, all components were designed for atmospheric testing and high-pressure combustion testing. The starting point for determining the highest pressures and temperatures the rig would experience was arrived at by assuming cruising conditions for 40:1 pressure ratio engine operating at 35,000 feet. An atmospheric table was referenced to obtain the temperature and pressure at an altitude of 35,000 feet and isentropic relations used to determine the theoretical engine inlet conditions, which were calculated to be 139 psia and 660°F. Anticipated future testing includes the possibility of PIV, so the combustion chamber was designed to allow for multiple optical viewports and/or instrumentation access points. Provisions were made to allow either two small quartz windows or one large one, or for one of the smaller windows to be replaced with an instrumentation plate.

The airbox was designed to be large enough so as to not restrict the swirler airflow on the outside swirlers in the array, and to allow for relatively easy adjustment of the insertion depth to one of three pre-determined distances. A series of nine very closely-spaced slider-type feed-thrus were designed to accommodate this demand for adjustment of fuel nozzle insertion depth

without complete rig disassembly, while also being able to withstand the expected 139psia and 660°F inlet conditions. The fuel circuit was designed with the constraint that the entire test rig must also fit into the high-pressure chamber for future testing, and was constructed to allow for total disassembly and cleaning of all components if necessary. Steel tubing was used to carry the fuel rather than flexible tubing or a custom-made manifold due to the extreme conditions experienced both inside and outside of the airbox in the high-pressure chamber, as well as the desire to modification/alteration of the fuel circuit should the need arise. A 3D CAD rendering of the test rig is shown below in figure 2-17, and a photo of the horizontal test rig with the LDI rig attached is shown in figure 2-18. A cutaway view showing the LDI test rig in relation to the high-pressure chamber is shown in figure 2-19, which illustrates the relative location of the chamber, LDI rig, and optical portholes on the chamber sleeve, as well as the extreme proximity of the fuel circuit to the chamber sleeve.

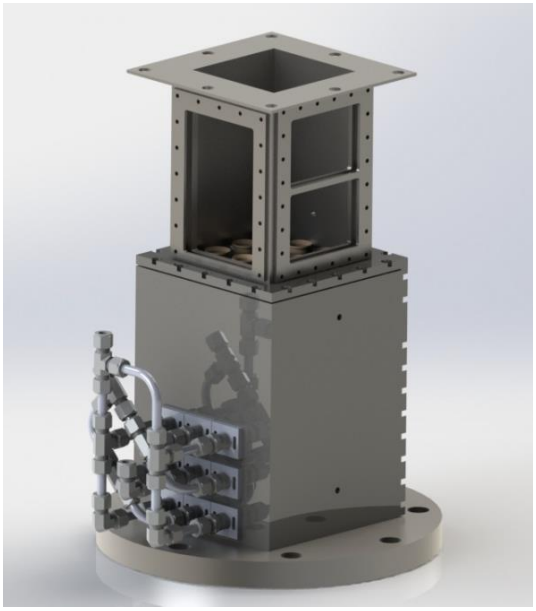

Figure 2-17: 3D CAD Model of LDI Combustion Chamber, Airbox, and Fuel Circuits

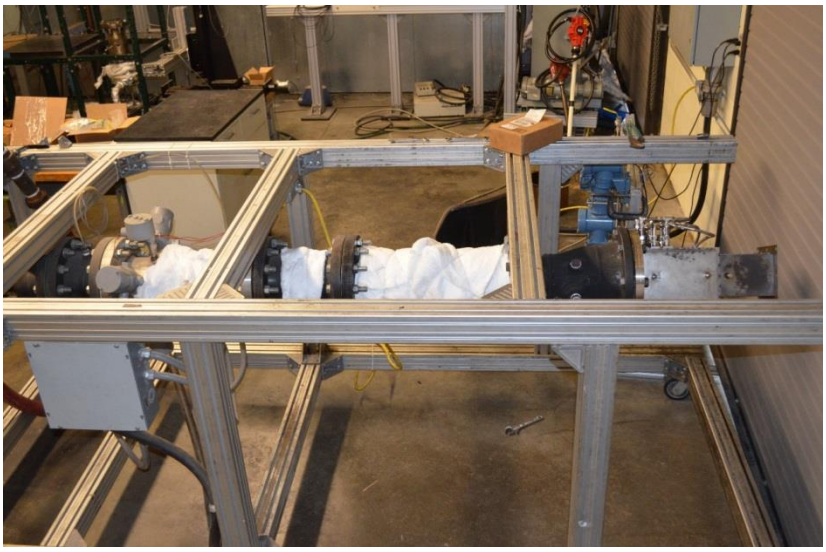

Figure 2-18: Test Setup with Horizontal Rig, Heater, and LDI Rig

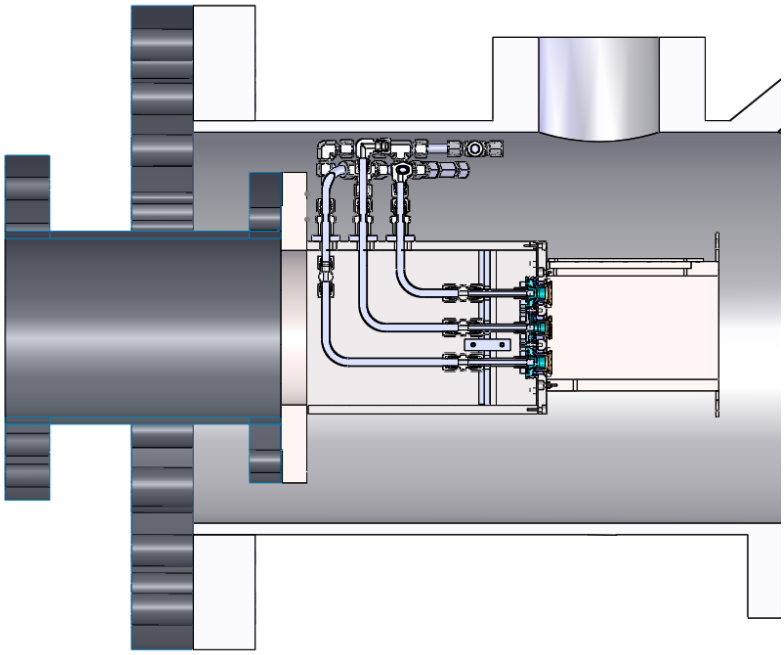

Figure 2-19: CAD Model of LDI Rig in High Pressure Combustion Chamber

Chapter 3 : Test Matrix

As previously stated, the atmospheric combustion testing consisted of three swirler configurations and two fuel nozzle insertion depths. For each of these six cases, five conditions were investigated to gauge the performance of the design at simulated low-power and high-power settings. For each condition, two values of fuel flow rate per circuit were recorded, and the equivalence ratio later calculated from the total fuel flow rate and the measured air flow rate. A series of pictures were also taken for conditions 3, 4, and 5 to illustrate the flame characteristics (color, uniformity, steadiness, shape, etc.), and standard video was recorded for the duration of testing for all six test cases. High-speed video was also captured for certain conditions where acoustic instabilities were encountered, and will be expanded upon later on in later chapters. A summarization of the test plan for each case is shown below in table 3-1.

Condition Number	Circuit 1	Circuit 2	Circuit 3
1	Ignition	X	X
2	LBO	X	X
3	Stable, Lean	X	X
4	Stable, Lean	Stable, Lean	X
5	Stable, Lean	Stable, Lean	Stable, Lean

Table 3-1: Steady-State Combustion Pictures and ϕ Test Plan

Conditions 1, 2, and 3 are designed to gauge stability at low fuel flow rates and equivalence ratios at with only circuit 1 activated, to find the lower operability limit of the LDI configuration as a whole. Condition 4 is designed to investigate how the center swirler alters the aerodynamics and combustion dynamics of the array, and what effect it has on operability limits with various central swirlers and neighboring swirlers. The fuel circuits were selected to mimic cruise conditions/flow rates for a full-scale engine. Condition 5 is intended to investigate the performance of the array at full-power conditions, i.e. SLTO and/or climb, to gauge the flame

uniformity among the various fuel circuits and individual swirler cups, and determine a suitable global equivalence ratio and compare that with equivalence ratios for commercially used combustors. A summary of the various test conditions, parameters, and data to be collected is shown below in table 3-2.

Data Collected	Configurations	Nozzle Depth	Nozzle FN	Circuits Active
Pictures	1,2, 3	Deep, Shallow	0.9	1, 1+2, 1+2+3
Video	1,2, 3	Deep, Shallow	0.9	1, 1+2, 1+2+3
HS Video	1,2, 3	Deep	0.9	1+2, 1+2+3
Steady-State Burning φ	1,2, 3	Deep, Shallow	0.9	1, 1+2, 1+2+3
LBO	1,2, 3	Deep, Shallow	0.9, 3.0	1
Ignition	1,2, 3	Deep, Shallow	0.9, 3.0	1
Acoustic Instability	1,2, 3	Deep	0.9	1+2+3

Table 3-2: Complete Testing Matrix

Additional testing was also performed with a larger fuel nozzle in circuit 1. This fuel nozzle had a flow number of approximately 3.0 and was meant to replicate actual turbine engine hardware to gauge the ignition capabilities of this design at real-world conditions. These conditions mirror those of engine startup conditions, where the inlet pressure is close to atmospheric and the pressure drop across the swirlers is still around 4% of atmospheric pressure.

Chapter 4 : Experimental Setup

All experiments were conducted at the University of Cincinnati Combustion Research Center (CRC) located on the Centerhill campus. Combustion testing was performed on the horizontal rig, which is supplied with air by a GA90FF compressor capable of 0.6 lb_m/s flow rates at 150psig pressure. A de-moisturizing system and settling tank are connected downstream

of the compressor, and a pressure regulator is attached as well to ensure consistent flow rates. A Merium 2100 Smart Gage series differential pressure transducer was used to monitor the pressure drop across the swirlers, and a type-K thermocouple monitored the air temperature shortly upstream of the swirler array. The air was heated by an Osram Sylvania 72kW heater capable of air temperatures of >700°F and the flow rate was measured with a MicroMotion CMF300 Coriolis-type flow meter. Fuel flow rates were measured by a MicroMotion CMF010 flow meter for each fuel circuit. The air temperature was held constant at roughly 400 °F and the pressure drop held constant at 4% of atmospheric pressure (~0.588 psig) for all testing. A schematic of the horizontal rig is shown below in figure 4-1.

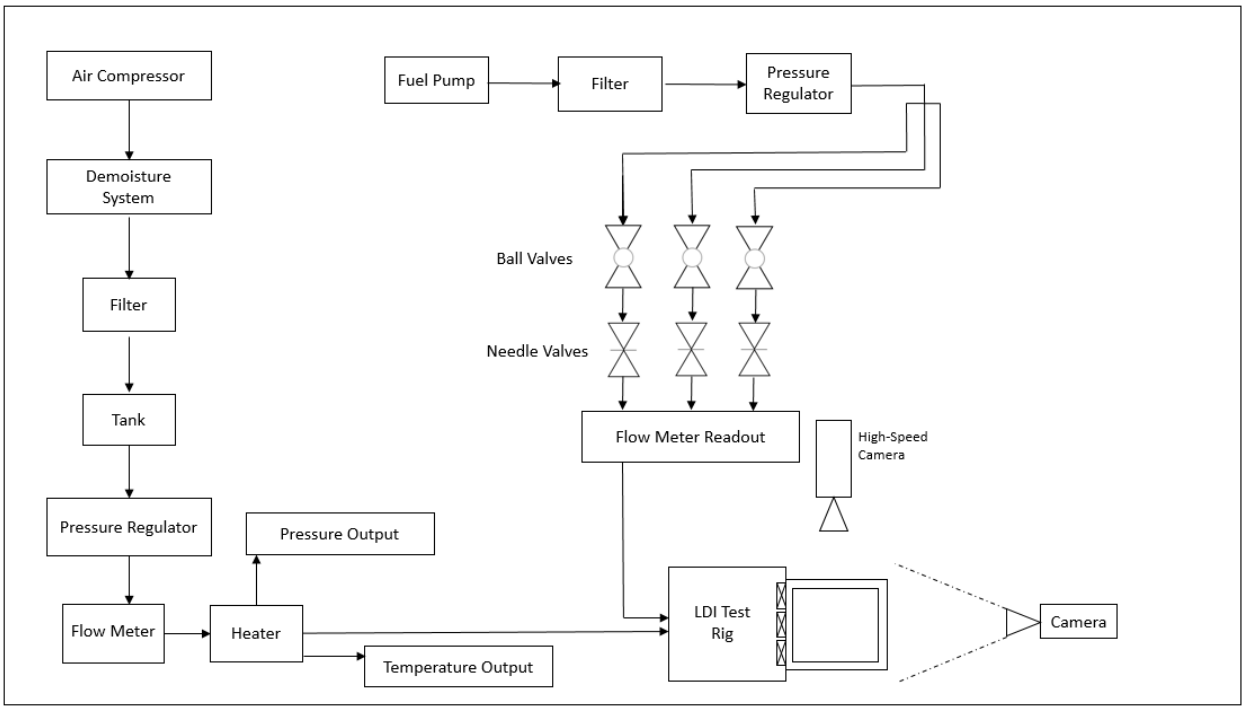

Figure 4-1: Schematic of Horizontal Rig Test Facility

Performance will be evaluated based on the equivalence ratio and visual images for each test case. The equivalence ratio will be divided into global and local sub-components; global is

total fuel flow rate compared to total air flow rate, and local is the air and fuel flow for each swirler. Note that while the local equivalence ratio is presented to give an idea of if the flame is lean or rich immediately at the swirler exit, it may not adequately describe whether or not the burning process is truly lean, and will be discussed further in the results section. Images taken will be from a head-on orientation to observe the flame pattern similar to an axial cross-section, as well as from an orthogonally-orientated optical porthole to observe the flame pattern near the swirler exit similar to a centerline-planar cross-section.

The test procedure for each of the six cases is as follows. The air pressure drop and temperature were set to the appropriate values and an ignition torch inserted into the ignition port in the combustion chamber. The fuel flow rate for circuit 1 was slowly increased until ignition occurred and the value was noted. The chamber was then allowed to heat up for a short time and the flow rate on circuit 1 slowly reduced until the flame extinguished or lifted off from the swirler sufficiently to be regarded as "blown out", and the flow rate again noted. The ignition procedure was then again repeated and the ignition flow rate recorded, then the flow was reduced until the flame was steady and stable but as fuel-lean as possible, and the flow rate again recorded. Circuit 2 was then activated and circuit 1 reduced to be slightly fuel-richer than each individual swirler cup on circuit 2. Two sets of values for circuits 1 and 2 were recorded to allow a slight variation in the ratio of fuel flow rates to each circuit; e.g. some cases permitted a lower global equivalence ratio when circuit 1 operated more fuel rich and vice versa. Circuit 3 was then activated and the procedure repeated, using the results from the previous case to aid in selecting which flow rate combinations to attempt and collect data for. Circuits 2 and 3 were then shut off and a final LBO test performed with circuit 1 only.

Ignition testing for the larger fuel nozzle cases was performed in the same manner as ignition with the smaller fuel nozzles: a blowtorch ignitor was inserted into a small hole in the chamber and replaced with a metal plug after ignition occurred. The blowtorch was inserted a similar distance into the chamber that would be typical of an ignition coil or other ignition device. After insertion the fuel flow rate was gradually increased until ignition occurred and the flame was found to be stable, and after re-insertion of the plug the flow rate was gradually decreased until liftoff or blowout occurred, and the flow rate recorded both for ignition and blowout. This was repeated 3-4 times for each case to obtain a representative average.

Chapter 5 : Results

The results of these experimental investigations will be divided into four parts: the equivalence ratios for the various configurations and test conditions, pictures of the steady-state burning conditions, data collected on the acoustic instabilities encountered during testing, and the fuel flow rates and equivalence ratios for ignition/LBO with the large fuel nozzle. The pictures will be organized such that all of the deep insertion images will be presented, then the shallow insertion, further sub-organized by configurations 1, 2, and 3, in that order, and finally by simulated operating condition, e.g. idle, cruise, and takeoff. The titles for each image will include this information, as well as a 3-digit hyphenated string designating the fuel flow rates to each of the three fuel circuits respectively, in lb/hr, and the calculated global equivalence ratio.

Data for the acoustic instabilities will be presented in a table detailing the fuel flow rates and subsequent equivalence ratios for each circuit where acoustic instabilities were encountered, with the global equivalence ratio for each case reported as well. A sample of the acoustic

spectrum recorded for one test case is included as well, both log scale and a linear scale, to illustrate the acoustic profile and dominant frequency for these instabilities. Both the fuel flow rates and the equivalence ratios will be reported for the ignition/LBO testing for the large fuel nozzles in the same manner as for the steady-state combustion testing. Each test was performed four times to obtain a representative average.

5.1 Equivalence Ratios for Steady-State Combustion

Results Comparison Table						
Equivalence Ratio	Deep Insertion			Shallow Insertion		
Circuits Active	Config. 1	Config. 2	Config. 3	Config. 1	Config. 2	Config. 3
1	0.21	0.18	0.18	0.42	0.35	0.31
1+2	0.55	0.48	0.48	0.70	0.55	0.62
1+2+3	0.74	0.77	0.76	1.06	1.04	0.94

Table 5-1: Steady-State Combustion Equivalence Ratios for Various Fuel Circuits Active

5.2 Steady-State Combustion Pictures

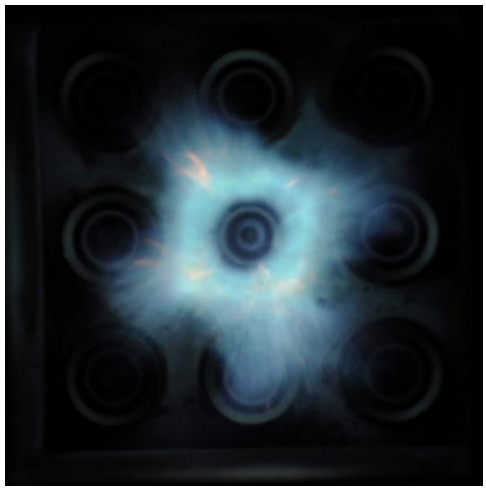

Figure 5-1: Configuration 1, Deep Insertion, Idle, 6-0-0, φ=0.21

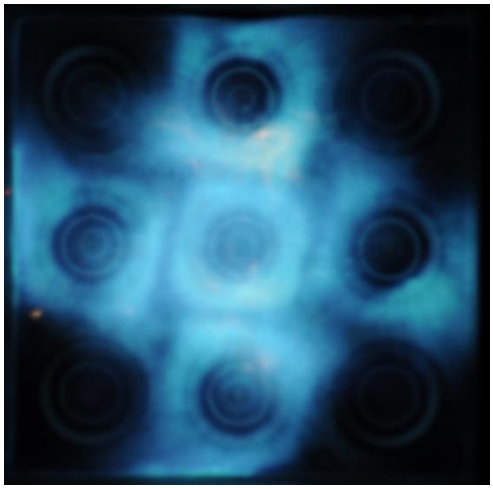

Figure 5-2: Configuration 1, Deep Insertion, Cruise, 4-12-0, φ=0.55

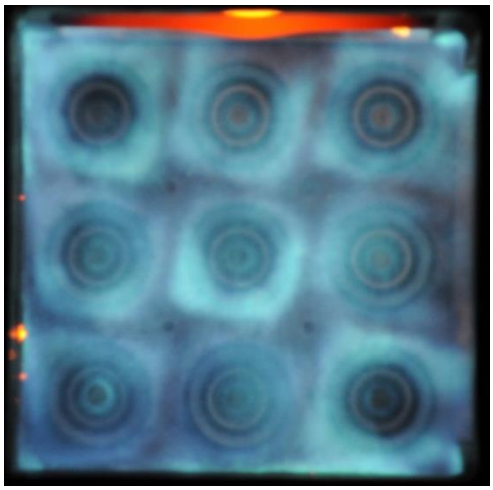

Figure 5-3: Configuration 1, Deep Insertion, SLTO, 3-8-10, φ=0.74

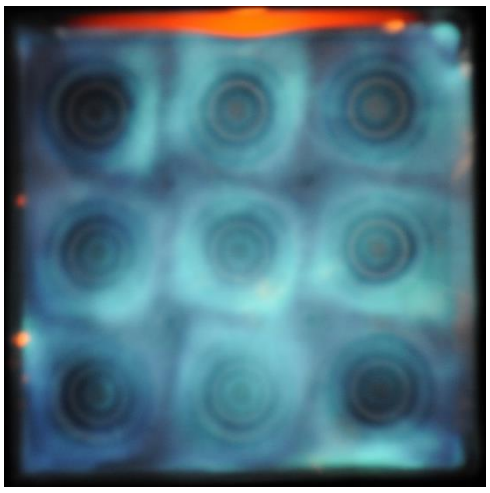

Figure 5-4: Configuration 1, Deep Insertion, SLTO, 3-9-9, φ=0.74

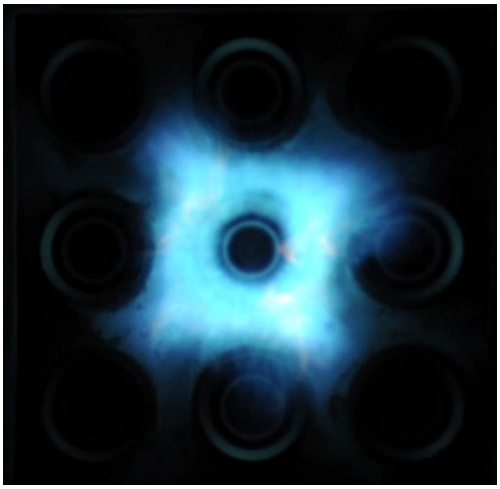

Figure 5-5: Configuration 2, Deep Insertion, Idle, 5-0-0, φ=0.18

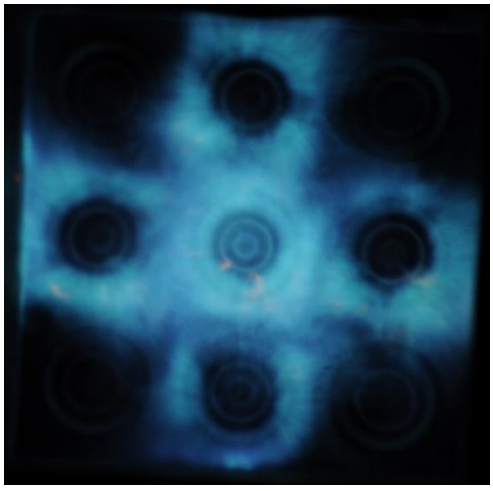

Figure 5-6: Configuration 2, Deep Insertion, Cruise, 2.5-12-0, φ=0.48

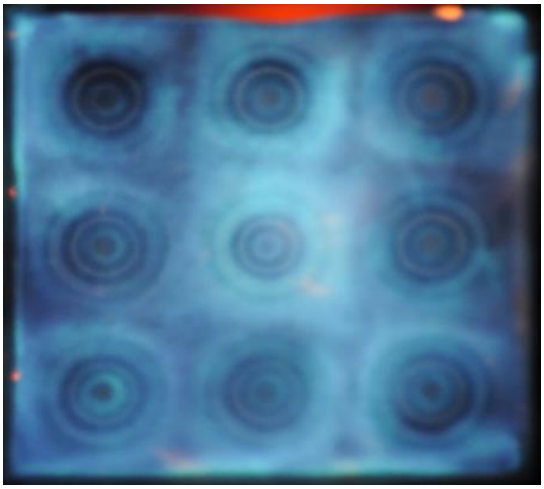

Figure 5-7: Configuration 2, Deep Insertion, SLTO, 2.5-9-11, φ=0.77

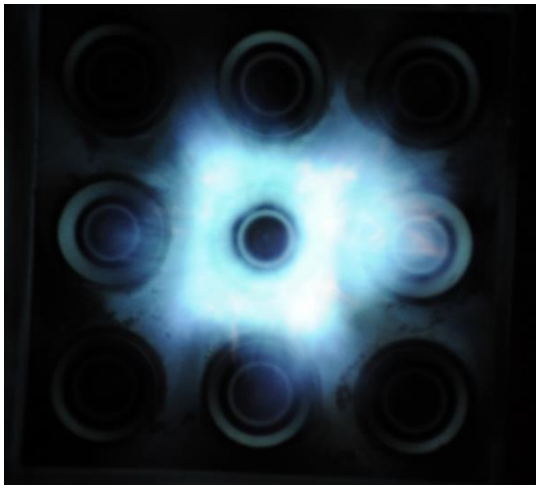

Figure 5-8: Configuration 3, Deep Insertion, Idle, 5-0-0, φ=0.18

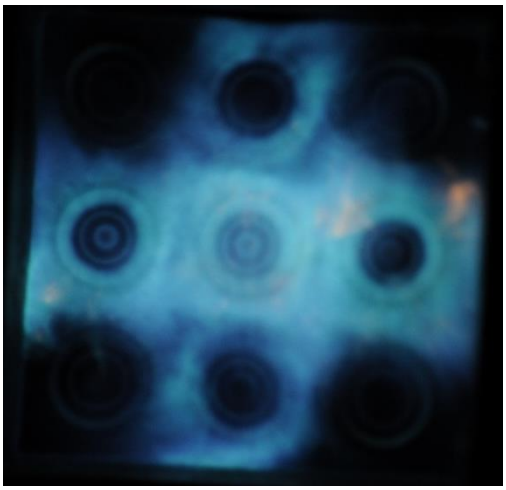

Figure 5-9: Configuration 3, Deep Insertion, Cruise, 3-12-0, φ=0.48

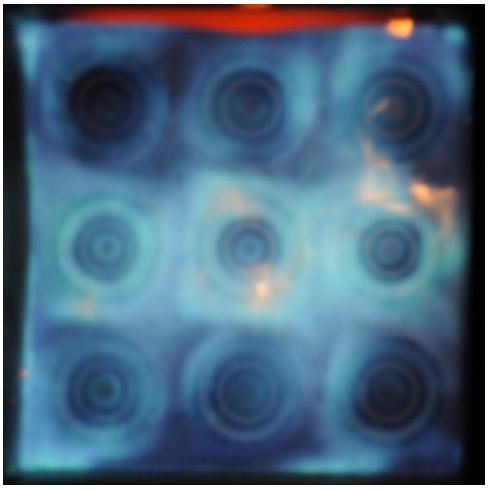

Figure 5-10: Configuration 3, Deep Insertion, SLTO, 3-9-11, φ=0.76

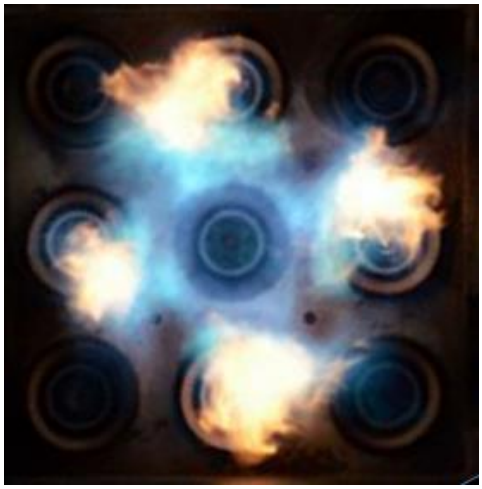

Figure 5-11: Configuration 1, Shallow Insertion, Idle, 12-0-0, φ=0.42

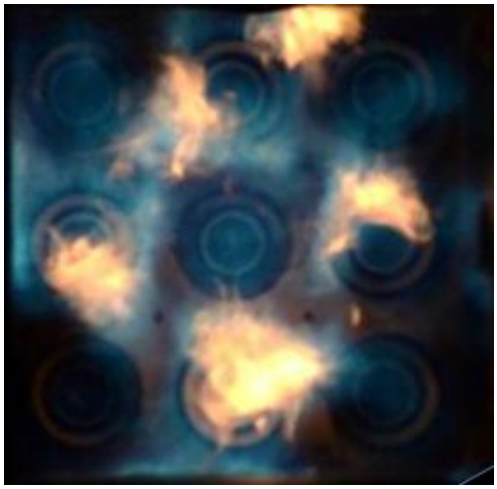

Figure 5-12: Configuration 1, Shallow Insertion, Cruise, 8-12-0, φ=0.70

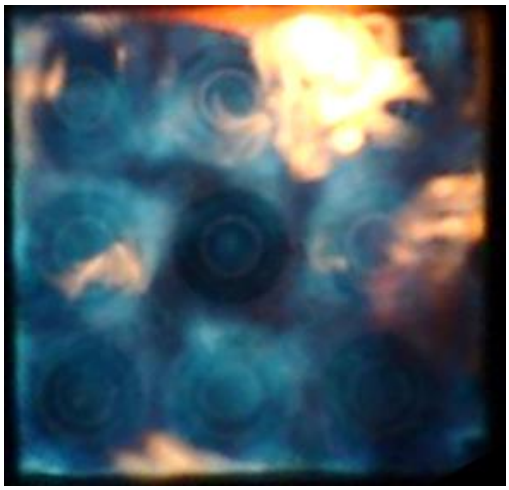

Figure 5-13: Configuration 1, Shallow Insertion, SLTO, 6-12-12, φ=1.06

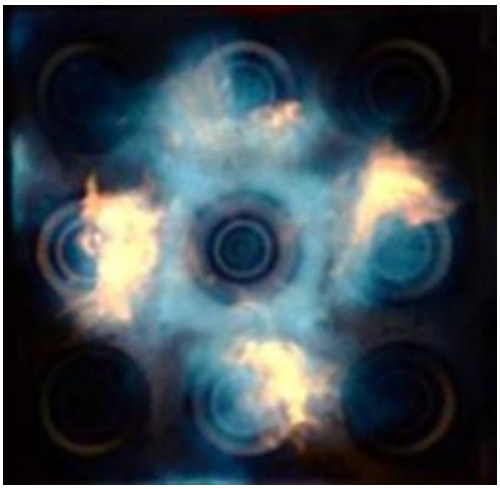

Figure 5-14: Configuration 2, Shallow Insertion, Idle, 10-0-0, φ=0.35

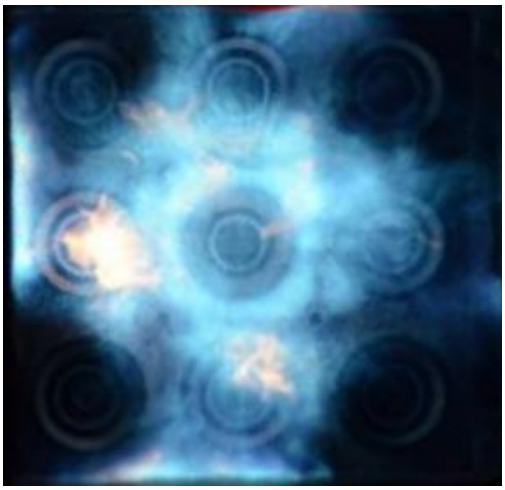

Figure 5-15: Configuration 2, Shallow Insertion, Cruise, 6-10-0, φ=0.55

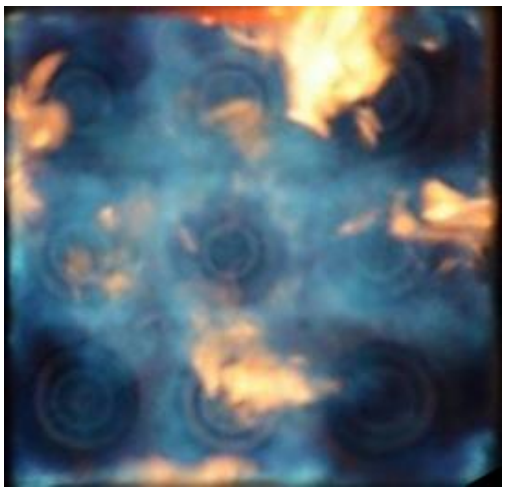

Figure 5-16: Configuration 2, Shallow Insertion, SLTO, 6-12-12, φ=1.04

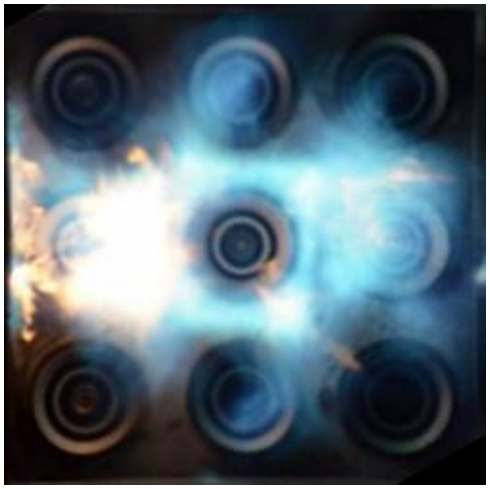

Figure 5-17: Configuration 3, Shallow Insertion, Idle, 9-0-0, φ=0.31

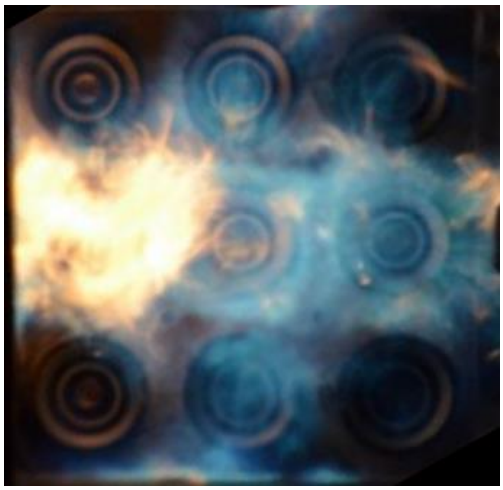

Figure 5-18: Configuration 3, Shallow Insertion, Cruise, 6-12-0, φ=0.62

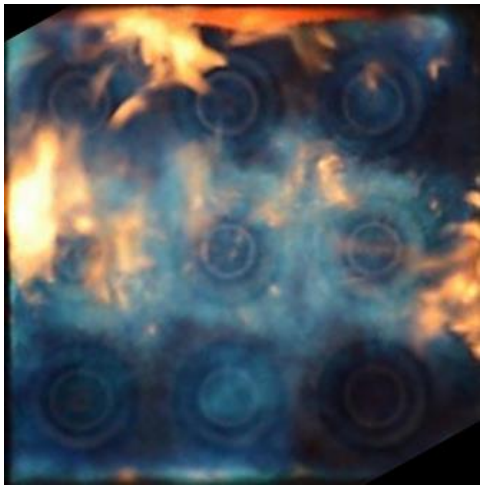

Figure 5-19: Configuration 3, Shallow Insertion, SLTO, 5-10-12, φ=0.94

5.3 Acoustic Instability

Configuration 1						
Circuit 1 ṁ (lb/hr)	Circuit 2 ṁ (lb/hr)	Circuit 3 ṁ (lb/hr)	Circuit 1 φ	Circuit 2 φ	Circuit 3 φ	Global φ
7	12	0	2.22	0.95	0.00	0.67
4	12	12	1.27	0.95	0.95	0.99
6	10	12	1.90	0.79	0.95	0.99
6	12	10	1.90	0.95	0.79	0.99
6	10	14	1.90	0.79	1.11	1.06

Table 5-2: Flow Rates for Acoustic Instability, Configuration 1

Configuration 2						
Circuit 1 ṁ (lb/hr)	Circuit 2 ṁ (lb/hr)	Circuit 3 ṁ (lb/hr)	Circuit 1 φ	Circuit 2 φ	Circuit 3 φ	Global φ
5	12	0	1.56	0.94	0.00	0.59
5	12	12	1.56	0.94	0.94	1.01
3	10	12	0.94	0.78	0.94	0.87
3	12	12	0.94	0.94	0.94	0.94
5	10	12	1.56	0.78	0.94	0.94

Table 5-3: Flow Rates for Acoustic Instability, Configuration 2

Configuration 3						
Circuit 1 ṁ (lb/hr)	Circuit 2 ṁ (lb/hr)	Circuit 3 ṁ (lb/hr)	Circuit 1 φ	Circuit 2 φ	Circuit 3 φ	Global φ
4	12	0	1.18	0.89	0.00	0.53
4	10	12	1.18	0.74	0.89	0.86
4	12	10	1.18	0.89	0.74	0.86
6	10	10	1.77	0.74	0.74	0.86

Table 5-4: Flow Rates for Acoustic Instability, Configuration 3

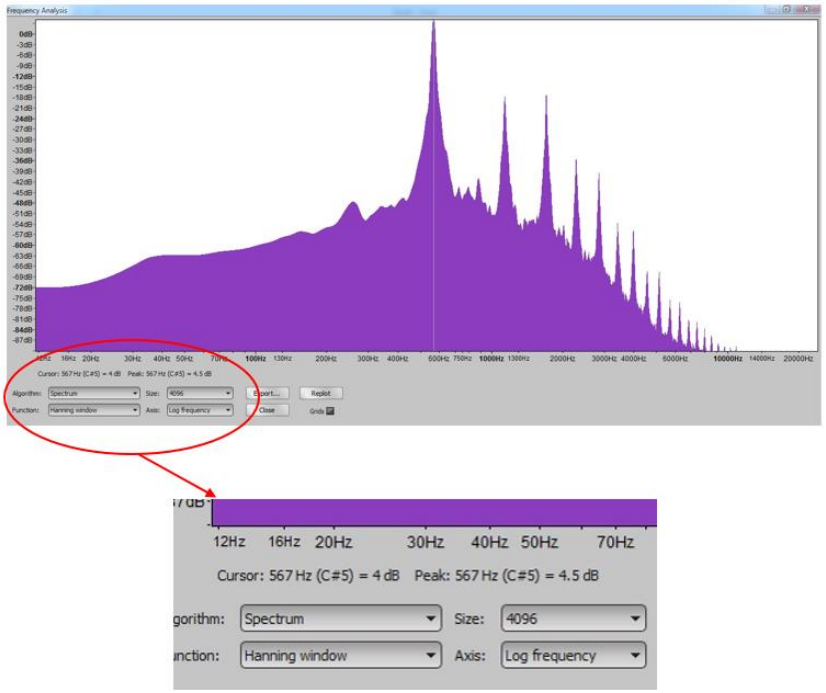

Figure 5-20: Output from Audacity showing Dominant Frequency of 567Hz

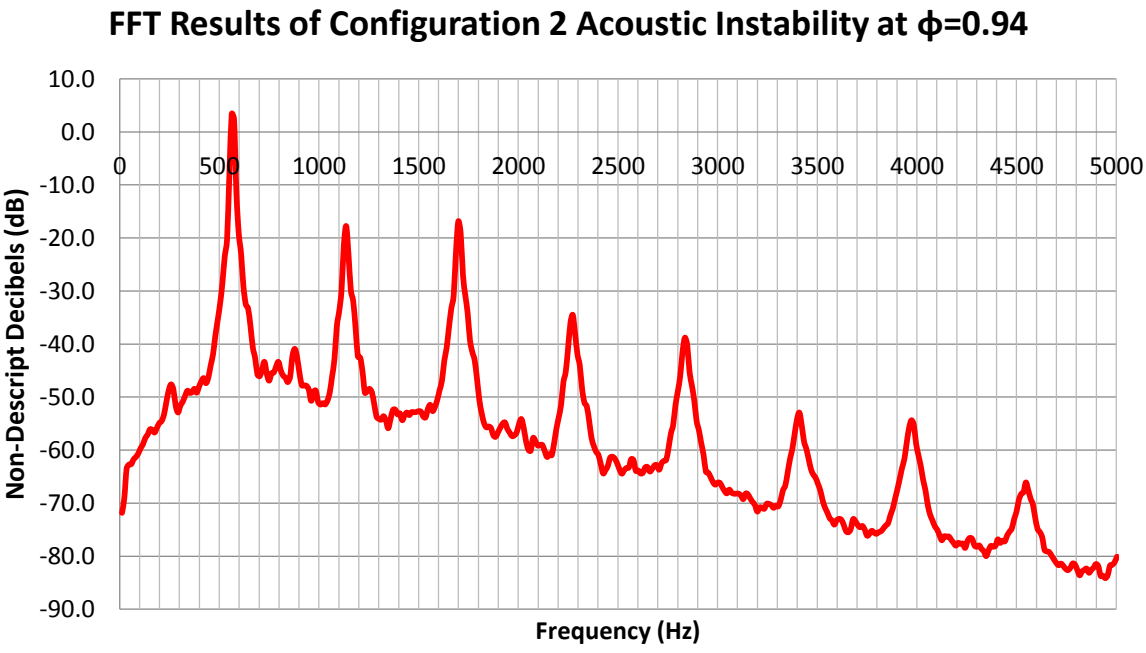

Figure 5-21: Sample Acoustic Spectrum for Acoustic Instability

5.4 Ignition and Lean-Blowout

Fuel Flow Rates (lb/hr) with FN 3.0 Fuel Nozzles				
		Configuration 1	Configuration 2	Configuration 3
Deep Insertion	Ignition	7.1	4.0	6.2
	LBO	6.2	3.6	4.4
Shallow Insertion	Ignition	12.0	8.4	XXX
	LBO	4.0	4.4	XXX

Table 5-5: Fuel Flow Rates for Ignition and LBO with FN 3.0 Fuel Nozzle

Ignition/LBO Equivalence Ratios with FN 3.0 Fuel Nozzles				
		Configuration 1	Configuration 2	Configuration 3
Deep Insertion	Ignition	0.25	0.14	0.20
	LBO	0.22	0.12	0.14
Shallow Insertion	Ignition	0.42	0.29	XXX
	LBO	0.14	0.15	XXX

Table 5-6: Equivalence Ratios for Ignition and LBO with FN 3.0 Fuel Nozzle

Ignition/LBO Equivalence Ratios with FN 0.9 Fuel Nozzles				
		Configuration 1	Configuration 2	Configuration 3
Deep Insertion	Ignition	0.25	0.24	0.20
	LBO	0.19	0.14	0.12
Shallow Insertion	Ignition	0.42	0.35	0.28
	LBO	0.28	0.30	0.27

Table 5-7: Equivalence Ratios for Ignition and LBO with FN 0.9 Fuel Nozzles

Chapter 6 : Discussion

This chapter will be divided into six sections: discussion of the equivalence ratio data from the previous chapter, comparison of the visual results with the isothermal LDV/PIV data and between the cases themselves, discussion of the standard video, discussion of the high-speed video, the acoustic instability phenomena, and finally the ignition and LBO testing with the large fuel nozzle. It should be noted again that the purpose of these tests is two-fold: firstly to investigate the performance of this LDI configuration across a wide range of test conditions, and secondly to draw comparisons with the aerodynamic PIV data collected by Endicott for the three configurations tested. The PIV data for Endicott's research and the relevant combustion pictures are shown side-by-side for a direct comparison. The pictures are taken with a head-on orientation, with a very distinct flame-front for many of the pictures. The axial location of this flame-front is estimated to be approximately 0.5 to 1.0 inches downstream of the flare exit, or y/D=0.5 to y/D=1.0, so three axial cross-sectional velocity profiles are presented at 0.3, 0.74, and 1.0 inches downstream to show how the velocity profiles changes with axial distance.

6.1 Steady-State Burning Equivalence Ratios

A comparison of the equivalence ratios calculated for steady-state combustion for the various test conditions are shown in table 5-1 above. These numbers were arrived at by considering the recorded fuel flow rates for each circuit and the air flow rate for each configuration and comparing them to the flow rates necessary for stoichiometric combustion, as shown below in equation 6-1.

$$\varphi = \frac{\dot{m}_{air\,(stoich)}}{\dot{m}_{fuel\,(stoich)}} * \frac{\dot{m}_{fuel}}{\dot{m}_{air}} \qquad \textbf{6-1}$$

The fuel flow rates used for each circuit were adjusted in fairly coarse increments, usually 0.5 to 1.0 lb/hr increments, so the "true" equivalence ratios for stable steady-state combustion for a particular test configuration may change by ± 5-10% or so. Again, the flow rates for up to three circuits had to be manipulated to obtain what was considered the best conditions for a stable, steady flame, and the numbers presented here are meant to be a stepping-off point for future high-pressure combustion testing.

The first thing to note is that the deeper insertion depth performed better than the shallow insertion depth for all tests performed in terms of the minimum fuel-to-air ratio required for stable combustion. This should come as no surprise as the deeper nozzle insertion depth allows for a longer time interacting with the counter-rotating air streams to break up the fuel droplets. The LDI design primarily relies on air stream interactions to break up the fuel droplets rather than heavy pre-filming or pre-vaporization used with the RQL and LPP designs respectively, as well as small flow number fuel nozzles to allow sufficient atomization at relatively low pressure drops and fuel-staging to improve operability range. For this reason, the insertion depth of the fuel nozzles is very important to ensure the fuel droplets are broken up by the air streams across a wide throttle setting. Additionally the insertion depth must be shallow enough so as to mitigate the risk of flashback or auto-ignition, one of the main goals of the LDI concept. All these considerations must be balanced to ensure good performance, safety, and good emissions for idle/sub-idle conditions as well as full-throttle takeoff.

The two insertion depths were chosen to explore the two extremes of this design: very deep insertion on the verge of prefilming with good performance and flame uniformity, and very shallow insertion with no issues with auto-ignition or flashback. Again, these tests were performed at atmospheric conditions with very small flow number fuel nozzles, and while the

results will clearly not be a 1:1 comparison with high-pressure combustion testing with large fuel nozzles, they should give a representative idea of the performance and stability of the rig as a whole. As previously-stated, the deeper insertion depth has better performance at the atmospheric pressure conditions tested, and likely for high-pressure combustion tests as well. However with the air preheated to 600-800°F, the shallower insertion depth will likely have higher resistance to auto-ignition and flashback as the ignition delay reduces with increasing air temperature.

The second thing to note about this data set is that configurations 2 and 3 performed better, in terms of the minimum fuel-to-air ratio required for stable combustion, than configuration 1 with circuit 1 and circuits 1 and 2 active, but very slightly worse with all three circuits active. These trends hold true for both the deep and shallow insertion depths. Both configurations which utilized a UCRI-1 swirler were expected to perform better based on Endicott's aerodynamic data due to the increase in size of the CTRZ, and generally the results show this to be true. The cases with all three circuits active may appear slightly worse due to the coarse fuel flow rate adjustments and are likely not significant. Configurations 2 and 3 show an improvement over configuration 1 for both insertion depths based on the results of table 5-1.

6.2 Comparison of Combustion Pictures with PIV Data

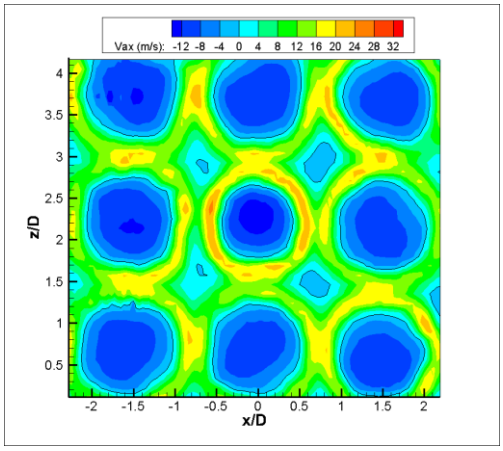

Figure 6-1: Configuration 1 Axial Velocity Contours at y/D=0.3

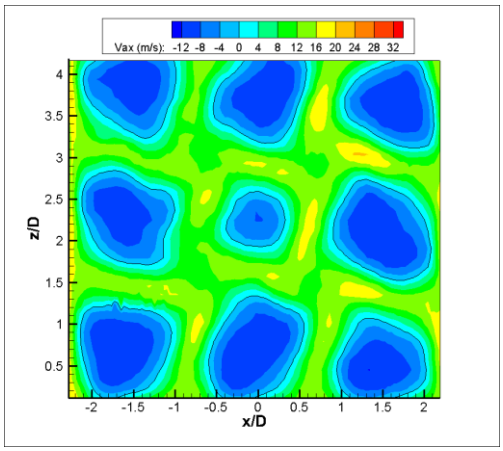

Figure 6-2: Configuration 1 Axial Velocity Contours at y/D=0.74

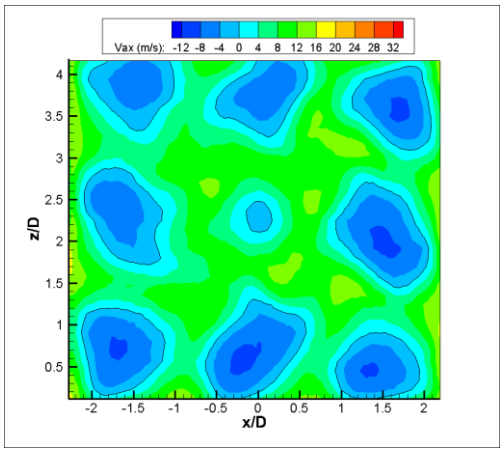

Figure 6-3: Configuration 1 Axial Velocity Contours at y/D=1.0

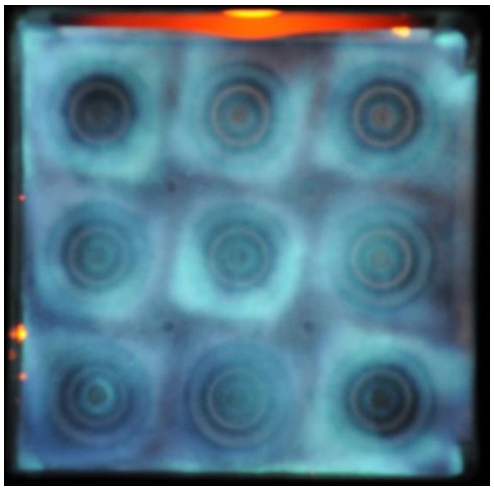

Figure 5-3: Configuration 1, Deep Insertion, SLTO, 3-8-10, φ=0.74

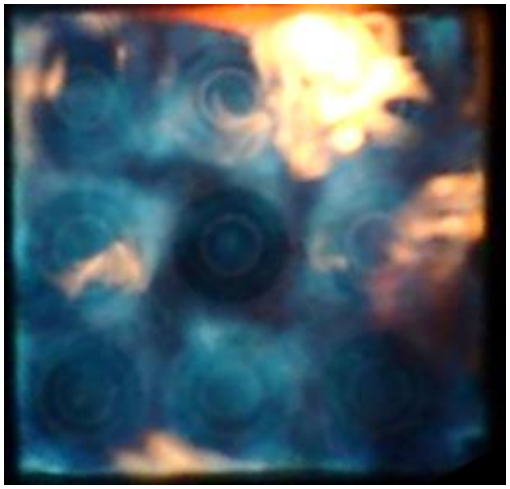

Figure 5-13: Configuration 1, Shallow Insertion, SLTO, 6-12-12, φ=1.06

The pictures on the preceding page compare the isothermal velocity data obtained by Endicott with the combustion pictures taken for this for configuration with all three fuel circuits active, and both insertion depths presented. Three axial stations were selected to show the progression of the aerodynamic structure through an axial distance which approximates the location were the flames from the individual swirl cups combine and form their distinct flame-front. Those axial distance are y/D=0.3, y/D=0.74, and y/D=1.0. The purpose of selecting these distances to compare the aerodynamic data with the combustion pictures is to compare and contrast both sets of data in a very identifiable, visual manner. The sharpness and shape of the individual flames in figure 5-3 is an excellent example of this, and by referencing the velocity profiles from figures 6-1, 6-2, and 6-3, it can be readily observed that the size and shape of the CTRZs correlate well with the patterns formed by the flames.

Note that one cannot directly compare the velocity profile with the flame characteristics, as the flame characteristics are dependent on much more than just the aerodynamic profile. However both sets of data do show similar trends which may not be evident when observing just the aerodynamic data or combustion data. Looking at figures 6-2 and 6-3, the overall orientation of the CTRZs can be seen to be "stretched" in a clockwise sense, or "clocked" with respect to the overall flow structure. Additionally, each individual burning zone for each swirl cup can be seen to be clocked in a similar orientation as well. The most obvious observation is the distinct square shape of the flame for each swirl cup: the aerodynamic data shows a circular CTRZ initially developing for each cup which then forms a very rough ovoid/polygonal shape with a slight "point" directed towards the four intermediate zones at the boundaries of four cups' flame fronts. Figures 6-4 and 6-5 below show close-up views of this region and the "points" produced by the swirlers' interactions.

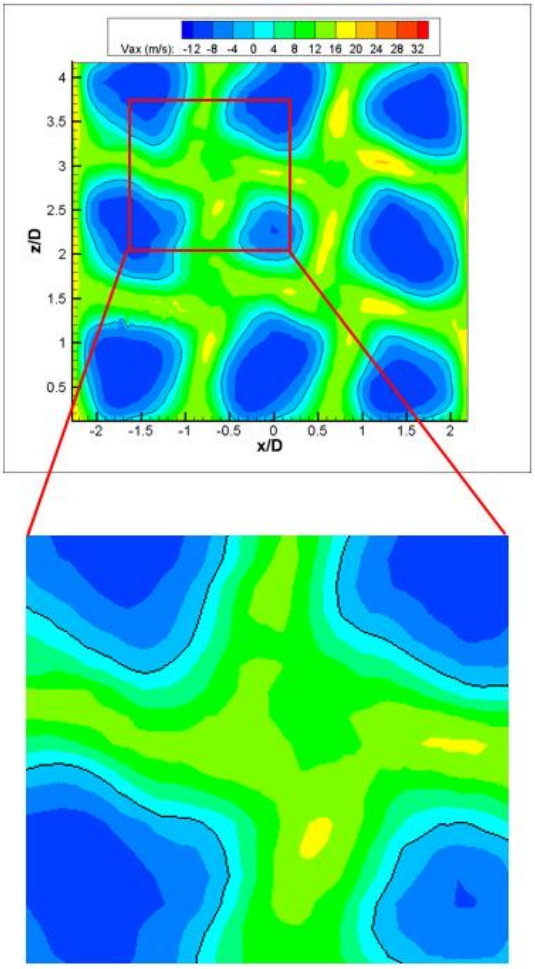

Figure 6-4: Magnification of CTRZ Interaction Zone

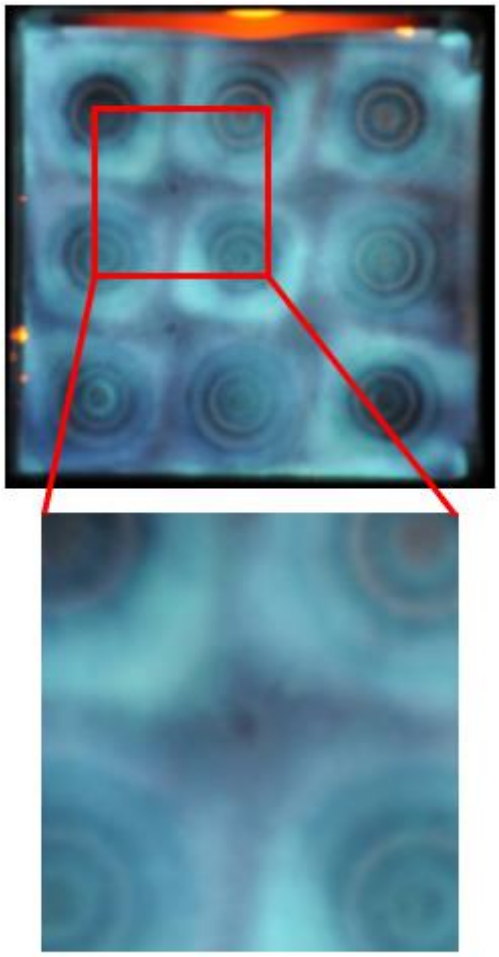

Figure 6-5: Magnification of Flame-Front Interaction

The overall clockwise clocking of the flow structure is due to the orientation of the secondary passage for each swirler. This passage rotates clockwise when viewed looking upstream, which is the same orientation as the overall flow structure. Standard swirler design theory for a dual-inlet swirler usually calls for a larger effective area for the secondary passages compared with the primary passage, and both UCRI-2 and UCRI-1 follow this design convention. This means that the overall swirl will follow the orientation of the secondary passage due to the higher mass flow and higher tangential momentum flux, which is precisely the case here as well.

Referencing figure 6-2 again, a second item to note is the reduction in both size and height of the central CTRZ. Figure 6-6 below gives more in-depth aerodynamic data for the velocity profile for configuration 1. Three vertical cross-sections are shown across each of the three rows of three swirlers. Symmetry is assumed for these set of measurements. The CTRZ of the central swirler exhibits the same slight reduction in size as that shown in figure 6-2, and that same reduction in size is seen in figure 5-2 as well. The overall flame is brighter, denser, and more compact than that of the surrounding eight swirl cups, which may be evidence of a stronger, more compact CTRZ and higher average positive axial velocity.

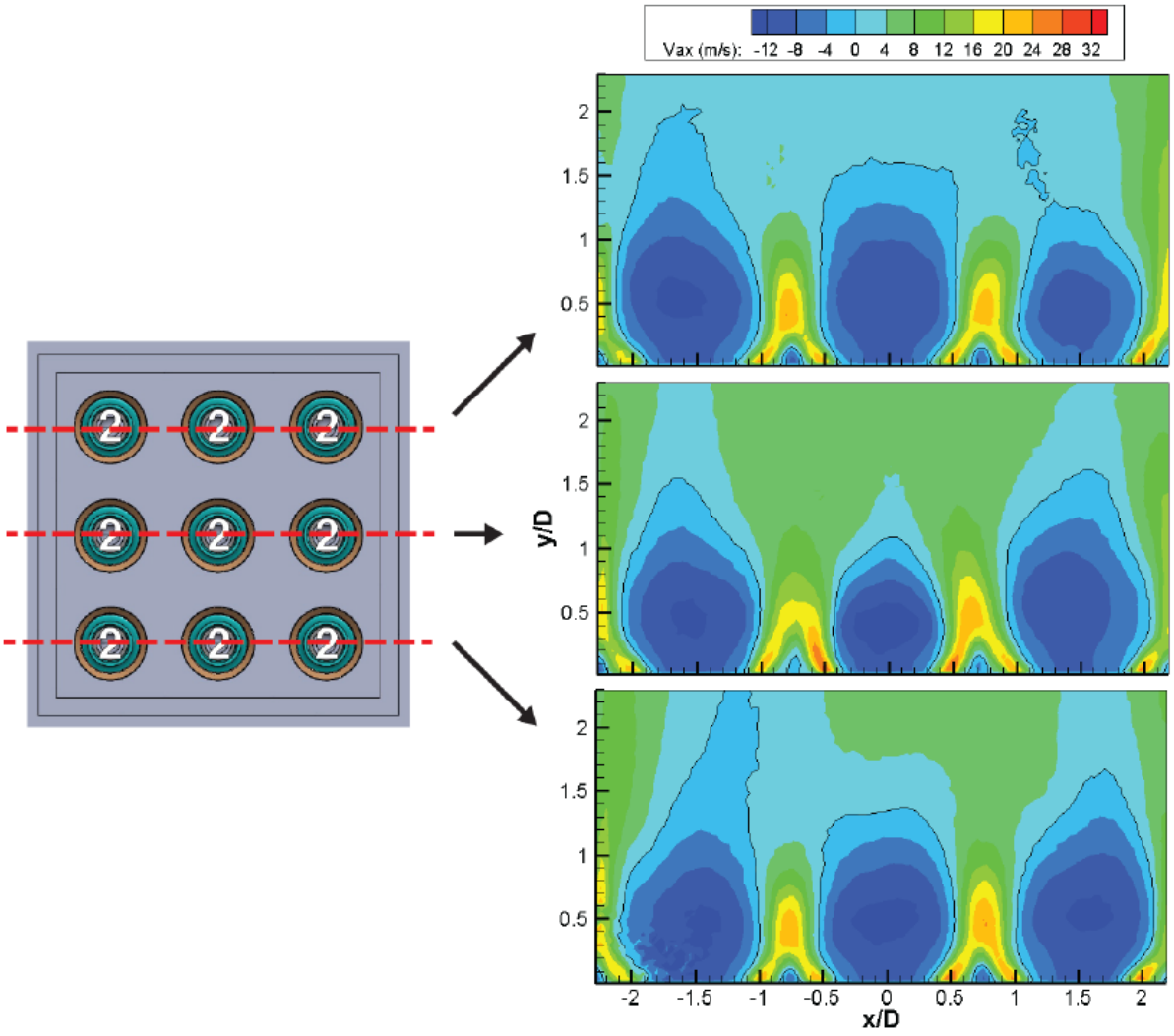

Figure 6-6: Vertical Cross-Sections of Axial Velocity for Configuration 1

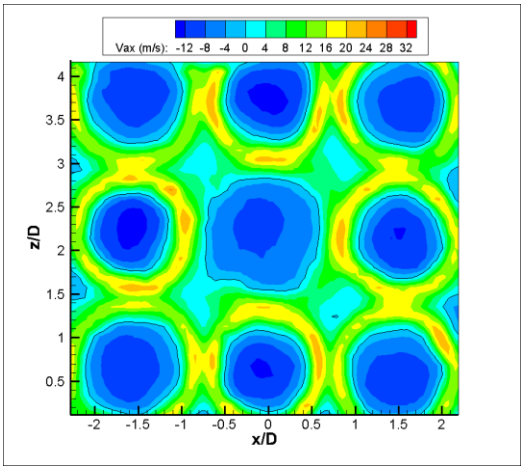

Figure 6-7: Configuration 2 Axial Velocity Contours at y/D=0.3

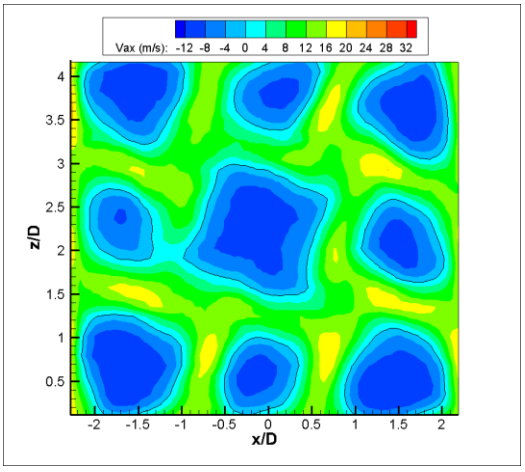

Figure 6-8: Configuration 2 Axial Velocity Contours at y/D=0.74

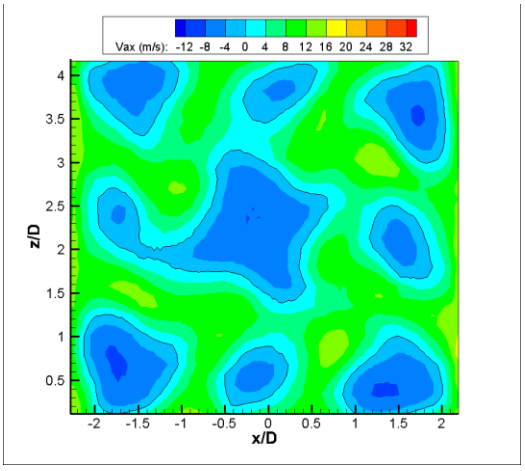

Figure 6-9: Configuration 2 Axial Velocity Contours at y/D=1.0

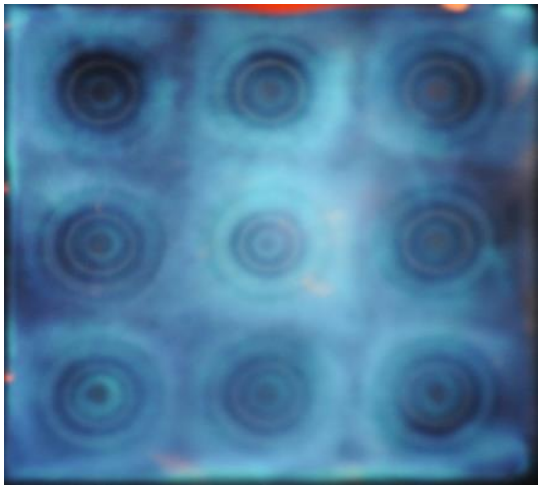

Figure 5-7: Configuration 2, Deep Insertion, SLTO, 2.5-9-11, φ=0.77

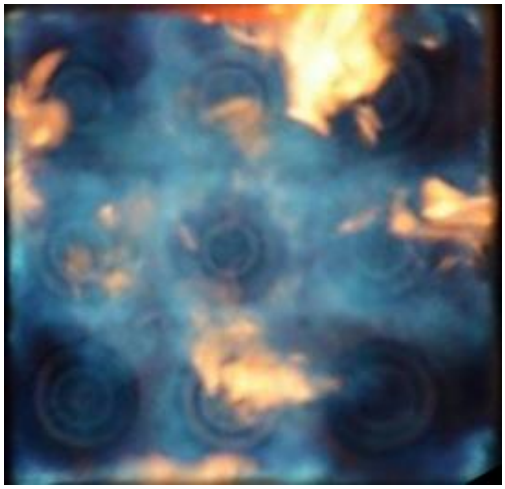

Figure 5-16: Configuration 2, Shallow Insertion, SLTO, 6-12-12, φ=1.04

Figures 6-7 through 6-9 above show the aerodynamic profile for configuration 2 at three stations downstream of the swirler, similar to figures 6-1 through 6-3. Here it can be seen in figure 6-1 that the center swirler's CTRZ has grown in size and the jets of positive axial velocity are now essentially gone. Progressing further downstream the CTRZ actually increases in size, which is the opposite of what happened with configuration 1. This is due to the center swirler's higher radial and tangential velocities, which serve both to reduce the magnitude of the positive axial velocity while increasing the size of the regions of negative axial velocity. The same overall clocking is present as well, with the corners of the CTRZ producing "points" which rotate with the overall flow swirling orientation.

A comparison of figures 6-2 and 6-8 reveals a very interesting observation. The "side" CTRZs for configuration 1 are approximately the same size as the "diagonal" ones from y/D=0.3 to y/D=1.0; however for configuration 2 the side CTRZs become smaller than the diagonal CTRZs from y/D=0.3 to y/D=0.74, with the trend continuing to y/D=1.0. This trend is mirrored in Kao's dissertation when investigating the periodic and uniform change in the characteristics of the size and shape of CTRZs with swirlers placed in an array. Comparing these observations to figure 5-7 however, the combustion pattern does not appear to follow this periodic change in CTRZ size/shape. The flow structure does not appear markedly different from the combustion pictures of the previous configuration. The main differences are the "blending" of the flame fronts between the center swirler and those of circuit 2 on the sides and improved overall flame uniformity. The sharpness of the square-shaped flame fronts is reduced and the center swirler's flame appears slightly brighter than that of configuration 1.

The PIV cross-sections in figure 6-10 show this same distinct periodic change in CTRZ characteristics, and may help to explain why the flame appears to be extinguished for the shallow

insertion depth testing shown in figure 5-16. The diagonal swirlers' recirculation zones are wider and weaker than those on the sides and are bound by two metal walls of the combustion chamber. Assuming that these swirlers have reacting CTRZs which mirror the non-reacting PIV data, this relatively weaker CTRZ will not anchor the flame as well as a smaller, stronger CTRZ, and when combined with fuel nozzles which are pushed relatively far downstream, these two factors may combine to force the flame to become detached and for combustion to happen downstream.

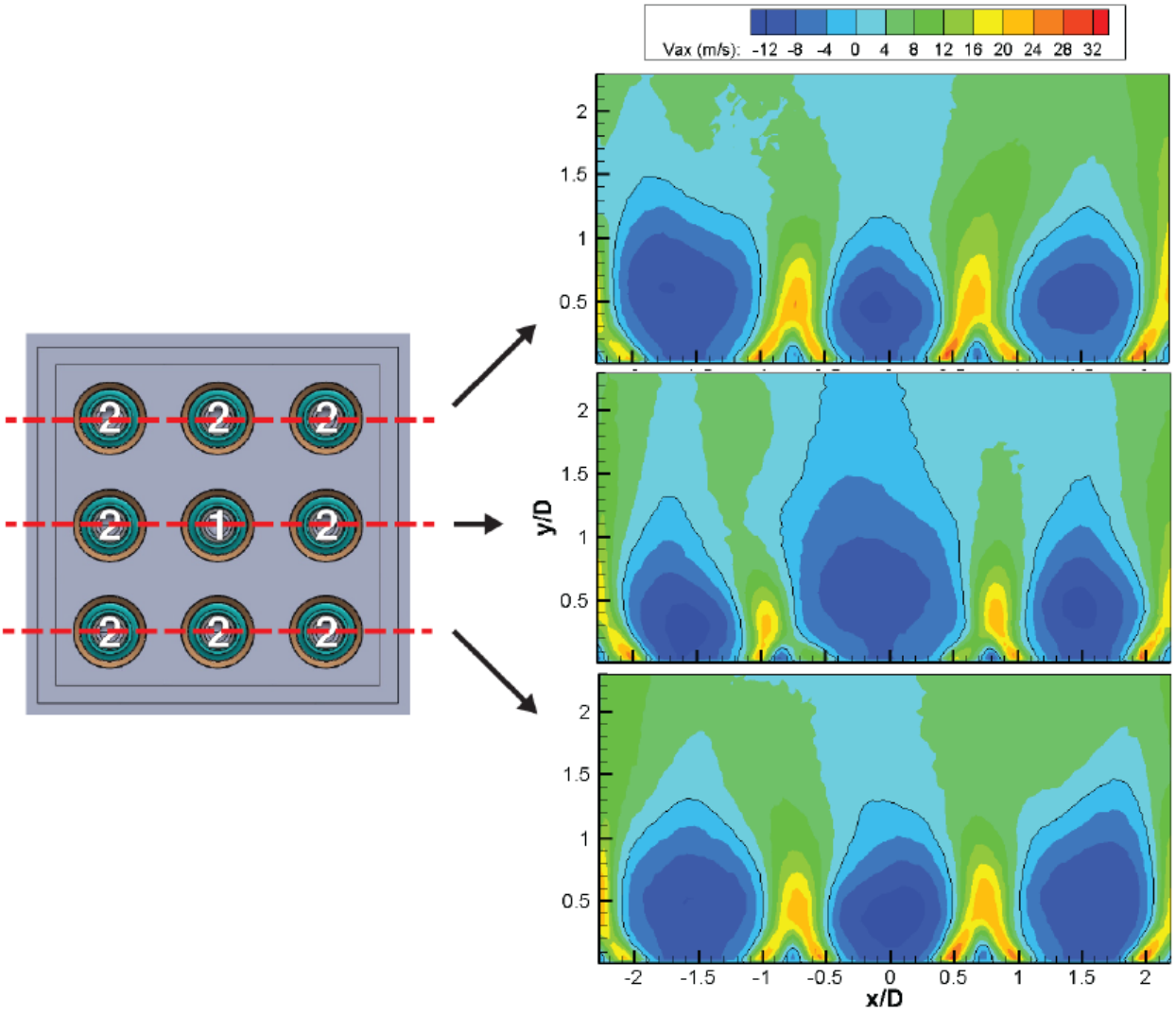

Figure 6-10: Vertical Cross-Sections of Axial Velocity for Configuration 2

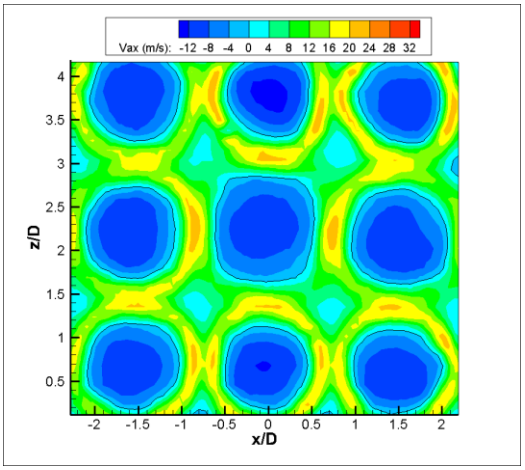

Figure 6-11: Configuration 3 Axial Velocity Contours at y/D=0.3

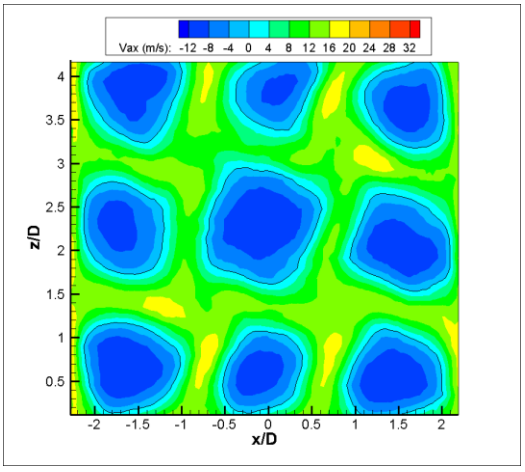

Figure 6-12: Configuration 3 Axial Velocity Contours at y/D=0.74

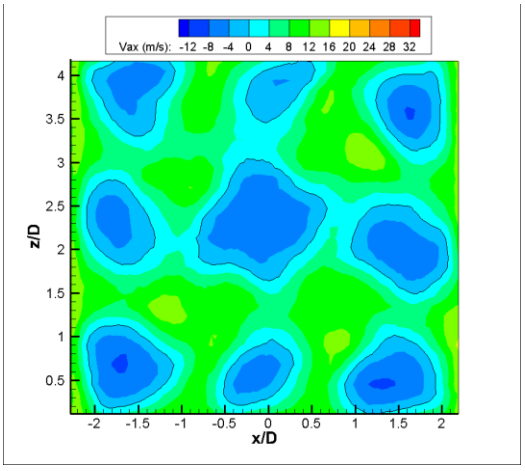

Figure 6-13: Configuration 3 Axial Velocity Contours at y/D=1.0

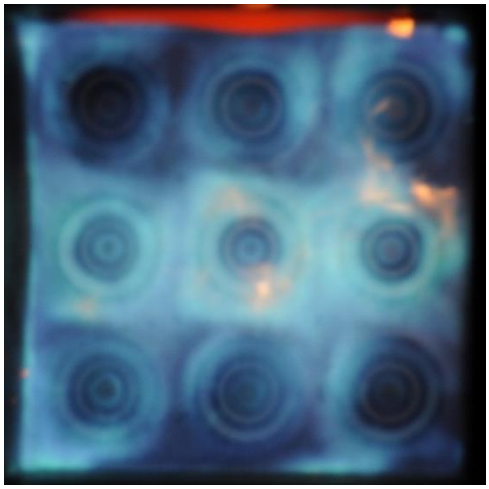

Figure 5-10: Configuration 3, Deep Insertion, SLTO, 3-9-11, φ=0.76

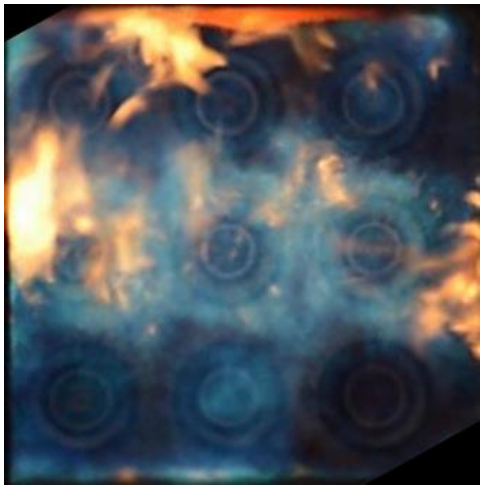

Figure 5-19: Configuration 3, Shallow Insertion, SLTO, 5-10-12, φ=0.94

Figures 6-11 through 6-13 above show the progression of the aerodynamic profile for configuration 3. Note that for all five pictures above, the UCRI-1 swirlers lie along the horizontal. In both figures 5-18 and 5-19 the flames above the UCRI-1 swirlers are brighter and bluer than the surrounding UCRI-2 swirlers, indicating higher fuel concentrations in accordance with the slightly reduced effective areas of all UCRI-1 swirlers. Again, the shallower insertion depth has less uniform flames with patches of orange-red and poorer overall performance. It is still difficult to make comparisons between the isothermal aerodynamics data and the combustion pictures, but the equivalence ratio for stable steady combustion is essentially the same between configurations 2 and 3, with only a 0.5 lb/hr increase for the center swirler for configuration 3. The effective area increases slightly as well from configuration 2 to configuration 3, so the equivalence ratio does not change appreciably.

Due to logistical constraints the fuel circuits were designed to allow the most flexibility for fuel staging and manipulation while having the fewest number of circuits possible. Obtaining measurement instrumentation for more than three fuel lines and designing a fuel manifold with more than three circuits would have been considerably more difficult than the three which were selected. An ideal scenario would have afforded separate fuel manipulation for each swirl cup, or to increase the number from three to four to manipulate the fuel separately for the two “side” UCRI-1 swirlers for this particular configuration. Since that is not the case, the fuel flow to all side swirl cups is the same, so the UCRI-1 swirl cups on circuit 2 are slightly more fuel-rich than they need to be to permit sufficient fuel to the two UCRI-2 swirlers on the same circuit. That being said, it is possible that this configuration could have allowed an even lower equivalence ratio than the one reported, and increasing the number of fuel circuits to accommodate this may be proposed for future testing if the logistical constraints can be adequately addressed.

Figure 6-14 below shows vertical cross sections of the axial velocity contours for all nine swirlers for configuration 3. With the addition of the two UCRI-1 swirlers on either side of the center swirler, the side CTRZs have returned to similar sizes and shapes as they were in configuration 1. The inclusion of a high-swirl swirler in the center of configuration 2 has certainly been shown to be beneficial to the operability limits and overall flame structure, and these additional high-swirl swirlers on either side make the size and shape of all outside CTRZs more uniform. Again due to the logistical constraints of having only three fuel circuits, the UCRI-1 swirlers on circuit 2 appear to operate slightly fuel-rich, so comparing the flame characteristics of the side swirl cups in figure 5-10 is difficult. Even with those UCRI-1 swirl cups operating fuel-rich, the overall equivalence ratio is still just as lean as configuration 2 for all three simulated flight conditions and just as lean as configuration 1 for the simulated idle and cruise conditions, and essentially the same for configuration 1 at takeoff conditions.

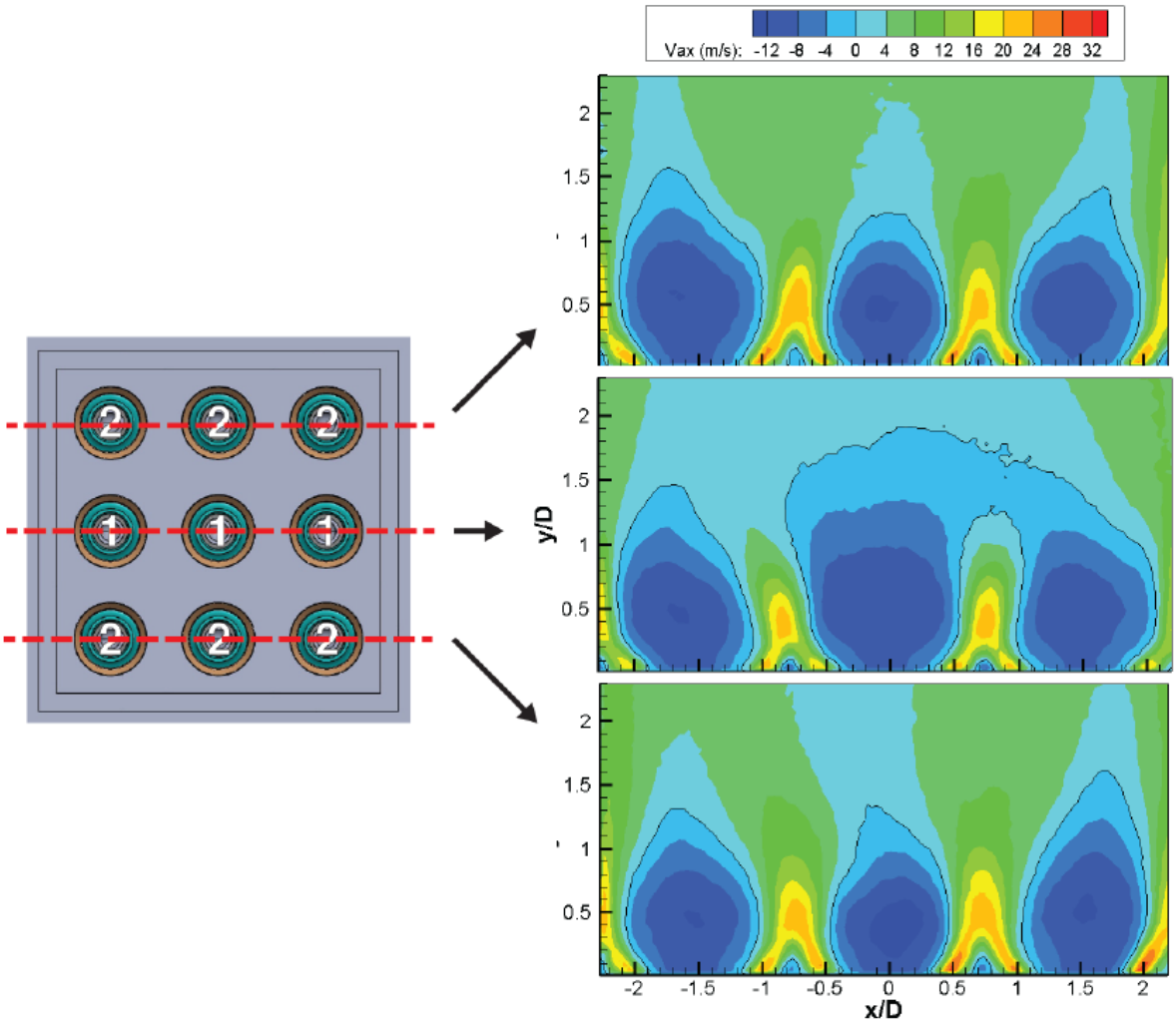

Figure 6-14: Vertical Cross-Sections of Axial Velocity for Configuration 3

6.3 Standard Video

Standard video was taken for all three configurations with both insertion depths to observe the flame stability and combustion characteristics at the various simulated flight conditions. While the photos are instructive in drawing real-time comparisons between the various cases and configurations and for presentation in this thesis, a video analysis is extremely useful for investigating the flame behavior over a full spectrum of tests. The videos were most useful for determining the flame steadiness at each test condition, as well as observing the

ignition process when circuits 2 and 3 were activated. These tests were meant to determine the lowest fuel flow rates needed for each circuit for each case, which means the flame was either close to or on the brink of stability. Analysis of the videos shows that reducing the fuel flow rate too much will reduce the overall stability and cause certain swirl cups to momentarily extinguish; e.g. for certain configurations one of the circuit 3 swirl cups would momentarily flicker when the fuel flow rate for circuit 2 was reduced, indicating a loss of stability and inadequate fuel flow rates to qualify as steady, stable combustion.

The premise of placing a high-swirl swirler in an array of low-swirl swirlers is to encourage swirler-swirler aerodynamic interaction and increase LBO range. Evidence of this enhanced interaction can be seen in the videos for configurations 1 and 2 when circuits 1 and 2 are active. Figures 6-15 and 6-16 below illustrate this point: in figure 6-15 some very bright blue areas can be seen on the flame-fronts between the center swirler and the neighboring swirlers on circuit 2, outlined in red below. These bright areas occur on all five swirlers at the border between two adjacent swirlers, and are indicative of a higher fuel concentration and subsequently poorer flame uniformity. However for figure 6-16, configuration 2, these spots only appear on the center swirler's flames and are somewhat more spread out than those of configuration 1. This provides further evidence that a high-swirl swirler in the center of the array is beneficial to overall flame uniformity and may be conducive to improved emissions performance. Additionally the flame was seen to be much steadier with circuits 1 and 2 active for configuration 3 than for other configurations with the same fuel circuits active. This is likely due to the increased swirler-swirler interaction that comes with having more high-swirl swirlers in the array, as well as the slightly higher fuel flow needed for circuit 2 to keep the two UCRI-2 swirlers on that circuit stable.

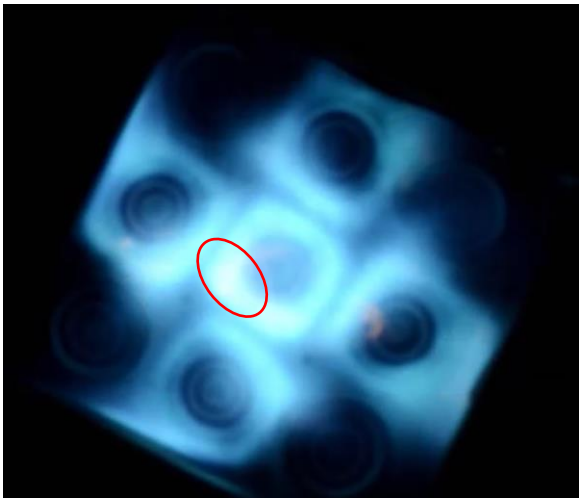

Figure 6-15: Image of Configuration 1 from Standard Video

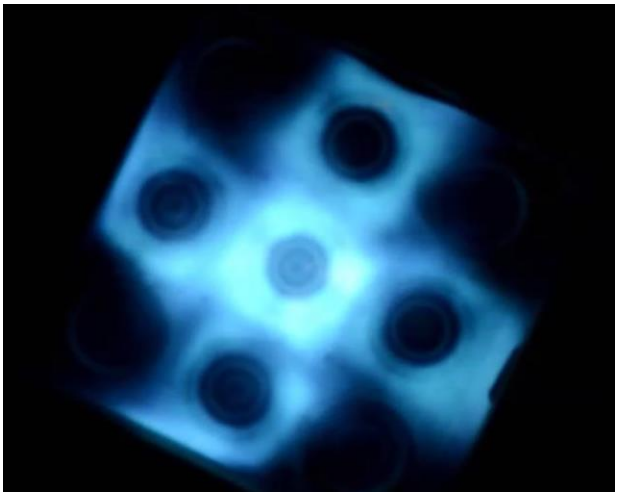

Figure 6-16: Image of Configuration 2 from Standard Video

These videos also served to reinforce the results from figures 5-3, 5-7, and 5-10, which all show that for the simulated takeoff condition with all circuits active the fuel flow rate for circuit 3 must be higher than circuit 2, by up to 25% more in the case of configuration 1. Attempting to set the flow rates to be equal caused circuit 3 to become unstable, with the flames on the corner swirl cups flickering and momentarily extinguishing then re-igniting. The likely reason for this is due to the corner swirlers' proximity to the two metal walls; while the swirl cups on circuit 2 are bordered by three swirlers and a wall, circuit 3 swirlers are bordered by two

walls and two swirlers. The circuit 2 swirlers benefit from more swirler interaction than those of circuit 3, sharing more air and fuel and encouraging better combustion performance, while the swirl cups on circuit 3 are further hampered by giving up heat to the wall, reducing their ability to maintain good combustion performance. This is likely an issue that is only experienced with this representative combustion test due to the two-wall condition; a full-scale engine would not have those two walls and each swirler would border at least three other swirlers.

Table 5-1 illustrates that the shallow insertion depth performs worse than the deeper insertion depth, and the videos are able to shed some light on the situation and explain why. The still images in figures 5-12 and 5-13 show that the center swirler's flame is not anchored, and increasing the flow rate to that circuit did not cause the flame to become anchored. The flame simply burns further downstream regardless of flowrate. This artifact is seen very clearly in figure 5-16, which shows a detached flame above the circuit 3 swirlers. Analysis of the video from the side showed the flames burning a few inches downstream of all corner swirlers, and again increasing the flow rate did not cause the flames to anchor while reducing the flowrate caused the flames to extinguish completely. The fact that this occurred only for the shallow insertion depth and not the deeper insertion likely means that the fuel is not atomizing properly prior to combustion. The droplets must progress further downstream to absorb enough heat and sufficiently reduce in size for combustion to occur, and when it does occur it produces an orange/red flame indicative of poor combustion and fuel-rich conditions. This indicates that the shallow insertion depth is not suitable for high-power throttle settings at these atmospheric pressure conditions.

Even with the poorer overall performance with the shallower insertion, configurations 2 and 3 still performed decently well with circuit 1 and circuits 1 and 2 active. The video shows

patches of orange flame kicking up every so often, but the majority of the flame is blue and stable as indicated by a still image taken from the video of configuration 2 at an equivalence ratio of roughly 0.5-0.6. Figure 6-17 shows a fairly uniform, stable flame on the center swirler, and some slight orange patches on the border between neighboring swirlers; but contrasting to configuration 1 whose center swirler was never even anchored, this configuration performed surprisingly well with the shallower insertion depth. Again, while the deeper insertion depth certainly performs better in nearly every criterion used to judge the performance of these tests, the shallower insertion depth still has some potential for producing a relatively uniform and stable flame in a high-pressure combustion environment.

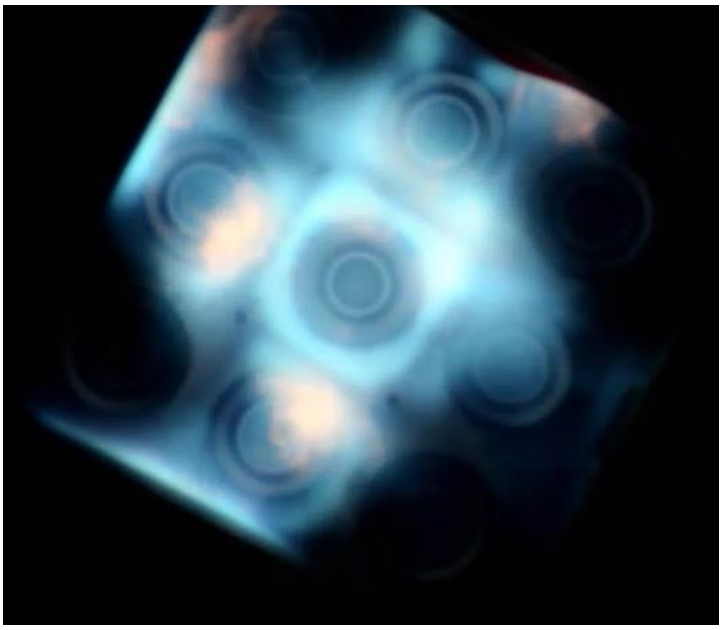

Figure 6-17: Still of Configuration 2 with Circuits 1&2 Active, Shallow Insertion

6.4 High-Speed Video

High-speed video was captured where acoustic instabilities were experienced for each configuration. Again, since no instabilities were experienced with the shallow insertion depth,

videos were only recorded for the deep insertion depth. These videos were meant to gain additional insight to the combustion dynamics and flame characteristics when instabilities were present. The recording speed and playback speed are noted for each case, and the total duration of the video as well as the number of flame "pulses" are recorded. These results are shown below in table 6-1. In this context, "pulse" refers to either the extinction and re-ignition of the flame or a surge in the axial distance the flame travels downstream. Note again that measurements were made for the acoustic intensity only for configuration 2, which was a by-product of obtaining a decibel-level reading to get an idea for how truly loud the instabilities were. For the results in table 6-1, fuel flow rates were simply selected which elicited acoustic instabilities and high-speed video was taken at those conditions to observe the flame properties.

High Speed Video Analysis					
Config.	**Time (s)**	**# Pulses**	**Fps (rec)**	**Fps (playback)**	**Frequency (Hz)**
1	**182**	**152**	**8800**	**15**	**490.0**
2	**182**	**197**	**8000**	**15**	**577.3**
3	**182**	**191**	**8000**	**15**	**559.7**

Table 6-1: Visual Frequency Analysis of High-Speed Videos

Note that the frequency of the flame oscillations coincides roughly with the frequency heard and recorded, which is detailed in the following section. A frame-by-frame analysis shows an interesting trend with regards to the "local" equivalence ratios for each swirl cup. When the fuel flow rate to the center nozzle drops to 3 lb/hr, the flame is seen to lift off from the swirler completely and temporarily extinguish, reigniting very shortly thereafter. However when the flow rate increases to 4 lb/hr, the flame stays anchored and does not extinguish even temporarily. Interestingly, the fuel flow rate for "local" stoichiometric combustion on a single swirl cup is

roughly 3.2 lb/hr, which means the flame stays anchored when fuel-rich and momentarily extinguished and reignites when fuel-lean. It may simply be a coincidence that this occurs around stoichiometric conditions, but this is certainly an expected trend that a more fuel-rich flame will maintain constant combustion through acoustic instabilities, and will not experience the transient extinction and re-ignition that a fuel-lean flame will.

The high-speed videos taken at these conditions also revealed that the flame extends only about 1 ½ inches downstream of the swirler exit. This very short, uniform global flame structure is indicative of very quick combustion and uniform fuel-air mixing. The very blue flame is evenly spread across all nine swirlers and is a potential indicator of low emissions and a relatively low, uniform temperature profile downstream of the swirlers. A short flame means reduced residence times which correlate to lower NO_x emissions, and the uniform flame means a uniform temperature profile which means no areas of high fuel concentration, which also correlates to lower estimated NO_x emissions. Again, note that these videos were taken when the global equivalence ratio was around 0.9-1.0, which is 15-20% more fuel-rich than the most fuel-rich case with all three circuits activated.

A frame-by-frame sequence of photos is included in figures 6-17 and 6-18 on the following two pages illustrating approximately one full "cycle" of combustion, from extinction to re-ignition to extinction again. The entire sequence takes place over $1/500^{th}$ of a second, and the time-step for each photo is $1/8000^{th}$ of a second. These pictures are from a high-speed video which was taken of configuration 2 when it experienced acoustic instability issues at a global equivalence ratio of 0.94, with fuel flow rates of 3, 12, and 12 lb/hr to the three circuits respectively. Note that the flame can be seen to start extinguishing in frame 8 on all swirl cups but the center cup, and in frames 9 and 10 the flame appears extinguished or very nearly

extinguished. In frame 11 the flame then reignites on the center swirl cup, and in frame 14, re-ignition begins on the surrounding swirl cups. This further evidences the theory that the center swirler, though it receives the same amount of fuel as the other eight swirl cups, anchors the flame during periods of transient instability, such as when these acoustic instability issues experienced. Again, this likely occurs due to heavy swirler-swirler interaction of the center swirler with all eight surrounding swirlers, with this heavy interaction being driven by the higher swirl number of the UCRI-1 swirler compared with the lower-swirl UCRI-2.

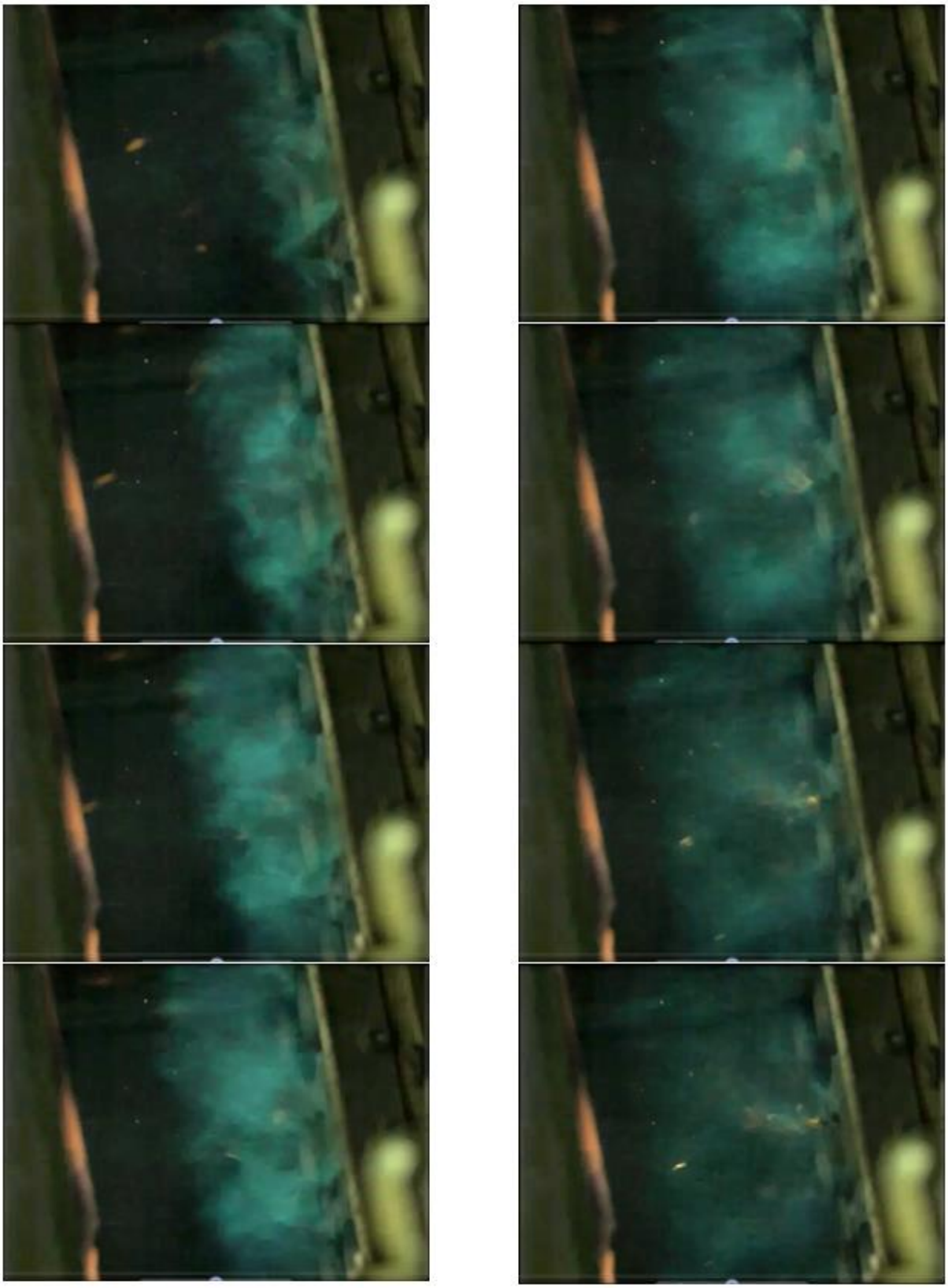

Figure 6-18: High-Speed Video Sequence of Configuration 2 at φ=0.94 (a)

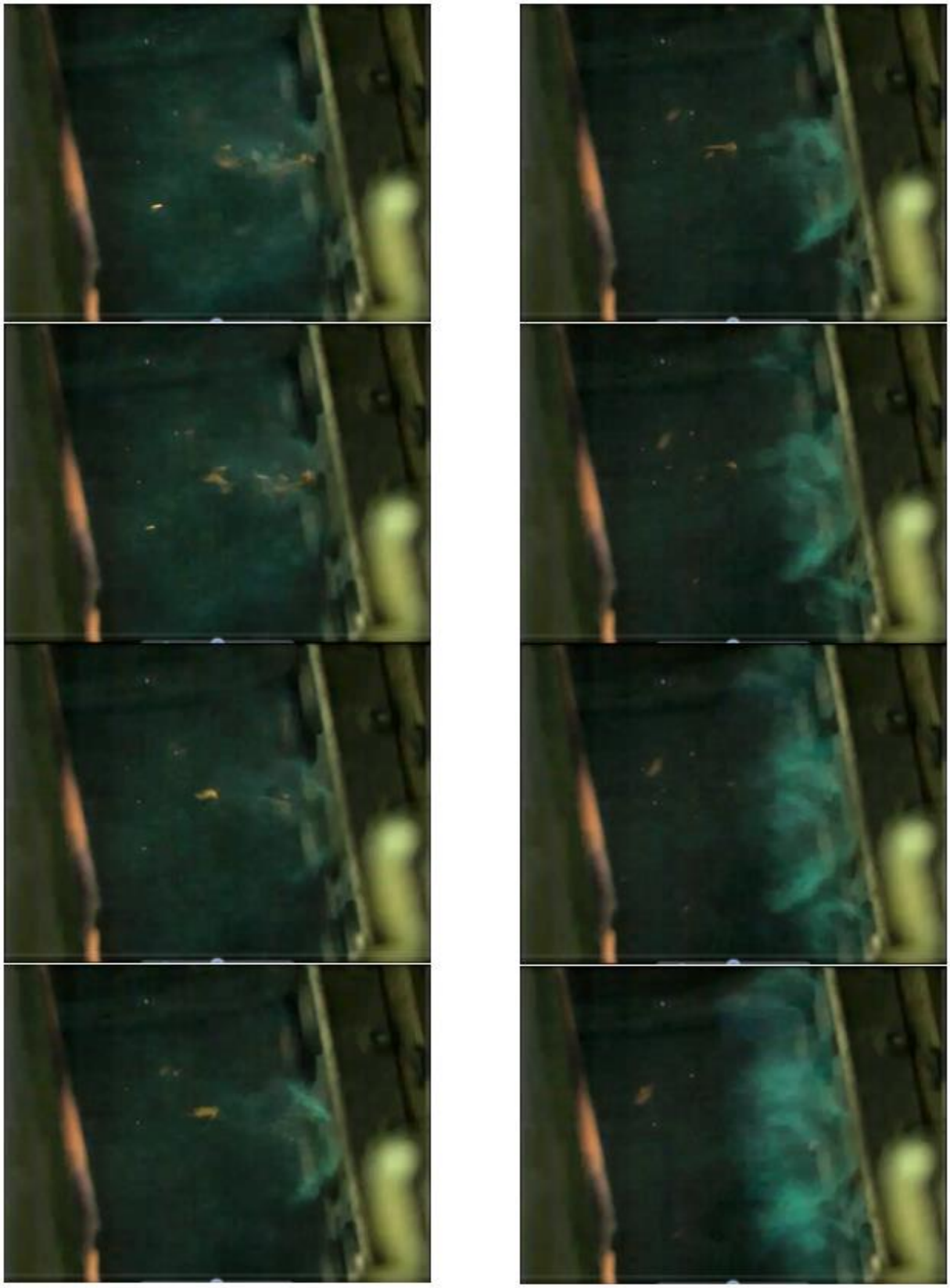

Figure 6-19: High-Speed Video Sequence of Configuration 2 at φ=0.94 (b)

6.5 Acoustic Instabilities

During the course of this testing, certain acoustic phenomena were experienced with all configurations at a variety of test conditions. This phenomena is colloquially known as the "howl" and is fairly well-documented by Lefebvre, producing an extremely loud tone around 500Hz. Due to the potential dangers presented by such loud acoustics in an actual turbine engine, this phenomena was investigated to gain some insight to when these instabilities occur. Due to the unique fuel-staging configuration and modular design of this combustor concept, the conditions at which these instabilities occur with respect to the fuel flow rates on the various fuel circuits could be investigated. Previous work has been done which links the combustor geometry to the strength and severity of these acoustics; however the geometry is something that is invariant during testing/operation, and difficult to alter if acoustic issues are found during preliminary combustion testing. A much simpler solution may be to adjust the local fuel flow rates and equivalence ratios for certain fuel circuits if these issues occur, or to avoid combinations of fuel flows to certain circuits where acoustics are known to occur. The results from this series of tests revealed a very distinct trend of acoustic intensity with respect to both the "local" and global equivalence ratios, both for the individual swirl cups and the entire combustor rig as a whole.

Tables 5-2, 5-3, and 5-4 list fuel flow rates and equivalence ratios for the three fuel circuits at which acoustic instabilities occur for all three configurations. Acoustic instabilities were only encountered with the deep insertion depth. There was a distinct, unmistakable difference between the "normal" combustion growl and the markedly louder "howl" characteristic of acoustic instability, so there is no misinterpretation between what constitutes instability and normal combustion sounds. An in-depth investigation of the change of acoustic

intensity with respect to the fuel flow rates of the various circuits was not performed, as that was not included in the scope of this thesis. However the sound level was measured for one set of tests to obtain a representative idea of how loud the acoustic instabilities were. By using a factory-calibrated decibel meter, the sound level intensity was measured at 132 dB for configuration 2, with the fuel flow rates set to 3 lb/hr, 12 lb/hr, and 12 lb/hr respectively for circuits 1, 2, and 3. This is contrasted by the average sound level intensity when no acoustic instabilities are present, roughly 102 dB.

An audio spectrum analysis was performed to determine the dominant frequency for configuration 2, which was found to be approximately 567Hz. The results of the analysis are shown above in figures 5-20 and 5-21. Figure 5-20 shows a log scale of the raw output from an audio processing program known as “Audacity”, which performs an FFT analysis of the audio data to obtain an arbitrary decibel intensity spectrum with respect to frequency. Note that the term “decibel” used here is simply the logarithmic relationship between two numbers, and is not the same as the colloquial definition of the decibel as is relates to human hearing and perceived noise levels. Figure 5-21 shows the same data in a linear scale to illustrate the falling peaks of the harmonics which accompany the dominant frequency.

Returning to tables 5-2 through 5-4, the fuel flow rates and equivalence ratios for each circuit are reported for each configuration, as well as the “local” and global equivalence ratio. Again, the term “local” may not, strictly speaking, be accurate, but does give enough information about the combustion properties on a local level to be of relative utility. The boxes which are highlighted in yellow denote equivalence ratios which fall between the range of 0.8 to 1.1. The significance of this range is that acoustic instabilities occur if at least one circuit operates within this equivalence ratio range. The only exception to this trend is the final test performed on

configuration 3, with local equivalence ratios for the three circuits of 1.77, 0.74, and 0.74 for circuits 1, 2 and 3 respectively. Again, this may be due to the fact that the center swirler cup is providing fuel to the surrounding swirl cups and increasing their local equivalence ratios, or that there are much more complicated interactions occurring in the flow-field which make this observation more of a guideline than a rule. This observation is supported by combustion fundamentals which state that the highest temperatures are reached for a flame which operates slightly fuel-lean of stoichiometric conditions, and the range is roughly centered on an equivalence ratio of one.

Additionally, the fourth set of sets done with configuration 2 is highlighted in yellow as well, and this particular test had the loudest acoustics out of all conditions tested. Following with the aforementioned trends, the equivalence ratios for all three circuits is 0.94, around where the highest flame temperatures are expected, which again evidences the idea that the acoustic instabilities are tied to the equivalence ratio indirectly and to the flame temperature directly. The second observation which arises from this particular test is that the more swirl cups which operate within this range, the more intense the instabilities will be. No significant trends were found between the three configurations; that is, instabilities were not found to be worse between configurations when standardized for similar equivalence ratios on similar fuel circuits. A brief summary of the observed trends is as follows:

1. At least one swirl cup must operate within the 0.8-1.1 range of equivalence ratio to experience acoustics
2. More swirl cups within the range equate to louder acoustics
3. Swirl cups operating closer to stoichiometric or conditions of highest flame temperature exhibit louder acoustics

From these trends it can be hypothesized that the temperature of the flame plays a role in acoustic instability, as temperature is linked with equivalence ratio and these observations all indicate that the acoustics are linked with equivalence ratio to some degree. It should also be noted that no acoustic issues were experienced with only circuit 1 activated: previous work had been done with LPP combustors at NASA and one of the primary reasons for a shift away from the LPP concept was acoustic instabilities at idle conditions. The likely reason for the lack of acoustics at simulated idle conditions for the LDI design is that the swirler cup burns outside of the previously-specified range of equivalence ratios where instabilities are experienced.

No instabilities were found to occur for any testing performed with the shallow insertion depth. The reasons for this are not known, but it may be due to the fact that testing done with the shallow insertion depth exhibited red/orange flames and higher fuel flow rates than those performed with the deeper insertion depth. These color flames are characteristic of lower temperatures, which may play a role in acoustic instability. Yet another reason may be due to fuel atomization or how thoroughly mixed the fuel/air mixture is. The LPP design referenced in the previous paragraph likely operated at similar equivalence ratios to this LDI design yet had higher inlet temperatures and a fuel supply which was more fully premixed and prevaporized. Acoustic issues were experienced only with the LPP design when it operated at similar equivalence ratios as the LDI design. Again for the LDI, acoustics were occurred only for the deeper insertion depth for similar equivalence ratios, which allowed slightly more time for the fuel to atomize and produce smaller droplets than the shallow insertion depth.

6.6 Large Fuel Nozzle Ignition/LBO Testing

The results of the ignition and lean-blowout testing with both sets of fuel nozzles are summarized in tables 5-6 and 5-7, and are fairly unexpected. The deeper insertion depths performed better than the shallow insertion depths, exhibiting lower equivalence ratios overall with the exception of the LBO performed with the deep insertion depth with configuration 1. The ignition/LBO tests performed with the smaller fuel nozzles do not necessarily have much utility when considering the size of fuel nozzles used in a typical turbine engine, and are shown here mainly to contrast the results obtained with the larger fuel nozzles. Very generally speaking, the larger fuel nozzles actually performed better than the smaller nozzles, which is non-intuitive. One would expect that smaller nozzles would exhibit better atomization and performance than larger ones with the very low fuel pressures and at the relatively small fuel flow rates used. However the opposite trend is true; the larger nozzles had lower or nearly identical ignition and LBO equivalence ratios than the smaller nozzles for all tests besides the shallow insertion testing with configuration 3, in which the flame was never truly anchored so the data was considered invalid.

These results, while slightly confusing, are very promising for future high-pressure testing, which will use an array of nine large fuel nozzles of the same flow number as the single nozzles used for these tests. Additionally, the very low equivalence ratios help validate this concept with regards to any issues which may be experienced during initial engine startup or blowout during startup, where the low inlet pressures may cause issues with fuel nozzles which may not provide sufficient atomization at such low fuel pressures and air flow rates. While no reference numbers could be found for actual turbine engines for comparison, the equivalence

ratios for all three configurations with the larger fuel nozzles and deep insertion depth are lower than those exhibited by typical gas turbine engines for the “idle” flight condition.

Yet another interesting item to note is that the LBO for configuration 1 is lower for the shallow insertion, which is expected to have poorer performance, than the deeper insertion. This may be due to the relatively high LBO of configuration 1 with the deeper insertion, which is almost 70% higher than configurations 2 or 3. Poorer LBO performance with the baseline configuration is not surprising, as the two configurations with UCRI-1 swirlers are expected to expand the operability range by encouraging more fuel-air and swirler-swirler interaction at lower fuel flow rates. In keeping with this expectation, configurations 2 and 3 all have lower or nearly identical LBO and ignition rates than configuration 1 for both insertion depths and both sets of fuel nozzles, with the only exception again being the shallow insertion tests with configuration 3.

These results help validate the hypothesis that having a high-swirl swirl in the center of this combustor array improves operability limits. For a given insertion depth and fuel nozzle type, configurations 2 and 3 both performed better than or essentially identical to configuration 1. The fact that the LBO/ignition performance is better for the larger fuel nozzles than the smaller ones is an unexpected result, but one which shows promise for future high-pressure combustion tests. As with the equivalence ratio results and the steady-state combustion pictures, the deeper insertion performs better than the shallow insertion, requiring lower fuel flow rates and equivalence ratios for both ignition and lean blow-out.

Chapter 7 : Conclusion

A lean-direct injection combustor concept was designed and tested to investigate its potential as a future replacement for the standard RQL and LPP combustors used in typical gas turbine combustors today. Its potential was gauged by its operability limits (ignition and LBO) with flow number 3.0 fuel nozzles typical of full-scale turbine engines, and the steady-state combustion properties with smaller fuel nozzles at atmospheric pressure. These properties included flame uniformity with various fuel circuits activated and varying fuel flow rates, combustion steadiness at fuel-lean conditions, and the lowest flow rates needed for steady combustion with various circuits activated. Standard and high speed videos were also taken to gain additional insight to the transient and long-term combustion properties, as well as an analysis of the acoustic instabilities experienced at certain local and global equivalence ratios, to aid in mitigating these issues with later testing. Three configurations of high/low-swirl swirler arrangements were tested as well as two fuel nozzle insertion depths. Three fuel circuits were also used to allow fuel staging and simulate different throttle/power settings.

The results of this testing show that this concept is able to achieve ignition, operate with various fuel circuits activated, and blowout at relatively low equivalence ratios. The equivalence ratios for all simulated flight conditions are very comparable to those seen by typical gas turbine engines used in industry. Some similarities were able to be drawn with Endicott's PIV data which predicated this work, although a direct comparison of cold-flow aerodynamics with combustion images cannot be done with full rigor. Of the three swirler configurations tested, the two with high-swirl swirlers in the center performed better across the board than the baseline configuration with only low-swirl swirlers, demonstrating lower equivalence ratios needed for ignition and LBO and slightly lower equivalence ratios for the simulated idle and cruise

conditions with circuit 1 and circuits 1 and 2 active respectively. These results demonstrated that the deeper fuel nozzle insertion depth exhibited better steady-state combustion, ignition, and LBO performance than a shallower insertion depth. Additionally, the investigation performed with the acoustic instabilities showed that care should be taken in future tests to ensure that no swirl cups operate "locally" between an equivalence ratio of 0.85 and 1.1 or instabilities will occur, and the more cups which operate in this range the worse those instabilities will be.

The very blue, uniform flame pattern observed with all configurations with a deeper insertion depth likely means quick, complete combustion and a uniform temperature profile shortly downstream of the swirler exit. This short, uniform flame is a characteristic of low NO_x emissions due to reduced residence time and no "hot-spots" of high fuel concentrations, as well as the low global equivalence ratios due to the heavy dependence of NO_x on temperature and subsequently the equivalence ratio. These very positive results indicate that this proof-of-concept design has demonstrated sufficient characteristics for producing a low-NO_x flame to proceed to the next round of testing in a high-pressure combustion environment to measure emissions and combustion performance parameters. Those tests will likely focus on the two high-swirl swirler configurations and the deeper fuel nozzle insertion depth unless any flashback or auto-ignition issues are experienced.

Chapter 8 : References

[1] Alkabie, H.S., and Andrews, G.E., "Reduced NO_x Emissions Using Low Radial Swirler Vane Angles." ASME Paper 91–GT–363, *ASME Gas Turbine and Aero Engine Congress and Exposition*, Orlando, FL, 1988

[2] Anderson, David. "Effects of equivalence ratio and dwell time on exhaust emissions from an experimental premixing prevaporizing burner." NASA TM X-71592, *20th International Gas Turbine Conference,* Houston TX, Mar. 1975

[3] Anderson, David. "Ultra-lean Combustion at High Inlet Temperatures." NASA-TM-81640 *26th Annual International Gas Turbine Conference,* Houston, TX, Mar. 1981

[4] Archer, S., and Gupta, S.K., "Effect of Swirl and Combustion on Flow Dynamics in Lean Direct Injection Gas Turbine Combustion." AIAA Paper 2003-1343, *41st AIAA Aerospace Sciences Meeting and Exhibit*, Reno, NV, 2003

[5] Beer, J.M and Chigier, J.M., "Combustion Aerodynamics." Applied Science Publishers LTD, London, 1972

[6] Bowman, Craig T. "Kinetics of nitric oxide formation in Combustion Processes." *International Symposium on Combustion*. Vol. 14. No. 1. Elsevier, 1973

[7] Cai, Jun. "Aerodynamics of Lean Direct Injection Combustor with Multi-Swirler Arrays." Dissertation, University of Cincinnati, 2006

[8] Cai, J., Jeng, S.-M., and Tacina, R., "Multi-Swirler Aerodynamics: Experimental Measurements." AIAA Paper 2001-3574, *37th Joint Propulsion Conference and Exhibit*, Salt Lake City, Utah, July 2001

[9] Correa, Sanjay M. "A review of NO_x formation under gas-turbine combustion conditions." *Combustion science and technology,* Vol. 87, pp. 329-362, 1992

[10] Daggett, D. L., and Geiselhart, Karl. A., "Ultra efficient engine technology systems integration and environmental assessment." NASA/CR-2002-211754, July 2002

[11] Endicott, Derick. "Experimental Development of a Lean Direct Injection Combustor Utilizing High-Low Swirl Intensity Combinations." Master's Thesis, University of Cincinnati, 2014

[12] Fleming, Gregg G., et al. "Using FAA's SAGE Model to Conduct Global Inventories and to Assess Route-specific Variability in Aviation Fuel Burn, Emissions, and Costs." *25th International Congress of the Aeronautical Sciences*. 2006

[13] Fletcher, R., and Heywood, J. "A model for nitric oxide emission from aircraft gas turbine engines." *9th Aerospace Sciences Meeting*. 1971

[14] Foust, Michael J., et al. "Development of the GE aviation low emissions TAPS combustor for next generation aircraft engines." *50th AIAA Aerospace Sciences Meeting,* Nashville, TN, Jan. 2012

[15] Friedl, Randall, "Atmospheric effects of subsonic aircraft: Interim assessment report of the advanced subsonic technology program." NASA Reference Publication 1400, 1997

[16] Fu, Yongqiang, "Aerodynamics and Combustion of Axial Swirlers." Dissertation, University of Cincinnati, 2008

[17] Fu, Yongqiang, and San-Mou Jeng. "Experimental investigation of swirling air flows in a multipoint LDI combustor." AIAA 2007-5685, *43rd AIAA/ASME/SAE/ASEE Joint Propulsion Conference & Exhibit*, Cincinnati OH, July 2007

[18] Fu, Y., Jeng, S.M., and Tacina, R.. "Characteristics of the swirling flow in a Multipoint LDI Combustor." *45th AIAA Aerospace Sciences Meeting and Exhibit,* Reno, NV. 2007

[19] Gupta, A.K, Lilley, D.G., and Syred, N., "Swirl Flows." Abacus Press, Tunbridge Wells, England, 1984

[20] Hayashi, S. "Compatibility between low-NO_x emissions and high-combustion efficiency by lean direct injection combustion." ASME 95-GT-276, *International Gas Turbine and Aeroengine Congress and Exposition*, Houston TX. June 1995

[21] Hussain, Abdul, et al. "Low NO_x primary zones using jet mixing shear layer combustion." 88-GT-308, *Gas Turbine and Aeroengine Congress and Exposition,* Amsterdam, Netherlands. 1988.

[22] Iannetti, A., et al. "Multi-Swirler Aerodynamics: CFD Predictions." AIAA 2001-3575, *37th AIAA/ASME/SAE/ASEE Joint Propulsion Conference and Exhibit*, Salt Lake City UT, 2001

[23] ICAO Annex 16 International standards and recommended practices, Environmental protection, *Volume II "Aircraft Engine Emissions", Part III, Chapter 2.* 3rd Ed, 2008

[24] Kao, Yi-Huan, et al. "Aerodynamics Comparisons Between Two Typical Gas Turbine Combustion Swirlers." *ASME Turbo Expo 2014: Turbine Technical Conference and Exposition*. American Society of Mechanical Engineers, 2014.

[25] Kao, Y.H., Tambe, S.B., and Jeng, S.M., "Aerodynamics of Linearly Arranged Rad-Rad Swirlers, Effect of Number of Swirlers and Alignment." *ASME Turbo Expo 2013: Turbine Technical Conference and Exposition*. American Society of Mechanical Engineers, 2013.

[26] Kao, Y.H., Tambe, S.B., and Jeng, S.M., "Aerodynamics Study of a Linearly-Arranged 5-Swirler Array." *ASME Turbo Expo 2014: Turbine Technical Conference and Exposition*. American Society of Mechanical Engineers, 2014.

[27] Kao, Yi-Huan, “Experimental investigation of aerodynamics and combustion properties of a multiple-swirler array.” Dissertation, University of Cincinnati, 2014.

[28] Lefebvre, A. H., and Ballal, Dilip R. *Gas turbine combustion*, CRC press, 3rd Ed. 2010.

[29] Lilley, D.G., “Swirl Flows in Combustion: A Review,” AIAA Journal, Vol.15, No.8, pp. 1063-1078. Aug, 1977.

[30] Marek, C. J., Leonidas, C. P., and Peter, W. V. "Preliminary studies of autoignition and flashback in a premixing-prevaporizing flame tube using Jet-A fuel at lean equivalence ratios." *NASA Technical Memorandum*, Lewis Research Center, Cleveland, Ohio, 44135, 1977.

[31] Marek, C. J., Smith, T. D., and Kundu, K. "Low emission hydrogen combustors for gas turbines using lean direct injection." *Proceedings of the 41st Joint Propulsion Conference,* Tucson, AZ, July, 2005.

[32] Niedzwiecki, R. W., and R. E. Jones. "The experimental clean combustor program: Description and status." NASA-TM-X-71547, *Air Transport Meeting,* Dallas TX, 1974.

[33] Semerjian, H., and A. Vranos. " NO_x formation in premixed turbulent flames," *International Symposium on Combustion*. Vol. 16. No. 1, Elsevier, 1977.

[34] Sheen, H.J., Chen, W.J., Jeng, S.Y., and Huang, T.L., “Correlation of Swirl Number for a Radial-Type Swirl Generator,” *Experimental Thermal and Fluid Science,* Vol. 12, pp.444-451, 1996.

[35] Smith, K. O. "Engine testing of a prototype low NO_x gas turbine combustor." *37th International Gas Turbine and Aeroengine Congress and Exposition*. Vol. 1. 1992.

[36] Stickles, R., and Barrett, J., “TAPS II Technology Final Report – Technology Assessment Open Report.” DTFAWA-1C-00046, *FAA Continuous Lower Energy, Emissions and Noise (CLEEN) Technologies Development*, June 2013.

[37] Tacina, Robert R. "Low NO_x potential of gas turbine engines." AIAA-90-0550, *28th Aerospace Sciences Meeting*, Reno, NV. Jan. 1990.

[38] Tacina, Robert, et al. "Sector Tests of a Low NO_x, Lean-Direct-Injection, Multipoint Integrated Module Combustor Concept." *ASME Turbo Expo 2002: Power for Land, Sea, and Air*. American Society of Mechanical Engineers, 2002.

[39] Tacina, Robert, et al. "A Low NO_x Lean-Direct Injection, Multipoint Integrated Module Combuster Concept for Advanced Aircraft Gas Turbines”, *Conference on Technologies and Combustion for a Clean Environment*. Oporto, Portugal. (2002).

[40] Tacina, R., Mao, C. and Wey, C., “Experimental Investigation of a Multiplex Fuel Injector Module for Low Emission Combustors,” AIAA Paper 2003-0827, *41st*

AIAA Aerospace Sciences Meeting and Exhibit, Reno, NV, 2003.

[41] Tacina, R., Mao, C.P., and Wey, C., "Experimental investigation of a multiplex fuel injector module with discrete jet swirlers for low emission combustors." AIAA 2004-135, *42nd AIAA Aerospace Sciences Meeting and Exhibit*, Reno NV, Jan. 2004

[42] Tacina, Kathleen M., and Changlie Wey. "NASA Glenn high pressure low NO_x emissions research." NASA/TM-2008-214974, 2008.

[43] Terasaki, T., and S. Hayashi. "The effects of fuel-air mixing on NO_x formation in non-premixed swirl burners." *International Symposium on Combustion*. Vol. 26, No. 2. Elsevier, 1996.

[44] Terasaki, T., and S. Hayashi. "Lean non-premixed combustion for low-NO_x gas turbine combustor." *Yokohama International Gas Turbine Congress, Yokohama, Japan*. 1995.

[45] Turns, Stephen R. *An introduction to combustion*. 3rd Ed. New York: McGraw-hill, 2012.